MAGNETIC AND THERMAL STUDIES OF Cu(II), Ni(II), Co(II) AND Fe(II) COMPLEXES OF LIGANDS DERIVED FROM 2-HYDROXYBENZALDEHYDE AND POLYMETHYLENEDIAMINES

AFIQ BIN AZIL

DISSERTATION SUBMITTED IN FULFILLMENT OF THE REQUIREMENT FOR THE DEGREE OF MASTER OF SCIENCE

DEPARTMENT OF CHEMISTRY
FACULTY OF SCIENCE
UNIVERSIY OF MALAYA
KUALA LUMPUR

2015

ACKNOWLEDGEMENT

I would like to express my deepest gratitude to my supervisor, Assoc. Prof. Dr. Norbani Abdullah, for without her assistance, support and guidance, this research would not have been possible.

I also want to thanks my colleagues from the Inorganic Chemistry Research Laboratory and all staff of the Chemistry Department, Faculty of Science, University of Malaya for their continuous support and assistance throughout my entire research.

Many thanks also to the members of Coordination Chemistry Research Group, Department of Chemistry, School of Science and Engineering, Kinki University, Higashi-osaka, Osaka, Japan, especially Prof. Dr. Takayoshi Kuroda-Sowa, for their kindness and hospitality in teaching me magnetochemistry.

I would like to acknowledge the Malaysia Ministry of Higher Education and University of Malaya for the financial grants: High Impact Research Grant (UM.C/625/1/HIR.MOHE/05) and Postgraduate Research Grant (PG023-2013A).

Last but not least, I dedicate this work to both my parents who managed to stand by me through the good and the bad time.

ABSTRACT

The main objective of this research was to synthesise and characterise magnetic and thermally stable metal complexes, designed as functional molecular materials. The ligands (H_2L1, H_2L2, and H_2L3) were Schiff bases prepared from 2-hydroxybenzaldehyde with 1,8-diaminooctane, 1,10-diaminodecane and 1,3-diaminopentane, respectively. The complexes were obtained from the reactions of these Schiff bases with $[M(CH_3(CH_2)_{14}COO)_2]$, where M = Cu(II) ($d^9$), Ni(II) ($d^8$), Co(II) ($d^7$) and Fe(II) ($d^6$) ions. A total of 16 complexes were obtained by step-wise and/or one-pot reactions (**Table 1**).

Table 1 Structural formulae of complexes; R = $CH_3(CH_2)_{14}COO$

Ligand	Synthetic Method	Structural formula
H_2L1	Step-wise	$[CuL1]$
		$[Ni(L1)]$
		$[Co(L1)]$
		$[Fe_2(R)_2(L1)(H_2O)_4].2.5H_2O$
H_2L2	Step-wise	$[Cu(L2)]$
		$[Ni(L2)].EtOH$
		$[Co_2(L2)(HL2)_2(EtOH)_4]$
		$[Fe^{II}Fe^{III}(R)(L2)(HL2)_2(H_2O)_2].H_2O$
	One-pot	$[Cu(L2)]$
		$[Ni_2(L2)(HL2)_2].H_2O$
		$[Co(L2)(HL2)]$
		$[Fe^{II}Fe^{III}(R)(L2)(HL2)_2(EtOH)_2].2EtOH$
H_2L3	Step-wise	$[Cu_2(R)(L3)(HL_3)]$
		$[Ni(R)(HL3)_2]$
		$[Co(R)(HL3)]$
		$[Fe(R)_2(HL3)]$

These complexes, except Ni(II), were soluble in chloroform. Ni(II) complexes were partially soluble in this solvent.

ABSTRAK

Objektif utama penyelidikan ini adalah untuk menyedia dan mencirikan kompleks magnetik dan stabil secara terma, yang direka bentuk sebagai bahan molekul berfungsi. Ligan (H_2L1, H_2L2, dan H_2L3) adalah bes Schiff yang disediakan daripada tindak balas 2-hidroksibenzaldehid dengan masing-masing 1,8-diaminooktana, 1,10-diaminodekana 1,3-diaminopentana. Kompleks pula diperoleh daripada tindak balas ketiga-tiga bes Schiff tersebut dengan $[M(CH_3(CH_2)_{14}COO)_2]$, iaitu M = ion Cu(II) ($d^9$), Ni(II) ($d^8$), Co(II) ($d^7$) dan Fe(II) ($d^6$). Sejumlah 16 kompleks diperoleh melalui tindak balas beberapa langkah dan/atau tindak balas satu langkah (**Jadual 1**).

Jadual 1 Formula struktur kompleks; R = $CH_3(CH_2)_{14}COO$

Ligan	Kaedah penyediaan	Formula struktur
H_2L1	Beberapa langkah	$[CuL1]$
		$[Ni(L1)]$
		$[Co(L1)]$
		$[Fe_2(R)_2(L1)(H_2O)_4].2.5H_2O$
H_2L2	Beberapa langkah	$[Cu(L2)]$
		$[Ni(L2)].EtOH$
		$[Co_2(L2)(HL2)_2(EtOH)_4]$
		$[Fe^{II}Fe^{III}(R)(L2)(HL2)_2(H_2O)_2].H_2O$
	Satu langkah	$[Cu(L2)]$
		$[Ni_2(L2)(HL2)_2].H_2O$
		$[Co(L2)(HL2)]$
		$[Fe^{II}Fe^{III}(R)(L2)(HL2)_2(EtOH)_2].2EtOH$
H_2L3	Beberapa langkah	$[Cu_2(R)(L3)(HL_3)]$
		$[Ni(R)(HL3)_2]$
		$[Co(R)(HL3)]$
		$[Fe(R)_2(HL3)]$

Kompleks-kompleks ini, kecuali Ni(II), larut dalam kloroform. Kompleks Ni(II) larut separa dalam pelarut ini.

Kompleks Cu(II) dari H_2L1 dan H_2L2 adalah mononukleus, tetapi mungkin wujud sebagai dimer. Semua kompleks ferum adalah Fe(II) dwinukleus, kecuali $[Fe(CH_3(CH_2)_{14}COO)_2(HL3)]$, yang merupakan kompleks Fe(III). Semua kompleks Co(II) adalah oktahedral, kecuali [Co(L1)] yang mempunyai geometri sesatah sisi empat sama.

Kecuali kompleks Ni(II) dari H_2L1, dan kompleks Ni(II) dan Co(III) dari H_2L2, yang diamagnetik, semua kompleks lain adalah paramagnetik.

Semua kompleks dari H_2L1 dan H_2L2 adalah stabil secara terma (suhu penguraian dalam julat 205 ^oC hingga 320 °C). Kestabilan terma kompleks dari H_2L3 adalah lebih rendah berbanding kompleks dari H_2L1 dan and H_2L2 (suhu penguraian dalam julat 142 °C hingga 209 °C). Semua kompleks tidak menunjukkan sifat cecair hablur.

Penemuan penyelidikan ini telah dibentangkan dalam satu seminar kebangsaan dan satu seminar antarabangsa, dan diterbitkan dalam satu jurnal ISI.

TABLE OF CONTENTS

CHAPTER 1 INTRODUCTION

This main objective of this research was to synthesize and fully characterize magnetic complexes formed from the reactions Cu(II), Ni(II), Co(II) and Fe(II) hexadecanoate with N_2O_2-tetradentate Schiff bases (**Figure 1.1**). These complexes were of interest as functional magnetic materials.

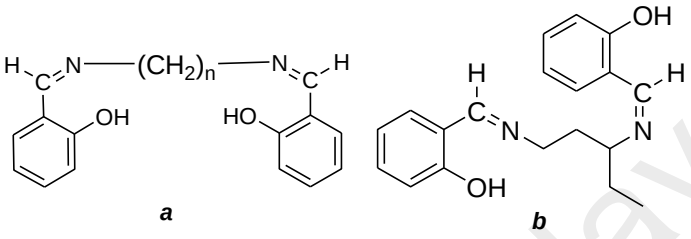

Figure 1.1 General structural formulae for Schiff bases studied in this research; n = 8, 10

This work was based on the findings by Ti that similar the Schiff base (**Figure 1.1**; *n* = 9) reacted with M(II) acetates (M = Zn, Cu, Ni and Co) [1] to form a dinuclear acetate complex for Cu(II), but mononuclear acetate complexes for the other metal(II) ions [1]. Also, literature reports of complexes formed for similar Schiff bases but with shorter alkyl chains (*n* less than 9) [2] were quite different from Ti (the acetate ion was not coordinated to the metal ion in the products). Hence, it was of interest to know the important factor(s) for the differences reported. In this work, the hexadecanoato ligand was chosen in order to induce mesomorphic properties to these complexes.

A total of three Schiff bases and sixteen complexes were prepared, using two methods, namely step-wise and one-pot method. The materials were characterized by elemental analyses, Fourier transform infrared (FTIR) spectroscopy, ^{1}H-nuclear magnetic resonance (NMR) spectroscopy (for Schiff bases), UV-vis spectroscopy, thermogravimetry (TGA), differential scanning calorimetry (DSC), room-temperature magnetic susceptibility (Guoy method) and optical polarizing microscopy (OPM). Selected complexes were further studied using variable-temperature magnetic

susceptibily using supeconducting quantum interference device (SQUID) magnetometer at the Joint Research Centre, Kinki University, Higashi-osaka, Osaka, Japan under the supervision of Prof. Dr. Takayoshi Kuroda-Sowa, during a three-month research attachment (1st September 2012 – 31st December 2012).

This thesis contains five chapters. **Chapter 1** is the introduction of the thesis. **Chapter 2** presents the theory and literature reviews related to Schiff bases and metal(II) complexes studied (structural, spectroscopic, magnetic, thermal and mesogenic). **Chapter 3** contains the experimental procedures for the synthesis of these materials and the analytical techniques employed. **Chapter 4** presents the results and discussion, and **Chapter 5** the conclusions and suggestions for future work. A list of references is included at the end of each chapter.

Some of the findings of this research were presented in one national and one international conferences either as oral or poster (**Appendices 1-X**), and published in one ISI international journal.

References

[1] Ti, T.J., *Synthesis and Characterization of Zn(II), Cu(II), Ni(II) and Co(II) Complexes as Molecular Spintronic Materials*, Msc Thesis, 2011, University of Malaya, Malaysia.

[2] Nathan, L.C., Koehne, J.E., Gilmore, Joshua M., Hannibal, Kelly A., Dewhirst, William E., and Mai, Tuyetha D. *Polyhedron*, 2003. **22**(6): p. 887-894.

CHAPTER 2 THEORY AND LITERATURE REVIEW

2.1 Introduction

The main objective for this research was to synthesize and characterize magnetic complexes formed from the reaction of hexadecanoates of Cu(II), Ni(II), Co(II) and Fe(II), with tetradentate Schiff bases formed from the reaction of 2-hydroxybenzaldehyde and diaminoalkanes. These complexes are potential molecular magnetic materials.

The Schiff bases and complexes were analyses by CHN elemental analyses, IR, H-NMR, and UV-vis spectroscopies, magnetic susceptibility at room temperature by the Guoy method, thermogravimetry (TGA), differential scanning calorimetry (DSC), and plane polarized optical microscopy (POM). Low-temperature susceptometry was also performed for selected complexes using a superconducting quantum interference device (SQUID) magnetometer.

Hence, this chapter focused on the concepts and literature reports relevant to this research.

2.2 Schiff Base

A Schiff base is an organic molecule containing the –C=N bond (imine) [1, 2] (**Figure 2.1**).

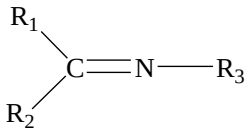

Figure 2.1 General structural formula of a Schiff base; R_1 = H, alkyl or aryl; R_2, R_3 = alkyl or aryl

These compounds are synthesized by the condensation reaction involving primary amines with either aldehydes or ketones. Three examples of such reaction are as follows:

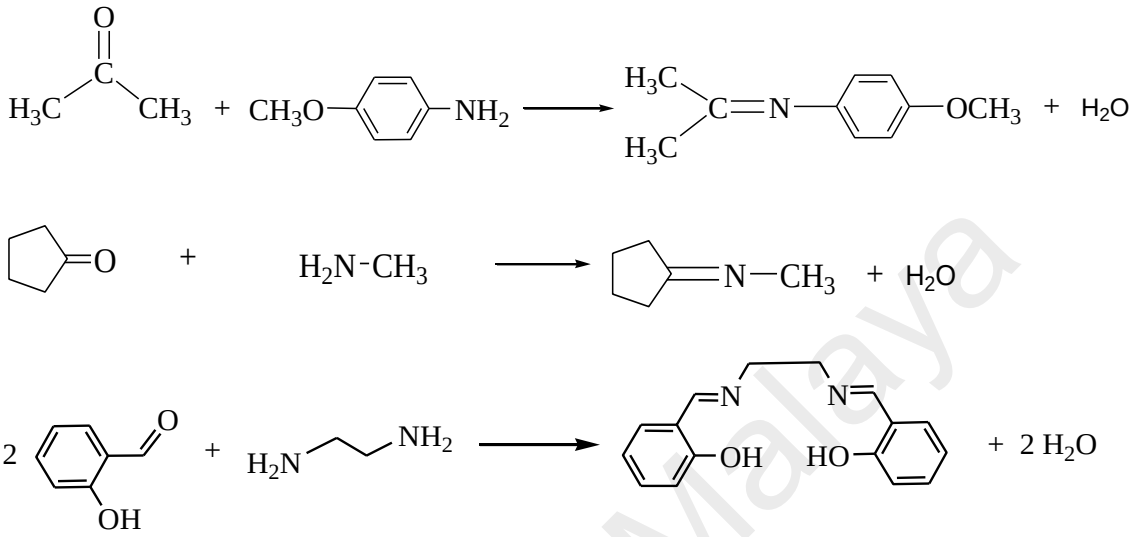

It is known that the hydroxyl group at the benzene ring of a Schiff base can undergo tautomerization, as shown below. However, the equilibrium favours the iminol form, as inferred from the presence of hydroxyl group in both their IR (~ 3500 cm^{-1})and -CH=N in ^{1}H-NMR (normally appears as a singlet at 8.0 – 9.0 ppm [3]).

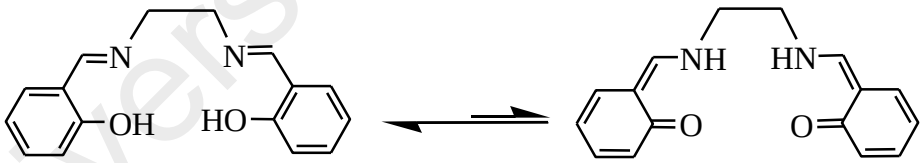

iminol ketoamine

It is also known that in the presence of water, a Schiff base can be hydrolyzed back to the starting amine and carbonyl. This is important especially during characterization involving heat. Since this dissociation occurs at the –C=N bond, alcohols (alcoholysis) also have similar effect on Schiff bases.

Schiff bases and/or their anions can coordinate a metal through the imine nitrogen and phenolic oxygen. These complexes play important roles in the development of coordination chemistry [4], mainly because they can be easily prepared

from a wide selection of readily available aromatic or aliphatic amines and carbonyls (aldehyde or ketone). Accordingly, Schiff bases with tunable physical and chemical properties may be designed. An example is a copper-Schiff base complex, designed and synthesized by Noyori as a catalyst for cyclopropanation of styrene [5].

2.3 Metal Complexes

A metal complex, also known as a coordination complex, is made of a central metal atom or ion surrounded by molecules or ions termed ligand or complexing agent. The term coordination refers to coordinate covalent bonds that exist between the ligands and the central atom [6] - [7].

2.3.1 Metal(II) carboxylates

Metal carboxylates are examples of coordination compounds made up from M^{2+} ion and $RCOO^-$ ion (R = alkyl or aryl). The simplest chemical formula for these compounds is $[M(RCOO)_2]$. First-row transition metal(II) ions have many useful properties, such as variability in geometries, oxidation states, colours, high density of polarizable *d* electrons and magnetism. Hence, these compounds can be used in various applications, such as photonic, magnetic fields and functional molecular material [8].

Various synthetic methods have been reported in the literature for the preparation of these complexes. Examples are methathesis [9], ligand-exchange [10] and one-pot reactions [11]. An example is $[Ni(NH_2CH(CH_3)COO)_2(H_2O)_2].2H_2O$, prepared from nickel(II) chloride in aqueous solution by adding DL-alanine and potassium hydroxide (one-pot reaction).

The structures of these carboxylates may be determined directly using X-ray crystallography (for crystals) or deduced using a combination of instrumental techniques (non-crystalline).

Crystals of most copper(II) carboxylates were found to exist as dimers adopting a structure known as paddle-wheel. Examples are copper(II) acetate dihydrate,

$[Cu_2(CH_3COO)_4(H_2O)_2]$ (**Figure 2.2**) [12] and copper(II) heptanoate, $[Cu_2(CH_3(CH_2)_5COO)_4]$ (**Figure 2.3**) [13].

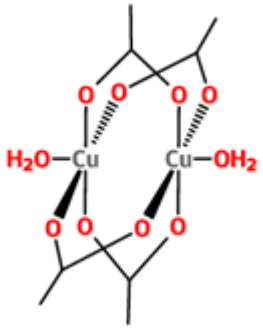

Figure 2.2 Paddle-wheel structure of $[Cu_2(CH_3COO)_4(H_2O)_2]$ [12]

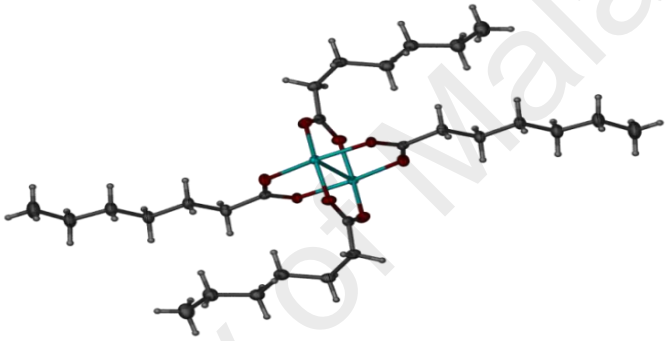

Figure 2.3 Paddle-wheel structure of $[Cu_2(CH_3(CH_2)_5COO)_4]$ [13]

However, copper(II) carboxylates were also found to have other structures, especially in the presence of other ligands. An example is a coordination polymer, $[Cu(ADC)(2,2'\text{-bpy})]_n$(**Figure 2.4**), isolated as crystals from the reaction of aqueous acetylenedicarboxylate ion (ADC) with aqueous copper(II) nitrate in the presence of piperidine. The Cu(II) atom in the crystal structure of this complex was in a square pyramidal coordination [14].

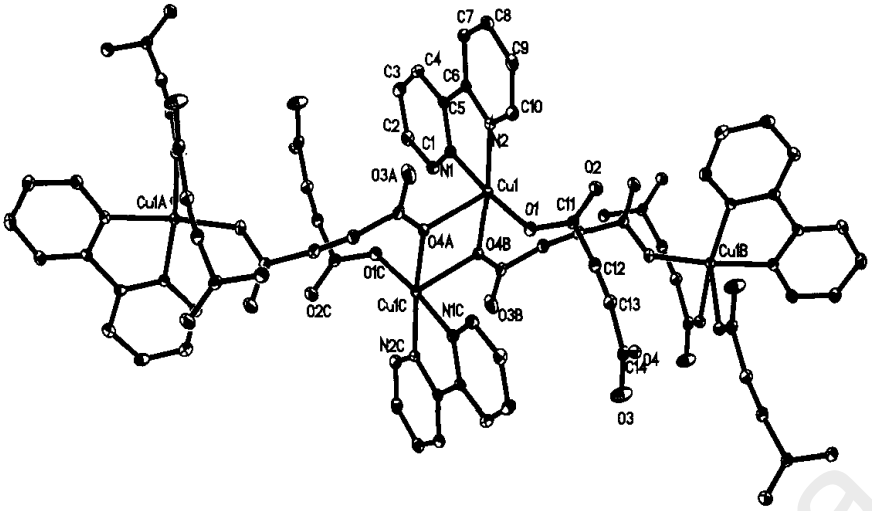

Figure 2.4 Crystal structure of $[Cu(ADC)(2,2'\text{-bpy})]_n$ [14]

Many nickel(II) carboxylates were also found in the paddle-wheel structure. For example, Kounavi obtained a dinuclear complex, $[Ni_2(O_2CPh))_4(L)_2]\cdot 2MeCN$ (L = 1-methyl-4,5-diphenylimidazole), showing this structure (**Figure 2.5**) [15].

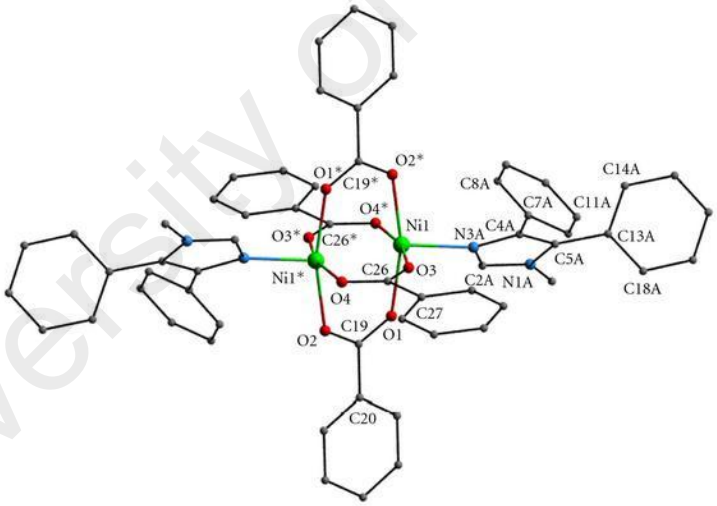

Figure 2.5 Crystal structure of $[Ni_2(O_2CPh))_4(L)_2]\cdot 2MeCN$ [15]

In comparison, cobalt(II) carboxylates normally adopt different structures, mainly because of the strong preference for the metal ion for octahedral geometry. For example, Guan obtained a distorted octahedral complex, $[Co_2(L)_{1.5}(OH)(H_2O)_2]\cdot 2H_2O$ (L = 2,5-dibenzoylterephthalate) (**Figure 2.6**) [16]. In this complex, the carboxylate ligand appeared to be in both chelating and bridging binding modes.

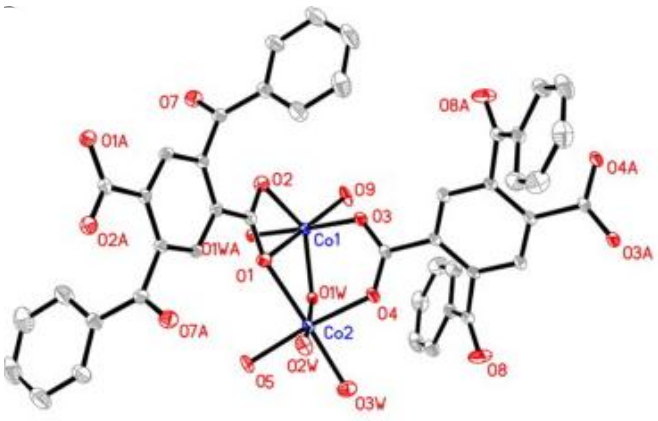

Figure 2.6 Crystal structure of $[Co_2(L)_{1.5}(OH)(H_2O)_2].2H_2O$ [16]

Similarly, iron(II) carboxylates nornally show structures in which the central metal is in an octahedral geometry. An example is a dinuclear Fe(II) carboxylate, $Fe_2[(HL)(H_2O)]$ (L = 4-$O_2CC_6H_4CH_2N(CH_2PO_3H_2)_2$), obtained as single crystals from the reaction of iron(II) sulphate heptahydrate with H_5L and piperazine in water.The structure of this crystal is shown in **Figure 2.7** [17].

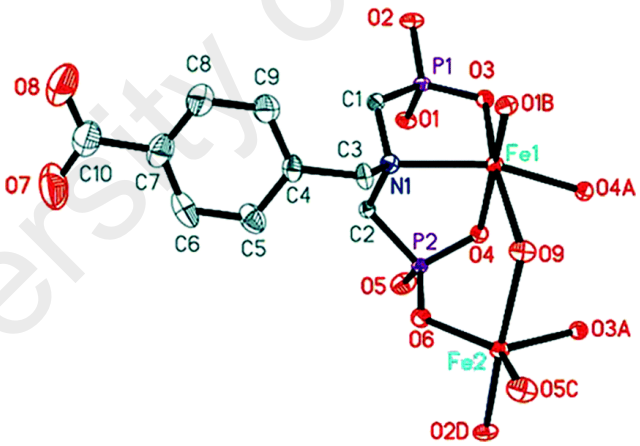

Figure 2.7 Crystal structure of $Fe_2[(HL)(H_2O)]$ [17]

For non-crystalline materials, instrumental methods normally used to deduce their structures are elemental analyses, IR and UV-vis spectroscopies, and magnetic susceptibility.

Elemental analyses give the percentage of elements (mainly C, H and N) in a sample, which can be used to determine its purity and calculate its simplest chemical formula. In these analyses, combustible samples (powders or liquids) are fully

combusted in oxygen so that all of its carbon atoms form carbon dioxide, all hydrogen atoms form water, and all nitrogen atoms form nitrogen oxides.

Fourier transform infrared spectroscopy (FTIR) is normally used to qualitatively identify functional groups and covalent bonds in compounds. The samples may be solid, liquid or gas. There are several methods for sample preparation: (a) a solid sample is grind together with KBr to a homogeneous consistency, and then pressed into a transparent disc;(b) a solid sample may be dissolved in volatile IR-transparent solvents, such as ethanol, and the solution placed onto a polished NaCl plate; (c) a liquid sample is normally analysed neat (no solvent), sandwiched between two NaCl plates; and (d) a gaseous sample is introduced into a special compartment (Teflon gas cell) connected directly to a gas line. IR spectroscopy can used to detect the binding mode of the carboxylate ion ($RCOO^-$) to the metal ion. The carboxylate ion has many ways to coordinate with the metal centre. It can attach as monodentate, bidentate, bridging or chelating. The COO group normally gives a very strong peak in the region of 1650 -1720 cm^{-1}. If hydrogen bonding from R-COOH is present, a broad peak is expected to appear in the region of 3000 – 2500 cm^{-1}. From many IR data of metal carboxylates collected by Deacon [18], it was found there is a good correlation between the difference in the wavenumbers for the asymmetric ($\bar{\upsilon}_{asym}$) and symmetric ($\bar{\upsilon}_{sym}$) stretching vibrations of COO of the carboxylate group ($\Delta = \bar{\upsilon}_{asym} - \bar{\upsilon}_{sym}$) and the binding mode of the ligand (**Table 2.1**).

Table 2.1 FTIR data (in cm^{-1}) for asymmetric ($\bar{\upsilon}_{asym}$) and symmetric ($\bar{\upsilon}_{sym}$) stretching vibrations of COO for selected metal carboxylates

Complexes	$\bar{\upsilon}_{asym}$**COO**	$\bar{\upsilon}_{sym}$**COO**	**Δ**	**Binding mode**
$Cu_2(OOCCH_3)_4(H_2O)_2$	1610	1410	200	bridging
$Ni(OOCCH_3)_2(H_2O)_4$	1550	1425	125	monodentate
$Cu(OOCCH_3)_4(Ph_3P)_2$	1552	1421	131	chelating

For example, Czakis reported that the FTIR spectrum of $Ni(4\text{-bpy})_2(CCl_3COO)_2{\cdot}2H_2O$ showed strong peaks for $\bar{\upsilon}_{asym}COO$ at 1693 cm^{-1} and $\bar{\upsilon}_{sym}COO$ at 1537 cm^{-1}, indicating bridging CCl_3COO[19].

UV-vis spectroscopymay be used to revealthe geometry of the central transition metal ion of the complex. In this spectroscopy, a complex is radiated in the region of 200 nm to 1000 nm, and functional groups within the molecules will absorb the energy to cause electronic transition from the ground state to the excited state. In transition metal complex, the focus is on the *d-d* transition band in the spectrum. A Cu(II) complex can be deduced to be either square planar, tetrahedral or octahedral if the value of λ_{max} for the *d-d* transition is found at about 500-600 nm, 700 nm, or 800 nm, respectively[20].

The electronic structure of the complex can be explained using crystal field theory. An octahedral metal complex will have ligand(s) coordinated at six different sites. In this geometry, the five *d* orbitals split into two energy levels, namely the triply degenerate t_{2g} orbitals (d_{xy}, d_{xz} and d_{yz}) of lower energy, and the doubly degenerate e_g orbitals ($d_z^2$and $d_{x^2-y^2}$) of higher energy. The splitting between the two set of orbitals is known as Δ_o (or 10 D_q) [21].An electronic transition between these levels involves absorption of photonic energy, which appears as a broad band in the visible region. For example, the UV-vis spectrum of $[Co(4\text{-bpy})(CCl_2HCOO)_2].1.5H_2O$ showed a broad band at 476 nm, assigned as $^4T_{1g}(F) \rightarrow {}^4T_{1g}(P)$ electronic transition [22].

The thermal stability of a complex may be measured by thermogravimetric analysis (**TGA**). The principle behind this analysis is to measure the mass loss as a function of temperature or time under an inert atmosphere (N_2). A sample is heated from room temperature up to 1000 °C. For example, TGA traces of $[M(4,4'\text{-bpy})_2(CCl_2HCOO)_2].2H_2O$ (M = Ni(I) and Zn(II)) and $[M(4,4'\text{-bpy})_2(HCOO)_2].2H_2O$ (M = Cu(II) and Co(II)) showed the dehydration

temperature of 65 °C for Ni(II), 60 °C for Zn(II), 100 °C for Cu(II), and 85 °C for Co(II) prior to the decomposition of the carboxylate ligand at 150 °C for Ni(II), 100 °C for Zn(II), 130 °C for Cu(II), and 115 °C for Co(II)[19, 22].

Metal carboxylates with long alkyl chains ($C_nH_{2n+1}COO$) were reported to have low-melting temperatures and may exhibit mesomorphisms (n > 6). Hence, these complexes are known as metallomesogens (metal-containing liquid crystal)[23-25]. Liquid crystal is matter in a phase intermediate between a solid phase and a liquid phase. Thus, it has both the properties of a solid and a liquid, such as ordered structure and fluidity.

There are two main types of liquid crystals: (a) thermotropic, where thephase transition between solid, liquid crystal and liquid is affected by heat; and (b) lyotropic, where the transition is affected by solvents. Terms normally used for liquid crystals are mesomorphism (liquid crystalline behavior), isotropic state (liquid state of liquid crystals), melting temperature (crystal-to-liquid crystal phase), mesophase (intermediate phase between solid and liquid) and clearing temperature (mesophase-to-isotropic liquid).

Different liquid crystals show different mesophases, depending on the structure of its molecules. Examples are nematic, smectic, calamitic (rod-like) and columnar (discotic or disc-like) (**Figure 2.8**) [24]. These mesophases may be shown by polarizing optical microscopy (POM), which is based on the concept that one of the characteristic of liquid crystal is birefringence. Optical textures are normally viewed upon cooling from the isotropic liquid state.

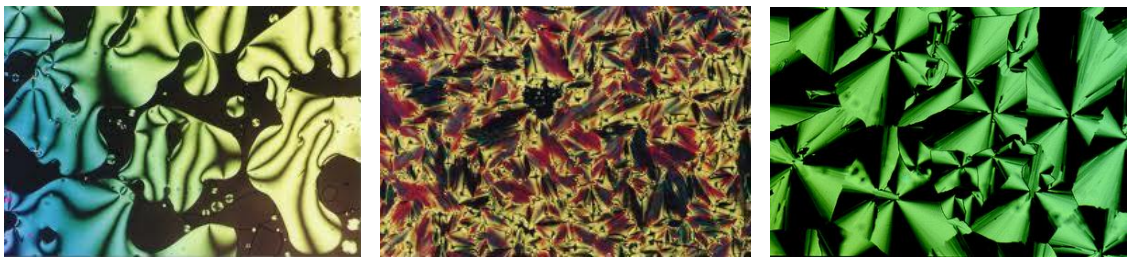

(a) (b) (c)

Figure 2.8 Photomicrographs of different mesophases captured by OPM: (a) nematic; (b) smectic; and (c) columnar

Transition metal ions can induce mesomorphism in non-mesogenic ligands. The molecular packing in the formation of the mesophase is greatly influenced by the coordination geometry of the metal centre. The objective in coordination compounds is to avoid intermolecular contacts and strong dipolar interactions that are strong enough to cause three-dimensional order. The addition of a long aliphatic chain to the rigid nucleus furnishes both the anisotropy and irregular packing needed to induce mesomorphism.

Differential scanning calorimetry (DSC) may be used to measure the enthalpy change (ΔH) and transition temperatures for solid and liquid crystals. The instrument consists of two pans, one for the sample while the other for the reference. The scan may be recorded as the sample is heated to below its decomposition temperature under N_2, and/or cooled. The ΔH value for crystal-to-mesophase transition is normally about 30 – 50 kJ mol^{-1}, and less than 1 kJ $mol^{-1}$for mesophase-to-mesophase transition. The value for mesophase-to-isotropic liquid transition is about 1 - 5kJ mol^{-1} [4]. For example, the peaks found for $[Rh_2(3,4\text{-}B_2OC_9H_{19})_4]$ (B = benzoate) have ΔH values of 1 kJ mol^{-1} for *Cr*-to-*Cr* transition, 19 kJ $mol^{-1}$for *Cr*-to-Col_htransition, and 4 kJ $mol^{-1}$$Col_h$-to-*I* transition[26].

2.3.2 Metal(II)-Schiff base complexes

Metal(II) complexes of Schiff bases were mainly designed for selected applications, such as biological, photochemical, and magnetic, and as metallomesogens. For magnetic applications, multinuclear complexes are favorable as these have a higher number of unpaired electrons.

(a) Structural studies

Many Schiff base complexes of Cu(II) were dinuclear [27-29]. Examples are: $[Cu_2(L)(NO_3)_3(H_2O)]$ (L = N′-(di(pyridin-2-yl)methylene)-5-methyl-1-(pyridin-2-yl)-1H-pyrazole-3-carbohydrazide), $[Cu_2(L^1)_2(NCNCN)_2]$ (L^1 = 2-[1-(2-dimethylamino-ethylamino)-ethyl]-phenol), and $[Cu^{II}L^1(\mu_{1,1}\text{-}N_3)]$ (L^1 = (E)-2-(4-aminobut-1-enyl)-6-ethoxyphenol). The structures of some of these dinuclear copper(II) complexes were deduced from their crystal structures. For example, the crystal structure of $[Cu^{II}L^1(\mu_{1,1}\text{-}N_3)]$ (L^1 = (E)-2-(4-aminobut-1-enyl)-6-ethoxyphenol)is shown in **Figure 2.9** [30]. For this complex, the copper is pentacoordinated to the phenolate oxygen and imine nitrogen, with the nitrogen of the azide ligand acting as a bridge between the two copper centers. The geometry at copper was distorted square pyramidal.

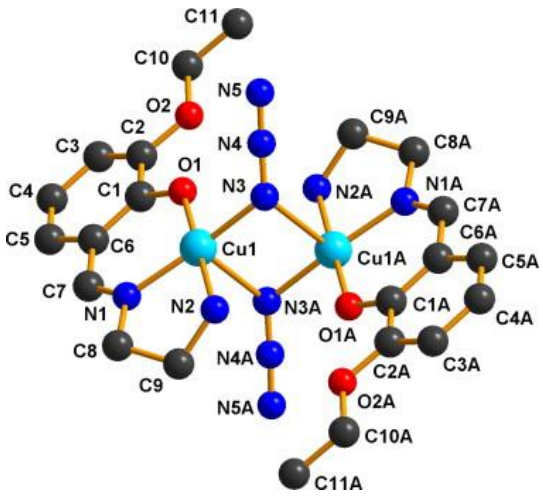

Figure 2.9 Molecular structure of $[Cu^{II}L^1(\mu_{1,1}\text{-}N_3)]$ crystals [30]

Another example is $[Cu_2(L)(NO_3)_3(H_2O)]$ (L = N′-(di(pyridin-2-yl)methylene)-5-methyl-1-(pyridin-2-yl)-1H-pyrazole-3-carbohydrazide), shown in **Figure 2.10** [28]. In this complex, both Cu(II) atoms are in a distorted tetrahedral geometry.

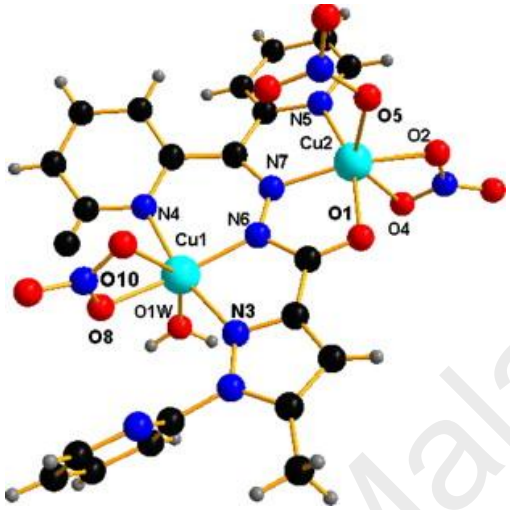

Figure 2.10 Molecular structure of $[Cu_2(L)(NO_3)_3(H_2O)]$ crystals [28]

An example of Cu(II) complex that self-assembled in solution to form a dimeric complex is reported by Akbar Ali[Cu(NNNS)X] (X = Cl^-, NO_3^-, H_2O;NNS = anionic forms of di-2-pyridyl ketone-4-N-methyl- and di-2-pyridyl ketone 4,4,-N dimethylthiosemicarbazone)(**Figure 2.11**) [29].

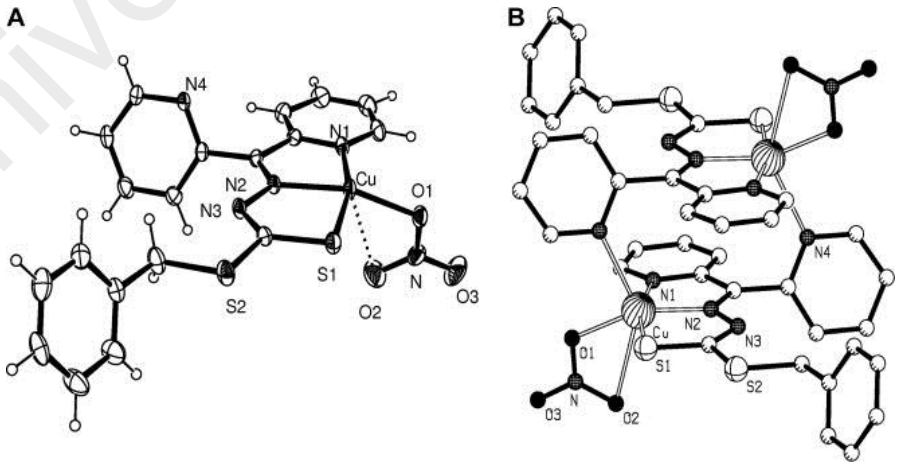

Figure 2.11 Monomeric and dimeric structures of$[Cu(NNNS)X]_2$ (X = NO_3^-) [29]

Schiff bases of Ni(II) also formed dinuclear complexes. Two examples are provided by Biswas, who obtained $[Ni_2L_2(o\text{-}(NO_2)C_6H_4COO)_2(H_2O)]$ and

$[Ni_2L_2(p\text{-}(NO_2)C_6H_4COO)_2(H_2O)]\cdot 0.5CH_3OH$ (L = 1-[(3-dimethylamino-propylimino)-methyl]-naphthalen-2-ol) [31]. Both complexes have almost similar structures (they differ in the position of the nitro group: *para* or *ortho*).

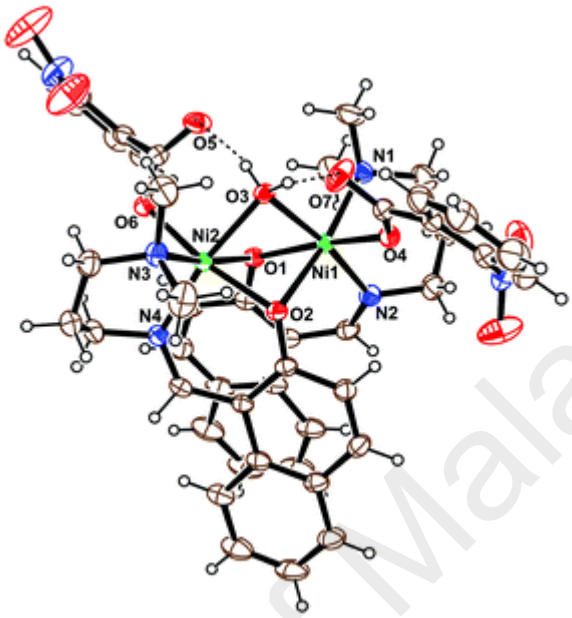

Figure 2.12 Molecular structure of $[Ni_2L_2(o\text{-}(NO_2)C_6H_4COO)_2(H_2O)]$ crystals [31]

However, many cobalt(II) were partially or fully oxidised in air to cobalt(III) during synthesis. An example is an octahedral mixed-valence $Co^{II}Co^{III}$ complex, $[Co_2(HL^1)_2(H_2O)_2](NO_3)$($H_3L^1$ = 2-ethyl-2-(2-hydroxybenzylideneamino)propane-1,3-diol)[32].In this complex, the Schiff base bridging both cobalt centres was incompletely deprotonated.

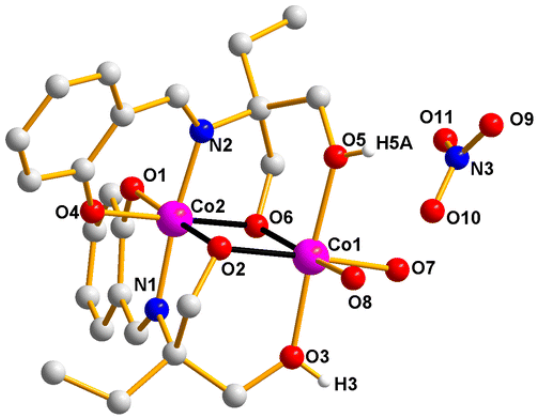

Figure 2.13 Molecular structure of mixed-valence $[Co_2(HL^1)_2(H_2O)_2](NO_3)$ [32]

Nowak reported that monomeric [FeL1(MeOH)$_2$] (L1 = (*E*,*E*)-{dimethyl-2,2′-[1,2-phenylenebis(iminomethylidyne)]bis(3-oxobutanato)(2–)-*N*,*N*′,O^3,O^3′}) formed an octahedral coordination polymer by substituting methanol with neutral axial ligand, such as 4,4'-bipyridine (**Figure 2.14**) [33].

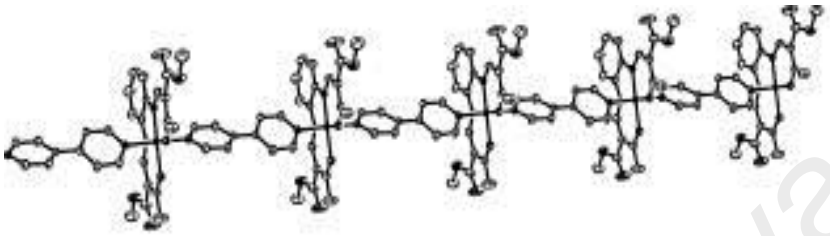

Figure 2.14 An Fe(II) cordination polymer, {[Fe(L1)(4,4'-bipyridine)]$_n$ [33]

A facile analytical technique to ensure the formation of complexes of Schiff bases is IR spectroscopy. For these complexes, the most important functional group is C=N (imine), which normally appears as a strong peak at 1600 – 1650 cm^{-1}[34]. This is lower than the corresponding Schiff bases, indicating coordination of the metal ion to the imino N atom. Additionally, a peak for the M-O bond usually appears at about 400 cm^{-1}, while the M-N bond appears at about 500 cm^{-1}. For example, the ν*C*=N stretching absorption appeared at 1617 cm^{-1}for *fac*-*Λ*-[Fe(*R*-L)$_3$](BF$_4$)$_2$·MeCN (*R*-L = 1-phenyl-N-(1-methyl-imidazol-2-ylmethylene)ethanamine]) [35], and at 1622 cm^{-1} for[Ni$_2$L$_2$(*o*-(NO$_2$)C$_6$H$_4$COO)$_2$(H$_2$O)] (L = 1-[(3-dimethylamino-propylimino)-methyl]-naphthalen-2-ol) [31].

UV-vis spectroscopy is similarly used to determine the geometry of the metal - Schiff base complexes. For example, the UV-vis spectrum for [Cu$_2$(L)(NO$_3$)$_3$(H$_2$O)] showed a *d-d* peak at 697 nm, indicating distorted octahedral geometry [28]. Tomczyk reported spectroscopic properties of Ni(II) complexes with (±)-*trans*-*N,N*′-bis(salicylidene)-1,2-cyclohexanediaminesubstituted with different substituent (Figure 2.15) [36]. All spectra showed bands at 546-576 nm, indicating distorted square coordination geometry around Ni(II).

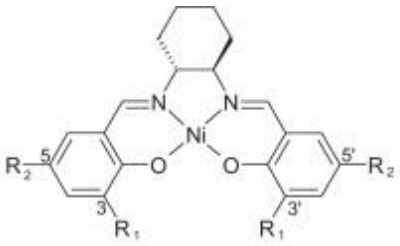

R_1 = H	R_2 = H	[Ni(salcn)]
R_1 = *t*-Bu	R_2 = H	[Ni(salcn(Bu))]
R_1 = *t*-Bu	R_2 = *t*-Bu	[Ni(salcn(2Bu))]
R_1 = *t*-Bu	R_2 = OMe	[Ni(salcn(BuOMe))]

Figure 2.15 Structural formula of Ni(II) complexes of differently substituted Schiff bases

Anacona reported that the UV-vis spectrum of [Co(L)Cl(H_2O)] (L = derived from cephaclor antibiotic and 1,2-diaminobenzene) [37]showed two bands at 425 nm and 460 nm for metal–ligand charge and $^4T_{1g}(F) \rightarrow {}^4T_{2g}(F)$ transition respectively, suggesting an octahedral geometry for the Co(II) ion. However, the electronic spectrum of [Co(salen)(OTf)] (**Figure 2.16**) showed low energy NIR absorptions [2]. Since Co(salen)(OTf) complexes contains both Co^{III}(salen)(OTf) and $Co^{II}(salen^{\bullet+})$(OTf) character, it was inferred that there were four possible origins for the NIR absorptions: a ligand-to-metal charge transfer in Co^{III}(salen)(OTf), a metal-to-ligand charge transfer in $Co^{II}(salen^{\bullet+})$(OTf), a ligand-to-ligand charge transfer in $Co^{II}(salen^{\bullet+})$(OTf), and an intraligand π-to-π* transition of a phenoxyl radical.

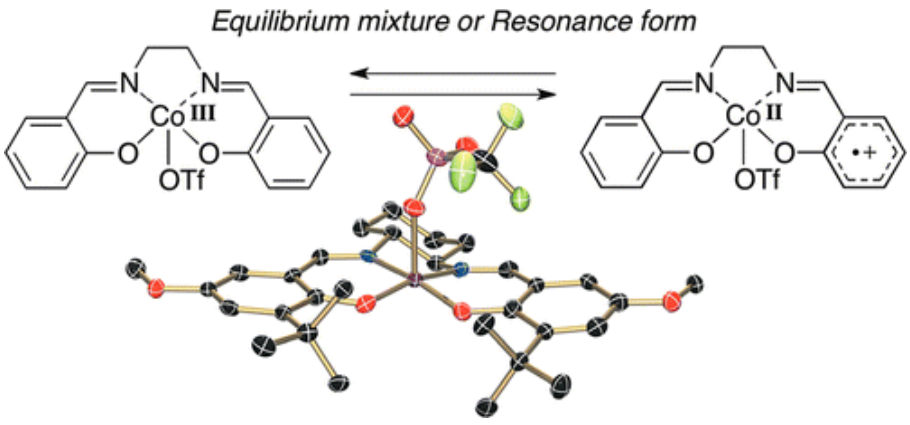

Figure 2.16 Equilibrium for Co(L-OMe)(OTf) [2]

(b) Magnetic properties

First-row transition metal ions, such as Cu(II) ($3d^9$), Ni(II) ($3d^8$), Co(II) ($3d^7$), and Fe(II) ($3d^6$) ions, normally form magnetic complexes with Schiff bases. Magnetic materials have found important applications, such as data storage devices, sensors, switches, motors, medical devices and generators.

There are many types of magnetisms, namely diamagnetism, paramagnetism, ferromagnetism, antiferromagnetism and ferrimagnetism. Diamagnetism is due to the interaction of the magnetic field with the motion of the electrons in their orbits. A diamagnetic materials has a magnetic field opposite of the applied magnetic field, thus being repelled. All materials contain diamagnetic component even though the materials exhibit paramagnetism. Diamagnetism is not affected by temperature, and the strength of interaction is proportional to the molecular weight of a material.

Paramagnetism is a form of magnetism that occurs only in the presence of an externally applied magnetic field [21]. It can be characterized by the attraction of a material into the applied magnetic field. Paramagnetic materials will lose any magnetization once the applied field is removed. Usually paramagnetic materials will have at least one unpaired electron and the interaction varies according to temperature. There is also some materials that exhibit temperature-independent paramagnetism (TIP). This can happened when the magnetic ground state can couple with excited states through the Zeeman perturbation, given that the energy gaps are small. The values are normally really small and comparable to the diamagnetism but of opposite sign. TIP is applicable to both diamagnetic and magnetic compounds. Magnetic ground state coupled with nonthermally populated excited states give rise to a weak temperature-independent contribution.

Ferromagnetism is an occurrence whereby a material form a permanent magnet or attracted to a magnet even after the external applied field is removed. It can be

characterized by molecular spins that are oriented in a parallel fashion, also known as the long range ordering. It is the strongest type of magnetism and sometimes the force is strong enough to be felt. This long range order can disappear at above certain temperature, known as the Curie temperature.

Antiferomagnetism is the opposite of ferromagnetism. It usually occurs at very low temperature (up to absolute zero). The spins of two adjacent molecular spins are antiparallel. This antiparallel coupling will disappear above certain temperature that is known as Néel temperature, which is different for different material. At very low temperature, the material will not respond to any externally applied field due to the antiparallel coupling rigidity. Upon heating some of the atoms break free and start to align with the applied field. This process continues until the Néel temperature is achieved.

Ferrimagnetism is somewhat similar to antiferromagnetism whereby two adjacent molecular spins are antiparallel. The difference is that in ferrimagnetism, these two adjacent spin has different magnitude of magnetic moment thus resulting in a non-zero net magnetic moment even in the absence of applied field.

Magnetic susceptibility (χ) is a quantitative measure of the extent to which a material may be magnetized in relation to a given applied magnetic field. χ is equal to the ratio of magnetization, *M* within the applied magnetic field, *H*.

$$\chi = \frac{M}{H} \qquad \text{(Equation 2.1)}$$

Based on Curie law, molar magnetic susceptibility (χ_m) can be obtained from Equation 2.2, where *N* is Avogadro's number, g is the gyromagnetic factor of free electron, β is Bohr magneton, *k* is the Boltzmann constant and *S* is the spin quantum number.

$$\chi = \frac{Ng^2\beta^2}{3kT} S(S+1) \qquad \text{(Equation 2.2)}$$

The above equation serve as the basis for other derivation as different molecular structure requires different modification to the calculation. A measurement of magnetic susceptibility can be done either using the Guoy balance at room temperature or superconducting quantum interference device (SQUID) magnetometer, which is more accurate and has a wide temperature range.

An example of $\chi_M T$ versus T plots obtained by SQUID for a dinuclear Cu(II) complexes, $[Cu^{II}L(\mu_{1,1}\text{-}N_3)]$ (L = (E)-2-(4-aminobut-1-enyl)-6-ethoxyphenol) is shown in **Figure 2.17** [30]. At 300K, the complex shows a maximum value of 0.89 $cm^3\,mol^{-1}K$, which was higher than expected for two uncoupled S = ½ (0.75 $cm^3\,mol^{-1}\,K$ (g = 2.00). From the fitted curve based on the Bleaney-Bowers equation (**Equation 2.3**), the J value obtained was $-10.16\ cm^{-1}$. Thus the copper complex was said to have a weak antiferromagnetic interaction.

$$\chi_M = \frac{N\beta^2 g^2}{kT}\frac{2e^{J/kT}}{1+3e^{J/kT}}(1-\rho)+\frac{N\beta^2 g^2 \rho}{4kT}+\mathrm{TIP} \qquad \text{(Equation 2.3)}$$

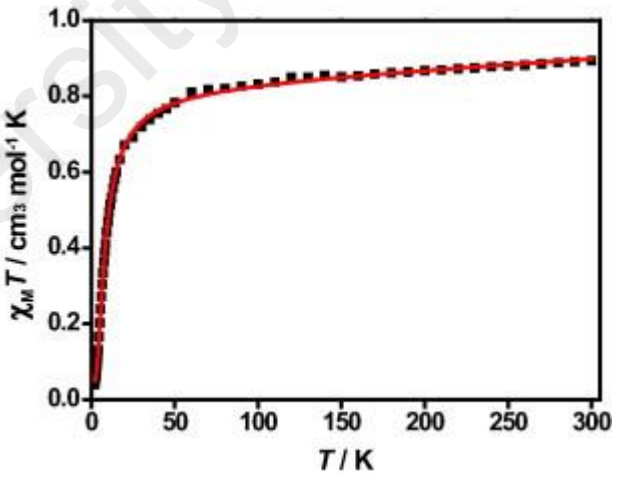

Figure 2.17 $\chi_M T$ versus T of $[Cu^{II}L^1(\mu_{1,1}\text{-}N_3)]$ [31]

Similarly, Biswas found that $[Cu_2(L)(NO_3)_3(H_2O)]$ (**Figure 2.10**) gave $\chi_m T$ value of 0.60 $cm^3\,mol^{-1}$ K at room temperature, which is lower than the expected value, and decreased to zero upon cooling [29]. The shape of the curve indicates a strong antiferromagnetic coupling. The best-fit parameters gave the values of

$J = -184.3$ cm^{-1} and $g = 2.07$. Based on literature data, the exchange coupling in dinuclear complexes with Cu_2O_2 core depends on several factors, namely the Cu–O(R)–Cu angle, the Cu–O distance and geometrical distortions. Nevertheless, several compounds have been found to deviate from this linear relationship. The reasons for these deviations are mainly the geometrical distortions, such as the variations in Cu–O bond distances and/or the distortion of the square pyramidal geometry towards trigonal bipyramidal.

A dimeric state Cu(II) complex attached to a pentadentate Schiff base, $[Cu_2(L^1)_2(NCNCN)_2]$ (HL^1 = 2-[1-(2-dimethylamino-ethylamino)-ethyl]-phenol) was reported to have the effective magnetic moment (μ_{eff}) of 1.7 B.M. at 300 K, and 0.3 B.M. at 18 K. The $\chi_M T$ vs. T plot (**Figure 2.18)** indicates spin-spin coupling in the asymmetrically dibridged dicopper(II) core [38].The geometry of each copper was square planar (**Figure 2.18**).

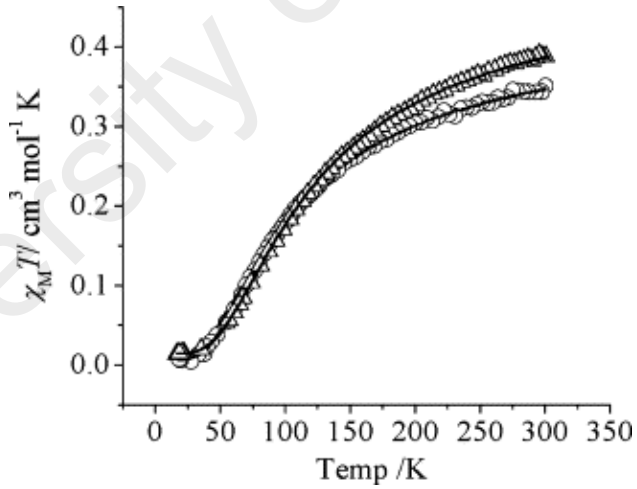

Figure 2.18 $\chi_M T$ versus Tplots for $[Cu_2(L^1)_2(NCNCN)_2]$ [38]

Magnetic interaction was also reported for multinuclear nickel(II) complexes. For example, the magnetic susceptibility data for $[Ni_2L_2(o\text{-}(NO_2)C_6H_4COO)_2(H_2O)]$ (L = 1-[(3-dimethylamino-propylimino)-methyl]-naphthalen-2-ol)) showed intradimer ferromagnetic interaction and interdimer antiferromagnetic interaction [31]. The $\chi_M T$ value at 300 K was 2.78 cm^3 mol^{-1} K, which was higher than the expected

value of two non-interacting Ni(II)S = 1 spin centers (1.0 cm^3 mol^{-1} K). Upon cooling, the $\chi_M T$ values correspond well with an S = 2 ground state resulting from the occurrence of ferromagnetic coupling between the two S = 1 centers. The results also gave the values of J = 25.4 cm^{-1} and g = 2.27 for this complex.

Magnetic data can also give information on the geometry and oxidation state of metal ion in a complex [2]. For example, the magnetic moment value (μ) for [Co^{II}(L-OMe)] (L = derived from cephaclor antibiotic and 1,2-diaminobenzene) was about 2.1 B.M. in the temperature range 20–320 K. This was consistent with square-planar Co(II) (d^7; S = ½; μ = 2.828 B.M.). In contrast, the μ value for [Co(L-OMe)](OTf) was about 3.0 B.M. in the temperature range 50–320 K. This was in agreement with the spin-only value of 2.828 B.M. for Co(III) (d^6; S = 1) or may be the result of coupling between the ligand radical (S = $^1/_2$) and Co(II), since the value of J was −4.5 cm^{-1} (very weak antiferromagnetic coupling) at temperatures lower than 50 K.

Magnetic measurements at different temperatures are essential in the study of spin crossover (SCO) behavior of octahedral complexes involving metal ions with d^4-d^7ground state valence electronic configurations and ligands of intermediate field strength (normally N-donors). In these complexes, the metal ions may change from low spin (LS) to high spin (HS) in respond to external perturbation, such as heat. Hence, these complexes are potential functional materials in sensors and memory devices[39]. For example, the χ_MT vs T plot for an iron(II) complex (d^6), *fac-Λ*-[Fe(*R*-L)$_3$](BF$_4$)$_2$·MeCN *R*-L = 1-phenyl-N-(1-methyl-imidazol-2-ylmethylene)ethanamine]), (**Figure 2.19**) shows thermal SCO behavior from LS to HS with wide hysteresis loop near room temperature [35].

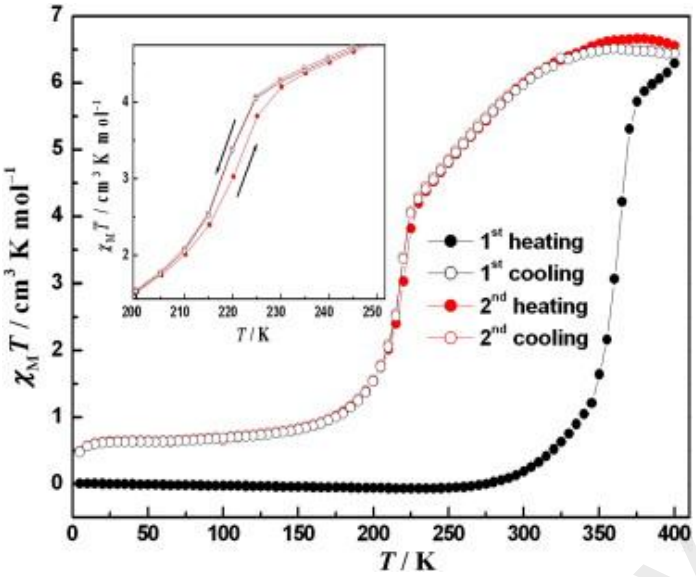

Figure 2.19 Plots ofχ_MT vs T of *fac-Λ*-[Fe(*R*-L)$_3$](BF$_4$)$_2$·MeCN [35]

Dinuclear iron(II) complexes normally show gradual and incomplete SCO behavior. For example, the χ_MT value for three complexes, namely [Fe{(phen)$_2$}$_2$(**4**)]4BPh$_4$ (phen = 1,10-phenanthroline) (**4** = (2,5-dibromo-N,N-bis(pyridine-2-ylmethylene)benzene-1,4-diamine) (*11*), [Fe{(phen)$_2$}$_2$(**10**)]4X (**10** = 2,5-Di-(2-thienyl)-N,N-bis(pyridine-2-ylmethylene)benzene-1,4-diamine) (X = BPh$_4$ (*12*) or PF$_6$ (*13*)) [40], was less than the anticipated value for two HS iron(II) ions (6.0 cm^3 K mol^{-1}, assuming g = 2).Complex [Fe{(phen)$_2$}$_2$(**4**)]4BPh$_4$ was said to have incomplete spin-crossover as even at 5 K, the χ_MT is 1.2 cm^3 K mol^{-1} (**Figure 2.20**).

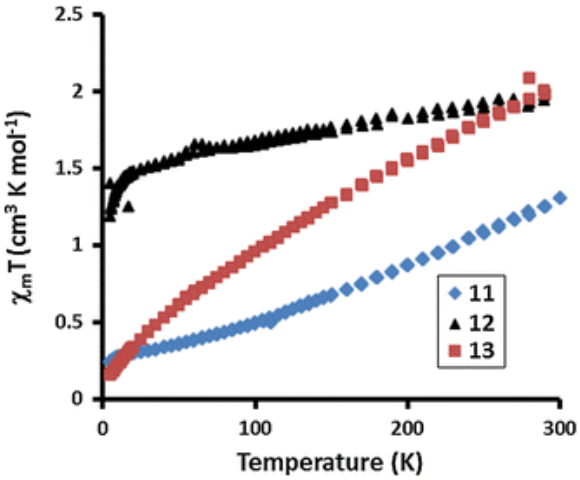

Figure 2.20 Plots of $\chi_M T$ vs T for dinuclear Fe(II) complexes, *11* = [{Fe(phen)$_2$}$_2$(**4**)]4BPh$_4$; *12* = [{Fe(phen)$_2$}$_2$(**10**)]4BPh$_4$; *13* = [{Fe(phen)$_2$}$_2$(**10**)]4PF$_6$

Magnetic properties can be harnessed for the application of spintronics (or spin transport electronics), which involves the study of active control and manipulation of spin degrees of freedom in solid-state systems. The advantages of incorporating the spin degree of freedom to current semiconductor devices are speed increased for data processing, decreased power usage, smaller size and possibility of quantum computing [41, 42].William Thomson first discovered magnetoresistance phenomenon in 1851 [43]. This was later called as anisotropic magnetoresistance (AMR) originated from the larger probability for *s-d* scattering of electrons in the direction of the magnetic field.

The prototype device that is already in use in industry as a read head and a memory-storage cell is the giant-magnetoresistive (GMR) sandwich structure discovered in 1988 [44-46]. This consists of alternating ferromagnetic and nonmagnetic metal layers. Device resistance varies from small (parallel magnetizations) to large (antiparallel magnetizations) according to the relative orientation of the magnetizations in the magnetic layers. This change in resistance, known as magnetoresistance, can be used to detect changes in magnetic fields. GMR technologies have also involved magnetic tunnel junction devices where the tunneling current depends on spin

orientations of the electrodes. A magnetic tunnel junction (MTJ) is formed by a pinned layer and a free layer separated by a thin insulating layer (normally aluminium oxide) [47].

The current GMR technology can be further enhanced by synthesizing new materials that have larger spin polarization of electrons or making improvements or variations in the existing devices that allow for better spin filtering. Another way is to find novel ways of both generation and utilization of spin-polarized currents.

Tunnel magnetorisstance (TMR) is another example of metal-based spintronic devices that was discovered by M. Jullière. It consist of two ferromagnetics separated by a thin insulator. Based on Jullière model, the spin of electrons is conserved in the tunneling process. Then the tunneling of up- and down-spin electrons are two independent processes, so the conductance occurs in the two independent spin channels. TMR can be used as a form of memory [48]. The read-heads of modern hard disk drives and magnetoresistive random access memory (MRAM) also function on the basis of TMR.

(c) Metallomesomorphisms

Suitably designed metal(II)-Schiff base complexes also exhibited mesomorphisms. Examples are complexes of 5-((4-^{n}alkoxyphenyl)azo)-N-(3-ydroxypropyl)salicylaldimine (n = 8,10,12,14) [49]. All of the ligands were not mesomorphic due to the strong intermolecular hydrogen bonding of the two hydroxyl groups (phenolic and alcoholic OH). However, the copper(II) complexes showed liquid crystalline properties (**Figure 2.21**). Their melting temperatures decreased as the alkyl chain increases, they were thermally stable (decomposition temperature ~ 280 °C).

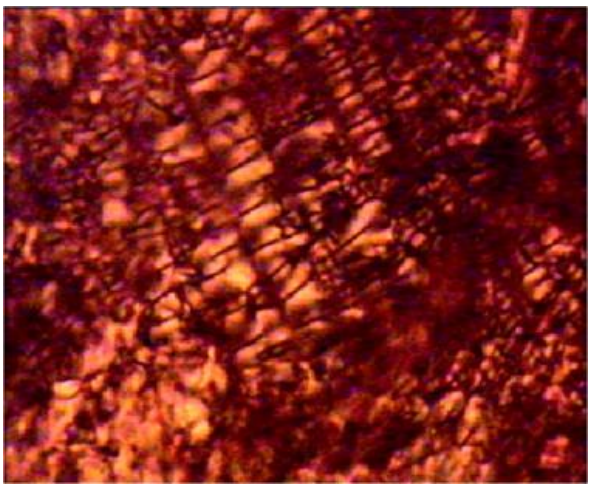

Figure 2.21 SmA mesophase of Cu(II) complex (n = 10)

A Ni(II) complex of *N*,*N*′-bis(4-(4′-*n*-hexadecyloxy)salicylidene)-1,2-phenylenediamine)(Ni-16opd) also exhibited mesomorphisms, even though the ligand was not mesogenic [50]. Upon cooling from the isotropic phase, the complex showed spherulitic growth which coalesced to a fan-like texture at 130 °C with large homeotropic regions, suggesting a columnar mesophase (Col) (**Figure 2.22**).

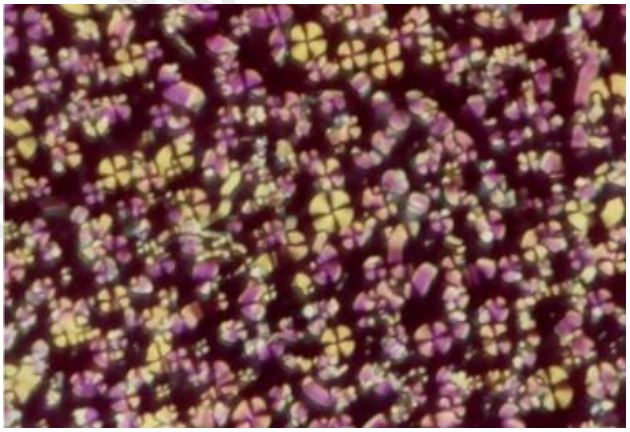

Figure 2.22 Columnar mesophase of Ni-16opd [46]

Another example of mesomorphic Ni(II) complex is Ni-18dch (the ligand was *N*,*N*′-bis[4-(4′-*n*-alkoxy)-salicylidene]-1,2-cyclohexanediamine) [51]. Upon cooling from the isotropic liquid (233 °C), a typical broken fan-shaped texture with several homeotropic regions developed at 227 °C (**Figure 2.23**). Its DSC trace shows an enthalpy at 227 °C (ΔH = 30.1 kJ mol^{-1}) for the I-Col mesophase transition.

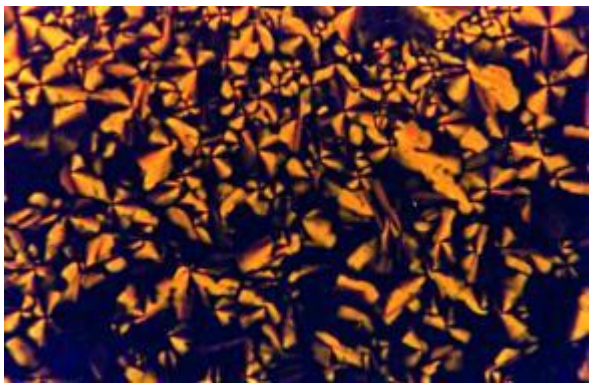

Figure 2.23 Columnar mesophase for Ni-18dch [47]

An example of a mesomorphic iron(II) complex is [Fe(II)n_4] (n_4 = Schiff base obtained from the reaction of 9,9'-diaminobis(tricarbollide)Fe(II) with 4-butoxybenzaldehyde[52]. Its mesophases are shown in **Figure 2.24**.

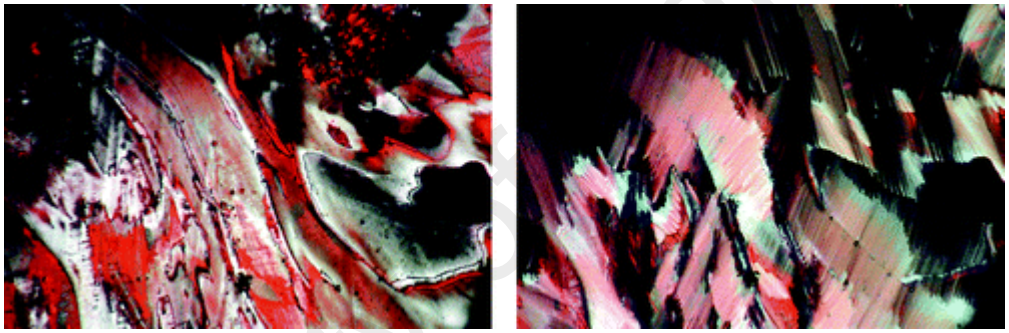

Figure 2.24 Nematic mesophase (left) and SmA mesophase (right) for Fe(II)n_4 [48]

References

[1] Brown, W.H., Poon T., and Wiley, J., *Introduction to Organic Chemistry*. 2005: Wiley Hoboken, NJ.

[2] Kurahashi, T. and Fujii, H., *Inorg. Chem.*, 2013. **52**(7): p. 3908-3919.

[3] Ghaffari, A., Behzad, M., Dutkiewicz, Grzegorz., Kubicki, Maciej., and Salehi, Mehdi, *J. Coord. Chem.*, 2012. **65**(5): p. 840-855.

[4] Yamada, S., *Coord. Chem. Rev.*, 1999. **190**: p. 537-555.

[5] Nozaki, H., Takaya, H., Moriuti, S., and Noyori, R., *Tetrahedron*, 1968. **24**(9): p. 3655-3669.

[6] McNaught, A.D., *Compendium of chemical terminology*. Vol. 1669. 1997: Blackwell Science Oxford.

[7] Cotton, F., Wilkinson, G., and C. Murillo, *Advanced Inorganic Chemistry*, 1999, Wiley, New York.

[8] Chen, S.H., Shi, H., Conger, Brooke M., Mastrangelo, John C., and Tsutsui, Tersuo, *Adv. Materials*, 1996. **8**(12): p. 998-1001.

[9] Zhang, W., Liu, S., Ma, Changqin., and Jiang, Dehua, *Polyhedron*, 1999. **17**(22): p. 3835-3839.

[10] Kögerler, P., Williams, P., Parajon-Costa, BS., Baran, EJ., Lezama, L., Rojo, T., and Müller, Achim, *Inorg. Chimica Acta*, 1998. **268**(2): p. 239-248.

[11] Abdullah, N., and Kamarazaman, Z., *American Institute of Physics Conference Series*. 2009.

[12] Van Niekerk, J., and Schoening, FRL, *Nature*, 1953. **171**: p. 36-37.

[13] Abdullah, N., and Al-Hakem, Y., Abdullah, Nazirah., Samsudin, Habibah., and Tajidi, Nur Syamimi Ahmad, *Asian J. Chem.*, 2014. **26**(4): p. 987-990.

[14] Ming Xing, L., Min, S., Hui, Dai., Bao Li, An., Wen Cong, Lu., Yu, Zhu., and Chen Xia, Du, *Chinese Chem. Lett.*, 2005. **16**(10).

[15] Kounavi, K.A., Manos, M.J., Tasiopoulos, Anastasios J., Perlepes, Spyros P., and Nastopoulos, Vassilios, *Bioinorganic Chem. Apps.*, 2010. **2010**.

[16] Guan, L., Zhou, Y.-H. and H. Zhang, *Inorg. Chem. Comm.*, 2010. **13**(6): p. 737-740.

[17] Zhou, W., Zhu, Y.-Y., Jiao, Cheng-Qi., Sun, Zhen-Gang., Shi, Shao-Ping., Dai, Lu-Lu., Sun, Tong., Li, Wen-Zhu., Ma, Ming-Xue., and Luo, Hui, *Cryst. Eng. Comm.*, 2014. **16**(6): p. 1174-1186.

[18] Deacon, G. and R. Phillips, *Coord. Chem. Rev.*, 1980. **33**(3): p. 227-250.

[19] Czakis-Sulikowska, D., A. Czylkowska, and A. Malinowska, *J. Therm. Anal. Cal.*, 2002. **67**(3): p. 667-678.

[20] Devereux, M., O'Shea, D., O'Connor, Mark., Grehan, Helen., Connor, Gavin., McCann, Malachy., Rosair, Georgina., Lyng, Fiona., Kellett, Andrew., Walsh, Maureen., Egan, Denise., and Thati, Bhumika, *Polyhedron*, 2007. **26**(15): p. 4073-4084.

[21] Atkins, P., *Inorganic Chemistry*. 2010: Oxford University Press.

[22] Czakis-Sulikowska, D. and A. Czylkowska, *J. Therm. Anal. Cal.*, 2003. **71**(2): p. 395-405.

[23] Giroud-Godquin, A.M., *Coord. Chem. Rev.*, 1998. **178**: p. 1485-1499.

[24 Donnio, B. and D.W. Bruce, *Metallomesogens*, in *Liquid Crystals II*. 1999, Springer. p. 193-247.

[25] Date, R.W., Iglesias, E.F., Rowe, Kathryn E., Elliott, James M., and Bruce, Duncan W, *Dalton Transactions*, 2003(10): p. 1914-1931.

[26] Rusjan, M., Donnio, B., Guillon, Daniel, and Cukiernik, Fabio D, *Chem. Mat.*, 2002. **14**(4): p. 1564-1575.

[27] Mondal, S., Chakraborty, P. Aliaga-Alcalde, Núria., and Mohanta, *Polyhedron*, 2013. **63**: p. 96-102.

[28] Jana, A., Konar, S., Mandal, Tarak Nath., Das, Kinsuk., Ray, Sangita., Sarkar, Ananda., Liu, Cai-Ming., and Kar, Susanta Kumar, *Polyhedron*, 2012. **46**(1): p. 105-112.

[29] Biswas, A., Drew, M.G., Ribas, Joan., Diaz, Carmen., and Ghosh, Ashutosh, *Inorg. Chimica Acta*, 2011. **379**(1): p. 28-33.

[30] Mondal, S., Chakraborty, Priyanka, Aliaga-Alcade, Nuria, aand Mohanta, Sasankasekhar, *Polyhedron*, 2013. **63**: p. 96-102.

[31] Biswas, R., Diaz, C. Bauzá, Antonio., Barceló-Oliver, Miquel., Frontera, Antonio., and Ghosh, Ashutosh, *Dalton Transactions*, 2014. **43**(17): p. 6455-6467.

[32] Niu, M.-J., Sun, D.-W., Li, Huan-Huan., Cao, Zhi-Qiang., Wang, Su-Na., and Dou, Jian-Min, *D., J. Coord. Chem.*, 2013. **67**(1): p. 81-95.

[33] Nowak, R., Bauer, W., Ossiander, Tanja., and Weber, Birgit, *Eur. J. Inorg. Chem.*, 2013. (5-6): p. 975-983.

[34] Ray, A., Sadhukan, Dipali., Rosair, Georgina M., Gomez-Garcia, Carlos J., and Mitra, Samiran, *Polyhedron*, 2009. **28**(16): p. 3542-3550.

[35] Gu, Z.-G., Pang, C.-Y., Qiu, Dan., Zhang, Jie., Huang, Ju-Li., Qin, Long-Fang., Sun, An-Qi., and Li, Zaijun, *Inorg. Chem. Comm.*, 2013. **35**: p. 164-168.

[36] Tomczyk, D., Nowak, L., Bukowski, W., Bester, K., Urbaniak, P., Andrijewski, G., and Olejniczak, B., *Electrochimica Acta*, 2014. **121**: p. 64-77.

[37] Anacona, J. and J. Santaella, *Spectrochimica Acta Part A: Mol. and Biomol. Spec.*, 2013. **115**: p. 800-804.

[38] Mukherjee, A., Saha, M.K., Nethaji, Munirathinam., and Chakravarty, Akhil R., *Polyhedron*, 2004. **23**(13): p. 2177-2182.

[39] Halcrow, M.A., *Spin-Crossover Materials: Properties and Applications*. 2013: John Wiley & Sons.

[40] Wilson, D., B. Djukic, and M.T. Lemaire, *Trans. Metal Chem.*, 2014. **39**(1): p. 17-24.

[41] Awschalom, D.D. and M.E. Flatté, *Nature Physics*, 2007. **3**(3): p. 153-159.

[42] Wolf, S., Awschalom, D., Buhrman, RA., Daughton, JM., Von Molnar, S., Roukes, ML., Chtchelkanova, A Yu., and Treger, DM, *Science*, 2001. **294**(5546): p. 1488-1495.

[43] Thomson, W., *Proceedings of the Royal Society of London*, 1856. **8**: p. 546-550.

[44] Barnaś, J., Fuss, A., Camley, RE., Grünberg, P., and Zinn, W, *Phys. Rev.* B, 1990. **42**(13): p. 8110.

[45] Baibich, M.N., Broto, J., Fert, Albert., Van Dau, F Nguyen., Petroff, F., Etienne, P., Creuzet, G., Friederich, A., and Chazelas, J., *Phys. Rev. Lett.*, 1988. **61**(21): p. 2472.

[46] Chelikowsky, J.R., E. Kaxiras, and R.M. Wentzcovitch, *Physica Status Solidi* (b), 2006. **243**(9): p. 2133-2150.

[47] Moodera, J.S., Kinder, L.R., Wong, Terrilyn M., and Meservey, R., *Phys. Rev. Lett.*, 1995. **74**(16): p. 3273.

[48] Moodera, J.S., et al., *Phys. Rev. Lett.*, 1995. **74**(16): p. 3273.

[49] Rezvani, Z., Ghanea, M.A., Nejati, Kamellia., and Baghaei, Sara Abodollahzadeh, *Polyhedron*, 2009. **28**(14): p. 2913-2918.

[50] Bhattacharjee, C.R., Datta, C., Das, Gobinda., Chakrabarty, Rupam., and Mondal, Paritosh, *Polyhedron*, 2012. **33**(1): p. 417-424.

[51] Bhattacharjee, C.R., G. Das, and P. Mondal, *Eur. J. Inorg. Chem.*, 2011. (35): p. 5390-5396.

[52] Januszko, A., P. Kaszynski, and B. Grüner, *Inorg. Chem.*, 2007. **46**(15): p. 6078-6082.

CHAPTER 3 EXPERIMENTAL

3.1 Introduction

This research was based on the findings that a new Schiff base, H_2salnon (**Figure 3.1**) reacted with metal(II) acetates to form a dinuclear magnetic complex with Cu(II) ion, but mononuclear magnetic complexes with Ni(II) and Co(II) ions [1].

Figure 3.1 Crystal structure of H_2salnon

Hence, the initial objectives of this research were to find out the effect of changing: (a) the alkyl chain length in the Schiff bases, and (b) metal(II) acetates to metal(II) hexadecanoates, on the nuclearity and other properties (especially mesomorphism and spin crossover) of the metal(II) complexes (Cu(II), Ni(II), Co(II), Fe(II)) formed. The Schiff bases chosen were H_2saloct (8-carbon chain) and H_2saldec (10-carbon chain) shown in **Figure 3.2**.

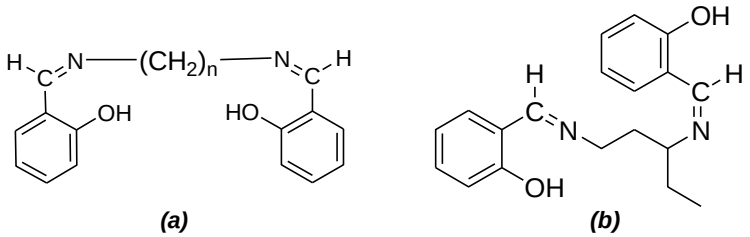

Figure 3.2 Structural formula of : (***a)*** H_2saloct (*n* = 8, *L1*); H_2saldec (*n* = 10, *L2*); and (***b)*** H_2salpen (*L3*)

The next objective of the research was to increase the nuclearity of the magnetic complexes, which is desirable in molecular magnetism. This was done based on the literature report that a Schiff base ligand formed a linear trinuclear complex with nickel(II) acetate or nickel(II) perchlorate (**Figure 3.3**) [2].

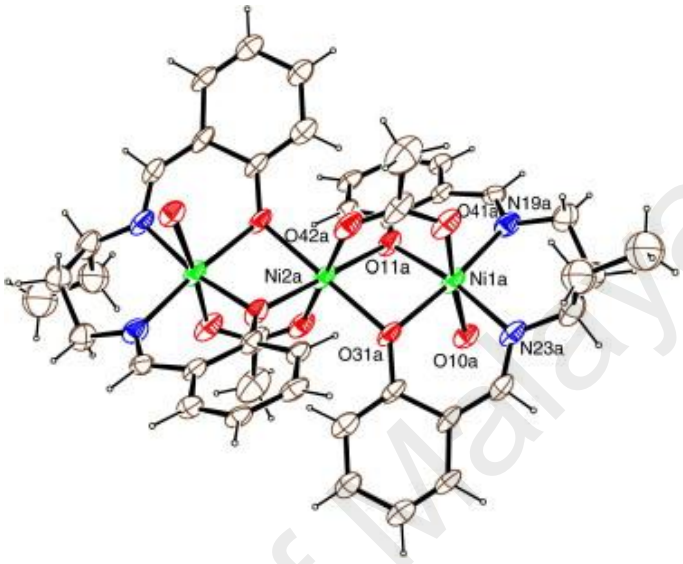

Figure 3.3 Crystal structure of $[Ni_3(salpen)_2(OAc)_2(H_2O)_2]\cdot 4H_2O$

The project involved the syntheses of the Schiff bases, ligand H_2L1, H_2L2 and H_2L3 with metal(II) complexes, deducing their chemical formulas by elemental analysis, ^{1}H-nuclear magnectic resonance spectroscopy, Fourier transform infrared spectroscopy, UV-visible spectroscopy, thermal stability by differential scanning calorimetry and thermogravimetry, mesomorphism by polarized optical microscopy, and magnetic properties by room-temperature magnetic susceptibility balance and variable-temperature superconducting interference device magnetometry.

3.2 Chemicals

The main chemicals used in the research are listed in **Table 3.1**.

Table 3.1 Chemicals used in the research

Chemical	Chemical Formula	Formula weight (g mol^{-1})	Purity (%)	Company
2-Hydroxybenzaldehyde	2-HOC_6H_4CHO	122.12	99	Merck
1,8-Diaminooctane	$H_2N(CH_2)_8NH_2$	144.26	98	Merck
1,10-Diaminodecane	$H_2N(CH_2)_{10}NH_2$	172.31	97	Acros
1,3-Diaminopentane	$H_2N(CH_2)_2CH(NH_2)CH_2CH_3$	102.18	97	Aldrich
Hexadecanoic acid	$CH_3(CH_2)_{14}COOH$	256.42	98	Aldrich
Sodium carbonate	Na_2CO_3	105.99	99	Merck
Copper(II) chloride dihydrate	$CuCl_2.2H_2O$	170.48	98	R&M Chemicals
Nickel(II) chloride hexahydrate	$NiCl_2.6H_2O$	237.71	98	R&M Chemicals
Cobalt(II) chloride hexahydrate	$CoCl_2.6H_2O$	237.93	99	R&M Chemicals
Iron(II) sulphate heptahydrate	$FeSO_4.7H_20$	278.02	99	Merck

3.3 Syntheses

The syntheses involved step-wise and one-pot reactions.

3.3.1 Schiff bases

(a) H_2L1

2-Hydroxybenzaldehyde (4.88 g; 40 mmol) was added to a solution of 1,8-diaminooctane (2.89 g; 20 mmol) in ethanol (100 mL), followed by a few drops of glacial acetic acid to act as a catalyst. The reaction mixture was heated under reflux for 3 hours, and the yellow solution formed was left overnight at room temperature. The yellow crystals formed were filtered, washed with cold ethanol and left to dry at room temperature. The yield was 5.37 g (76.1%). *Anal*. Calc. for $C_{22}H_{28}N_2O_2$ (FW, 352.47 g mol^{-1}): C, 75.0; H, 8.0; N, 8.0. Found: C, 75.3; H, 7.9; N, 8.2%.

(b) H_2L2

The procedure was the same as in **3.3.1(a)**, replacing 1,8-diaminooctane with 1,10-diaminodecane (3.45 g; 20 mmol). The product was yellow crystals and the yield

was 5.64 g (74.2%). *Anal*. Calc. for $C_{24}H_{32}N_2O_2$ (FW, 380.52 g mol^{-1}): C, 75.8; H, 8.5; N, 7.4. Found: C, 75.5 ; H, 8.8 ; N, 7.3%.

(c) H_2L3

The procedure was the same as in **3.3.1(a)**, replacing 1,8-diaminooctane with 1,3-diaminopentane (2.04 g; 20 mmol). The solvent was removed on a rotary evaporator to give a viscous yellow liquid. The yield was 5.27 g (84.8%). *Anal*. Calc. for $C_{19}H_{22}N_2O_2$ (FW, 310.39 g mol^{-1}): C, 73.5; H, 7.1; N, 9.0. Found: C, 72.8; H, 7.0; N, 8.8%.

3.3.2 $[M(CH_3(CH_2)_{14}COO)_2]$

(a) $CH_3(CH_2)_{14}COONa$

$CH_3(CH_2)_{14}COOH$ (24.68 g; 96.2 mmol) was added portion wise to an aqueous solution of Na_2CO_3 (5.10 g; 48 mmol) in distilled H_2O. The cloudy mixture formed was heated and stirred on a hot plate for 30 minutes. The solid formed was then filtered and dried in a warm oven (60 °C) overnight. The yield was 23.96 g (89.5%). *Anal*. Calc. for $C_{16}H_{31}O_2Na$ (FW, 278.41 g mol^{-1}): C, 69.0; H, 11.2. Found: C, 68.6; H, 11.4%.

(b) $[Cu(CH_3(CH_2)_{14}COO)_2]$

$CuCl_2.2H_2O$ (3.12 g; 18.3 mmol) was added to a hot solution of $CH_3(CH_2)_{14}COONa$ (10.23 g; 36.7 mmol) in ethanol (100 mL). The mixture was heated for another 30 minutes. A fine greenish-blue powder formed was filtered under suction, washed with distilled water followed by ethanol, and then dried in a warm oven (60 °C). The yield was 4.52 g (43.0%). *Anal*. Calc. for $C_{32}H_{62}CuO_4$ (FW, 574.38 g mol^{-1}): C, 66.9; H, 10.9 Found: C, 66.1; H, 11.0%.

(c) [Ni($CH_3(CH_2)_{14}COO)_2$]

$NiCl_2.6H_2O$ (2.17 g; 16.74 mmol) was added to a hot ethanolic solution of $CH_3(CH_2)_{14}COONa$ (5.12 g; 18.3 mmol). The mixture was then further heated for 30 minutes. A fine light green powder formed was filtered under suction, washed with distilled water followed by ethanol, and then dried in a warm oven (60 °C). The yield was 3.3566 g (35.2%). *Anal*. Calc. for $C_{32}H_{62}NiO_4$ (FW, 569.53 g mol^{-1}): C, 67.4; H, 10.9 Found: C, 66.9; H, 11.0%.

(d) [Co($CH_3(CH_2)_{14}COO)_2$]

$CoCl_2.6H_2O$ (2.18 g; 16.79 mmol) was added to a hot solution of $CH_3(CH_2)_{14}COONa$ (5.12 g: 18.3 mmol) in ethanol (100 mL). The mixture was then heated for another 30 minutes. A fine purple powder formed was filtered under suction, washed with distilled water followed by ethanol, and then dried in a warm oven (60 °C). The yield was 4.48 g (46.8%). *Anal*. Calc. $C_{32}H_{62}CoO_4$ for (FW, 569.76 g mol^{-1}): C, 67.5; H, 11.0 Found: C, 68.0; H, 10.8%.

(e) [Fe($CH_3(CH_2)_{14}COO)_2(CH_3CH_2OH)$]

$FeSO_4.7H_2O$ (5.10 g; 18.3 mmol) was added to a hot solution of $CH_3(CH_2)_{14}COONa$ (10.23 g; 36.7 mmol) in CH_3CH_2OH (100 mL). The mixture was then heated for another 30 minutes. A fine light brown powder formed was filtered under suction, washed with distilled water followed by ethanol, and then dried in a warm oven (60 °C). The yield was 8.26 g (73.7%). *Anal*. Calc. for $C_{34}H_{68}FeO_5$ (FW, 612.75 g mol^{-1}): C, 66.6; H, 11.2 Found: C, 66.4 ; H, 12.5%.

3.3.3 Reaction of H_2L1 with [M($CH_3(CH_2)_{14}COO)_2$]

(a) [Cu($CH_3(CH_2)_{14}COO)_2$]

[Cu($CH_3(CH_2)_{14}COO)_2$] (0.57 g; 1.0 mmol) was dissolved in ethanol (100 mL). The mixture was gently heated and stirred. H_2L1 (0.352 g; 1.0 mmol) was slowly added to

the mixture and the reflux continued for 3 hours. The colour of the solution changed from clear yellowish to dark brown. The solution was then left for two days at room temperature, and the solid formed was filtered. The yield was 0.38 g (92%). *Anal*. Calc. for $C_{22}H_{26}CuN_2O_2$ (FW, 414 g mol^{-1}): C, 63.8; H, 6.3; N, 6.7 Found: C, 63.2; H, 6.5; N, 6.8%.

(b) [Ni($CH_3(CH_2)_{14}COO)_2$]

[Ni($CH_3(CH_2)_{14}COO)_2$] (0.28 g; 0.49 mmol) and H_2L1 (0.35 g; 1.0 mmol) was reacted in the same manner as in **3.3.3(a)**. The colour of the solution changed from light green to dark green. The solution was then left for two days to let the product precipitate out. The filtered residue was then dried at room temperature. The yield was 0.19 g (39.7%). *Anal*. Calc. for $C_{22}H_{26}NiN_2O_2$ (FW, 409 g mol^{-1}): C, 64.6; H, 6.4; N, 6.9. Found: C, 64.8; H, 6.7; N, 6.8%.

(c) [Co($CH_3(CH_2)_{14}COO)_2$]

The same procedure was the same as in **3.3.3(a)**, replacing [Cu($CH_3(CH_2)_{14}COO)_2$] with [Co($CH_3(CH_2)_{14}COO)_2$] (0.57 g; 1.0 mmol). The colour changes of the solution was observed from light green to dark green. The precipitates from the reaction was filtered and dried at room temperature. The yield was 0.32 g (78.7%). *Anal*. Calc. for $C_{22}H_{26}CoN_2O_2$ (FW, 409.39 g mol^{-1}): C, 64.5; H, 6.4; N, 6.8. Found: C, 65.1; H, 6.5; N, 6.9%.

(d) [Fe($CH_3(CH_2)_{14}COO)_2$]

[Fe($CH_3(CH_2)_{14}COO)_2(CH_3CH_2OH)$] (0.42 g; 0.69 mmol) and H_2L1 (0.27 g; 0. 76 mmol) was reacted same as in **3.3.3(a).** The colour of the solution changed from clear yellowish to light brown. The brown solid formed was filtered and dried at room

temperature. The yield was 0.35 g (46.6%). *Anal*. Calc. $C_{54}H_{102}Fe_2N_2O_{13}$ for (FW, 1090.61 g mol^{-1}): C, 59.5; H, 9.2; N, 2.5 Found: C, 59.1; H, 8.6; N, 2.9%.

3.3.4 Reaction of H_2L2 with $[M(CH_3(CH_2)_{14}COO)_2]$

(a) Step-wise reaction

(i) $[Cu(CH_3(CH_2)_{14}COO)_2]$

H_2L2 (0.38 g; 1.0 mmol) was dissolved in ethanol (100 mL). The solution was magnetically stirred and heated for about 10 minutes. A suspension of $[Cu(CH_3(CH_2)_{14}COO)_2]$ (0.57 g; 1.0 mmol) in ethanol was slowly added to the yellow solution. The mixture colour turn green and left to be refluxed for 3 hours. After 3 hours of refluxed, the mixture was then left for a few days to let the product precipitate out. The yield was 0.30 g (67.9%). *Anal*. Calc. for $C_{48}H_{60}Cu_2N_4O_4$ (FW: 442.05 g mol^{-1}): C, 65.2; H, 6.8; N, 6.3 Found: C, 65.9; H, 7.0; N, 6.2%.

(ii) $[Ni(CH_3(CH_2)_{14}COO)(H_2O)_2]$

The procedure was the same as in **3.3.4(a)(i)**, replacing $[Cu(CH_3(CH_2)_{14}COO)_2]$ with $[Ni(CH_3(CH_2)_{14}COO)_2]$ (0.56 g; 0.1 mmol). The colour of the solution changed from light green to dark green. The solution was then left overnight before being filtered. Both the residue and the filtrate were kept. The yield was 0.33 g (68.3%). *Anal*. Calc. for $C_{26}H_{36}N_2NiO_3$ (FW: 483.2 g mol^{-1}): C, 64.6; H, 7.5; N, 5.8. Found: C, 65.0; H, 7.7; N, 5.5%.

(iii) $[Co(CH_3(CH_2)_{14}COO)_2]$

The procedure was the same as in **3.3.4(a)(i)**, replacing $[Cu(CH_3(CH_2)_{14}COO)_2]$ with $[Co(CH_3(CH_2)_{14}COO)_2]$ (0.57 g; 1.0 mmol). The colour of the solution changed from light green to dark green. The solution was then left for 2 days at room tempertaure. The dark green solid residue was filtered. The yield was 0.36 g (25.0%). *Anal*. Calc. for

$C_{80}H_{116}Co_2N_6O_{10}$ (FW: 1438.74 g mol^{-1}): C, 66.8; H, 8.1; N, 5.8. Found: C, 66.8; H, 7.6; N, 5.8%.

(iv) [Fe($CH_3(CH_2)_{14}COO)_2$.CH_3CH_2OH]

The procedure was the same as in **3.3.4(a)(i)**, replacing [Cu($CH_3(CH_2)_{14}COO)_2$] [Fe($CH_3(CH_2)_{14}COO)_2(CH_3CH_2OH)$] (0.28 g; 0. 46 mmol). The colour of the solution changed from clear yellowish to dark brown. The black gummy solid formed was filtered and left standing at room temperature. The yield was 0.29 g (40.4%). *Anal*. Calc. for $C_{88}H_{129}Fe_2N_6O_{11}$ (FW: 1558.69 g mol^{-1}): C, 67.8; H, 8.3; N, 5.4 Found: C, 67.6; H, 7.9; N, 5.5%.

(b) One-pot reaction

(i) [Cu(L2)]

1,10–diaminooctane (0.43 g; 2.50 mmol) was dissolved in about 100 mL of ethanol. The clear solution was slowly heated and stirred for about 10 minutes. Then 2-hydroxybenzaldehyde (0.61 g; 5.0 mmol) was slowly added to the hot solution. [Cu($CH_3(CH_2)_{14}COO)_2$] (0.90 g; 1.57 mmol) was added to the mixture. A few drops of glacial acetic acid was added as catalyst. The mixture was then refluxed for 3 hours. The precipitate formed was filtered. The yield was 0.63 g (90.1%). *Anal*. Calc. for $C_{24}H_{30}CuN_2O_2$ (FW: 442.06 g mol^{-1}): C, 65.2; H, 6.8; N, 6.3 Found: C, 66.5; H, 7.1; N, 6.3%.

(ii) [Ni_2(L2)($HL2)_2$].H_2O

1,10–diaminooctane (3.44 g; 20.0 mmol), 2-hyrdroxybenzaldehyde (4.88 g; 40.0 mmol) and [Ni($CH_3(CH_2)_{14}COO)_2$] (1.50 g; 2.63 mmol) was reacted together as in **3.3.4(b)(i)**. The precipitate formed was filtered and analysed. The yield was 1.01 g (87.8%). *Anal*. Calc. for $C_{72}H_{94}N_6Ni_2O_7$ (FW: 1272.9 g mol^{-1}): C, 67.9; H, 7.4; N, 6.4 Found: C, 67.2; H, 7.1; N,6.4%.

(iii) [Co(L2)(HL2)]

1,10–diaminooctane (0.86 g; 5.0 mmol), 2-hydroxybenzaldehyde (1.22 g; 10.0 mmol) and [$Co(CH_3(CH_2)_{14}COO)_2$] (1.42 g; 2.5 mmol) was reacted together using the same procedure as in **3.3.4(b)(i).** The black solution was left to cool to let the product precipitated out. The yield was 0.67 g (32.8%). *Anal*. Calc. for $C_{48}H_{61}CoN_4O_4$ (FW: 816.96 g mol^{-1}): C, 70.6; H, 7.5; N, 6.8 Found: C, 70.1; H, 7.6; N,6.7%.

(iv) [$Fe^{II}Fe^{III}(CH_3(CH_2)_{14}COO)(L2)(HL2)_2(EtOH)_2$].2EtOH

The procedure was the same as in **3.3.4(b)(iii)**, replacing [$Co(CH_3(CH_2)_{14}COO)_2$] with [$Fe(CH_3(CH_2)_{14}COO)_2(CH_3CH_2OH)$] (1.43 g; 2.3 mmol). The black solution was left to cool to let the product precipitated out. The yield was 1.95 g (50.7%). *Anal*. Calc. for $C_{96}H_{147}Fe_2N_6O_{11}$ (FW: 1672.92 g mol^{-1}): C, 68.2; H, 8.8; N, 4.9 Found: C, 68.0; H, 8.6; N, 4.7%.

3.3.5 Reaction of H_2L3 with [$M(CH_3(CH_2)_{14}COO)_2$]

(a) [$Cu(CH_3(CH_2)_{14})COO)_2$]

H_2L3 (0.12 g; 0.39 mmol) was dissolved in ethanol (100 mL). The solution was magnetically stirred and heated for about 10 minutes. A suspension of [$Cu(CH_3(CH_2)_{14}COO)_2$] (0.23 g; 0.4 mmol) in ethanol was slowly added to the yellow solution. The mixture colour turn green and left to be refluxed for 3 hours. After 3 hours of refluxed, the mixture was then left for a few days to let the product precipitate out. The yield was 0.13 g (64.8%). *Anal*. Calc. for $C_{54}H_{74}Cu_2N_4O_6$ (FW: 1001.3 g mol^{-1}): C, 64.7; H, 7.4; N, 5.6. Found: C, 64.5; H, 7.5; N, 5.8%.

(b) [Ni($CH_3(CH_2)_{14}$)$COO)_2$]

The procedure was the same as in **3.3.5(a)**, replacing [Cu($CH_3(CH_2)_{14}COO)_2$] with [Ni($CH_3(CH_2)_{14}COO$)Cl($H_2O)_2$] (0.15 g; 2.6 mmol). The colour of the solution changed from light yellow to light green. The solution was then left for 2 days before being filtered. Both the residue and the filtrate are kept. The yield was 0.19 g (77.2%). *Anal*. Calc. for $C_{54}H_{75}NiN_4O_6$ (FW: 934.89 g mol^{-1}): C, 70.2; H, 8.4; N, 5.9. Found: C, 69.5; H, 8.1; N, 5.9%.

(c) [Co($CH_3(CH_2)_{14}COO)_2$]

The procedure was the same as in **3.3.5(a)**, replacing [Cu($CH_3(CH_2)_{14}COO)_2$] with [Co($CH_3(CH_2)_{14}COO)_2$] (0.11 g; 0.2 mmol) and *H_2L3* (0.06 g; 0.2 mmol). The colour of the solution changed from light green to dark green. The solution was then left for 2 days at room tempertaure. The dark green solid residue was filtered. The filtrate was kept for further viewing. The yield was 0.11 g (80.3%). *Anal*. Calc. for $C_{35}H_{51}CoN_2O_4$ (FW: 623.7 g mol^{-1}): C, 67.5; H, 9.9; N, 4.5. Found: C, 67.5; H, 8.3; N, 4.5%.

(d) [Fe($CH_3(CH_2)_{14}COO)_2(CH_3CH_2OH)$]

The procedure was the same as in **3.3.5(a)**, replacing [Cu($CH_3(CH_2)_{14}COO)_2$] with [Fe($CH_3(CH_2)_{14}COO)_2$. CH_3CH_2OH] (0.4289 g; 0.70 mmol) and *H_2L3* (0.22 g; 0.71 mmol). The colour of the solution changed from clear yellowish to dark brown. The black gummy solid formed was filtered and left standing at room temperature. The yield was 0.1170 g (19.1%). *Anal*. Calc. for $C_{51}H_{83}FeN_2O_2$ (FW: 876.06 g mol^{-1}): C, 69.9; H, 9.55; N, 3.2. Found: C, 70.0; H, 10.3; N, 4.3%.

3.4 Instrumental Analyses

3.4.1 Elemental analyses

The percentages of carbon, hydrogen and nitrogen in a compound were determined on a Perkin Elmer CHNS/O analyser 2400 Series II. A small amount of the sample (1-2 mg) was placed in a tin capsule of dimension 5 mm x 8 mm, which was then folded into a tiny piece. It was then put into the analyser and heated up to 1000 ºC.

3.4.2 ^{1}H-Nuclear magnetic resonance spectroscopy

The ^{1}H-nuclear magnetic resonance spectra (^{1}H-NMR) were recorded on a JEOL FT-NMR Lambda 400 MHz spectrometer. A small amount of the sample was dissolved in a suitable deuterated solvent and placed inside an NMR tube.

3.4.3 Fourier transform infrared spectroscopy

The IR spectrum were recorded using a Perkin-Elmer Spectrum 400 FT-IR/FT-IR Spectrometer with a Pike Technologies GladiATR attachment.

3.4.4 Ultraviolet-visible spectroscopy

The ultraviolet spectra were recorded from 1000 – 300 nm with Shimadzu UV-vis-NIR 3600 spectrophotometer for both liquid and solid samples.

For solution, an exactly known mass of the solid was dissolved in a suitable solvent in a volumetric flask. Then part of the solution was placed into a 1cm quartz cuvette which is later put into the sample holder. The spectrum was recorded with the corresponding solvent as reference.

3.4.5 Differential scanning calorimetry

All the thermograms were obtained for differential scanning calorimetry (DSC) from a Perkin Elmer DSC 6 calorimeter within the temperature range of 35 – 300 ºC and scan rate of 10 ºC min^{-1}.

Mass of the sample (2 – 4 mg) was recorded using the microbalance before it was transferred into an aluminium crucible and placed inside the instrument. The analysis was performed under nitrogen gas with a flow rate of 10 cm^3 min^{-1}.

3.4.6 Thermogravimetry

Thermogram of all complexes were recorded using a Pyris Diamond TG/DTA Perkin Elmer instrument with temperature range of 50 – 900 ºC with scan rate of 20 ºC min^{-1} . The analysis was done under nitrogen with a flow rate of 10 cm^3 min^{-1}. An alumina pan was used as a sample holder. The sample (4 – 5 mg) was placed inside the pan and the instrument.

3.4.7 Room temperature magnetic susceptibility

The magnetic susceptibility was recorded using a Sherwood Auto Magnetic Susceptibility Balance. An empty glass tube was tared on an analytical balance before placing it on the instrument. The exponent of the reading was changed to 10^{-5} and tared again. Sample preparation started with the sample being ground finely and packed into the tube up to the optimum mark (4 cm in length) and the mass was recorded. The tube was then placed in the instrument before the weight and height of the sample was keyed in. The χ_g was recorded.

3.4.8 Variable temperature magnetic susceptibility

The measurement was done using a Quantum Design Magnetic Property Measurement System (MPMS) – XL EverCool superconducting quantum interference device (SQUID) magnetometer in Kinki University, Higashiosaka-shi, Osaka, Japan. About 10 mg of the sample was put inside a medicine capsule and insert halfway inside a straw which is roughly 10 centimeter from the top. The straw was then put inside the instrument to be analysed. The measurements were done at 1 Tesla or 10000 Gauss and the temperature range is 300 – 2 Kelvin. The raw data from the measurement was then further analysed using Microsoft Excel and Igor Software.

3.4.9 Polarized Optical Microscopy

Mesomorphism of samples were recorded with Olympus BX51 polarizing microscope equipped with a Mettler Toledo FP90 method controller and FP82HT hot stage. A tiny amount of the samples were sandwiched between two thin glass slides and placed on the hot stage. Then the samples were heated and cooled at various rate ranging from 1 – 10 °C min^{-1}.

References

[1] Ti, T.J., *Synthesis and Characterization of Zn(II), Cu(II), Ni(II) and Co(II) Complexes as Molecular Spintronic Materials*, M.Sc thesis, 2011, University of Malaya: Malaysia.

[2] Mukherjee, P., Drew, Michael, GB., Tangoulis, Vassilis., Estrader, Marta., Diaz, Carmen., and Ghosh, Ashutosh., *Polyhedron*, 2009. **28**(14): p. 2989-2996.

CHAPTER 4 RESULTS AND DISCUSSION

4.1 Introduction

This research was focused on the synthesis, structural deduction and characterization of magnetic metallomesogens as potential spintronic materials. It involved complexes of Cu^{II} (d^9),Ni^{II} (d^8), Co^{II}(d^7) and Fe^{II} (d^6) of three Schiff bases, H_2L1, $H_2L2$and H_2L3. The structural formulas of these Schiff bases and ligands are shown in **Figure 4.1**.This project was partly a continuation of previous research on complexes of similar Schiff base as H_2L1 and H_2L2, but with n = 9 [1].

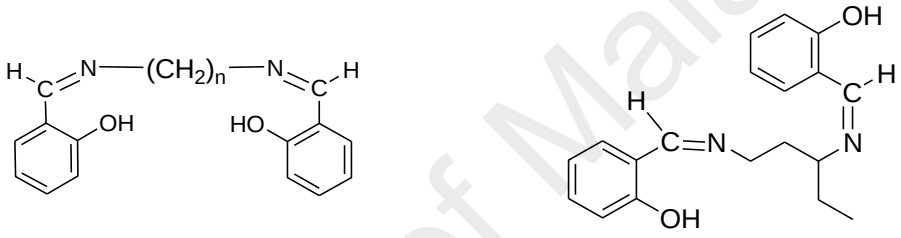

(a) (b)

Figure 4.1 Structural formulas of Schiff bases:(a)H_2L1(n = 8), H_2L2 (n = 10); (b)H_2L3

4.2 Synthesis, Structural Deduction and Characterisation of Complexes of H_2L1

The first phase of this research involved the synthesis of H_2L1 [2] and ascertaining its structure by elemental analyses, FTIR spectroscopy and ^{1}H-NMR spectroscopy. This was followed by syntheses of [$M(CH_3(CH_2)_{14}COO)_2$] (M = Cu(II), Ni(II), Co(II), Fe(II)) and deducing their chemical formulas by elemental analyses. Finally, H_2L1 was reacted with [$M(CH_3(CH_2)_{14}COO)_2$] [3], and the complexes formed were analysed by elemental analyses, FTIR spectroscopy, UV-vis spectroscopy, magnetic susceptibility, thermogravimetry (TGA), differential scanning calorimetry (DSC), and optical polarized microscopy (OPM).

4.2.1 Synthesis and characterization of H_2L1

H_2L1 was obtained as small yellow crystals from the reaction between 1,8-diaminooctane and 2-hydroxybenzaldehyde (mol ratio = 2:1). The solvent used was ethanol and the yield was 76.1%. However, its structure could not be ascertained by single-crystal X-ray crystallography due to poor diffraction. Hence, its structural formula was ascertained from the following instrumental data.

The results of the **elemental analyses**(75.3% C, 7.9% H, and 8.2% N) were in good agreement with the chemical formula $C_{11}H_{14}NO$ (75.0% C, 8.0% H, and 8.0% N). Its structural formula was supported by ^{1}H-NMR spectroscopy: the spectrum is shown in **Figure 4.2**, and the peak assignments are given in **Table 4.1**.

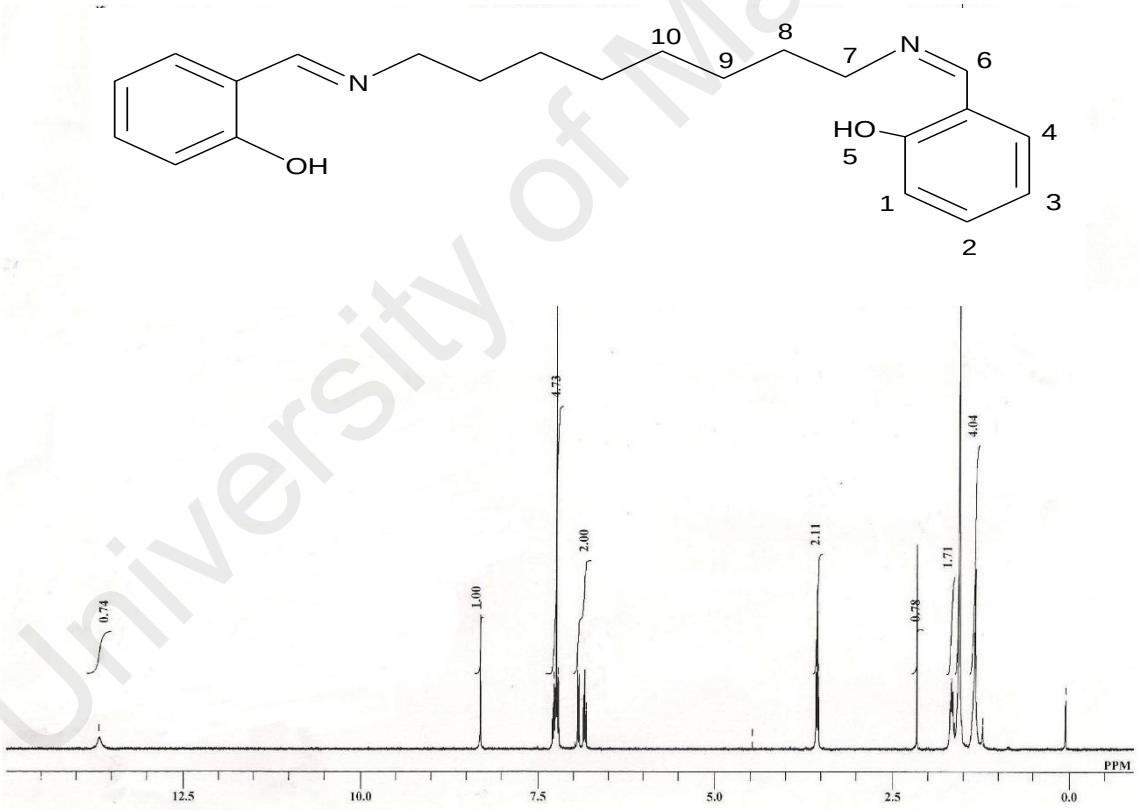

Figure 4.2^{1}H-NMR spectrum of H_2L1

Table 4.1 The ^{1}H-NMR peak assignment for H_2L1

Chemical Shift (ppm)	**Integral**	**Multiplicity**	**Assignment**
1.2 – 1.7	5.7	multiplet	H-8, H-9, H-10
3.5	2.1	triplet	H-7
6.8	1.0	triplet	H-3
6.9	1.0	doublet	H-4
7.2	1.0	triplet	H-2
7.3	1.0	doublet	H-1
8.3	1.0	singlet	H-6
13.6	0.74	singlet	H-5

Its **FTIR** spectrum and the data are shown in **Figure 4.3**and **Table 4.2** (which also includes the data for the corresponding complexes for later discussion). The spectrum shows a broad peak centered at 3406 cm^{-1} for the OH group, two strong peaks at 2921 cm^{-1} and 2850 cm^{-1} for the asymmetric and symmetric vibrations of CH_2 group respectively, a strong peak at 1633 cm^{-1} for the C=N (imine) bond, a strong peak at 1610 cm^{-1} for the aromatic C=C, and a medium peak at 1499 cm^{-1} for the aromatic ring.

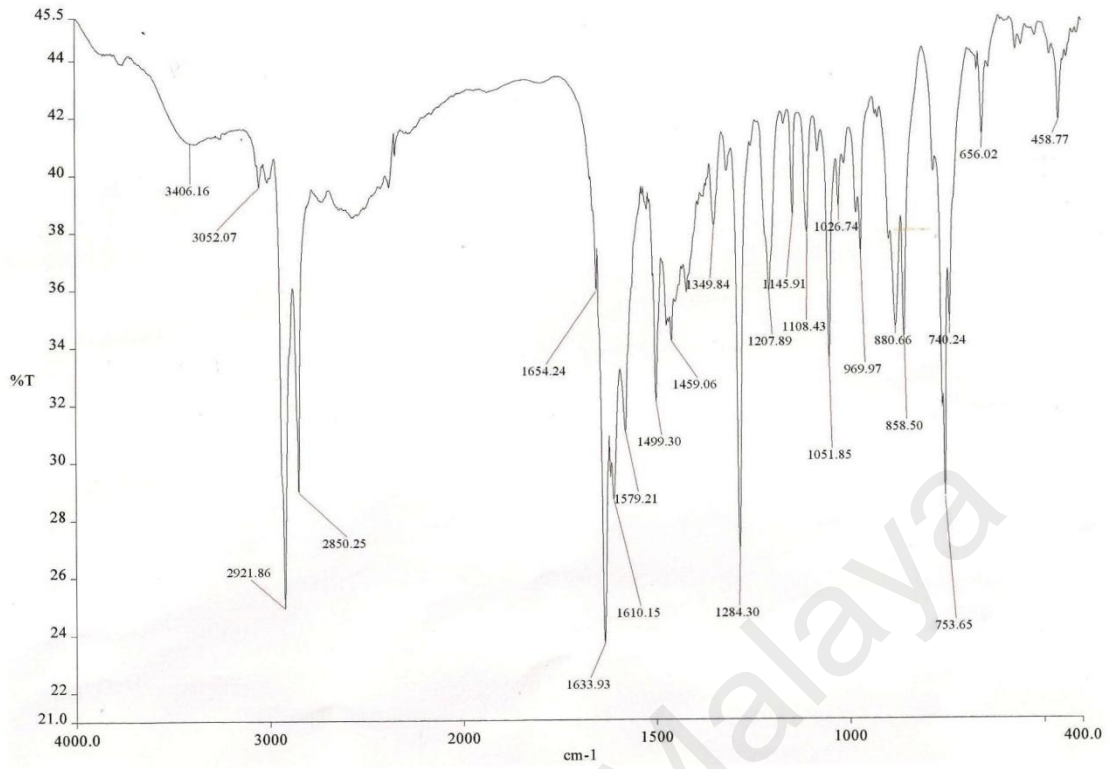

Figure 4.3 FTIR spectrum of H_2L1

Table 4.2 The FTIR data (in cm^{-1}) for H_2L1 and its metal(II) complexes.

Compound	Assignment / $\bar{\upsilon}$ (cm^{-1})					
	OH	CH_2 (asym)	CH_2 (sym)	C=N	M-O	M-N
H_2L1	3406	2921	2850	1633	-	-
$[Cu_2(L1)_2]$	-	2921	2850	1620	578	471
[Ni(L1)]	-	2922	2852	1612	560	460
[Co(L1)]	-	2918	2850	1617	550	463
$[Fe_2(CH_3(CH_2)_{14}COO)_2(L1)(H_2O)_4].2.5H_2O$	3200 - 3400	2917	2849	1617	509	461

From **TGA**, H_2L1 was found to lose 98.5% of its mass in the temperature range of 250 - 800 °C (**Figure 4.4**). Its **DSC** (**Figure 4.5**) shows one endothermic peak at onset temperature of 76.0 °C (ΔH = +41.6 kJ mol^{-1}), assigned to its melting temperature. When viewed under **OPM**, the sample was observed to melt at 77.9 °C and to clear to an isotropic liquid (I) at 78.4 °C. On cooling from I, it showed an optical texture at 51.6 °C (**Figure 4.6**).

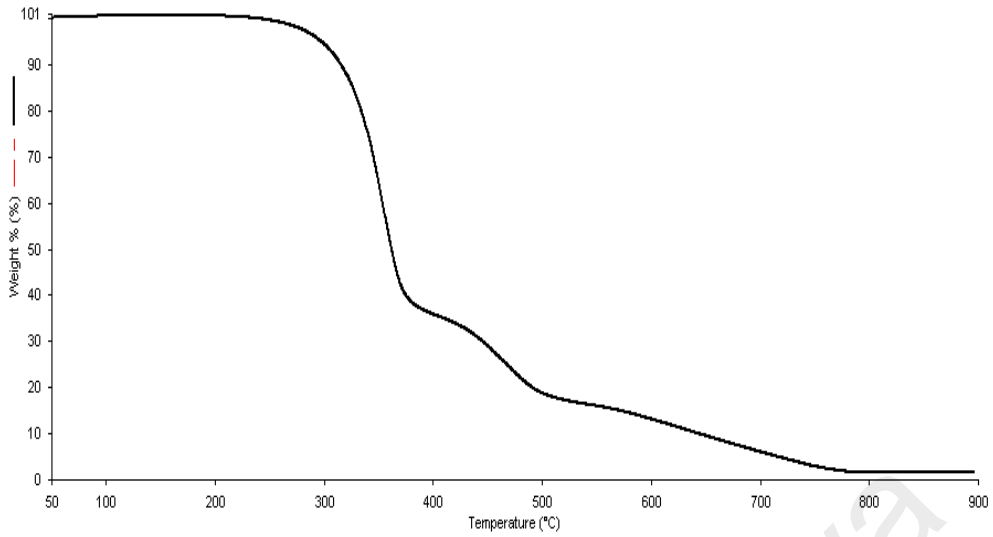

Figure 4.4 TGA thermogram of H_2L1

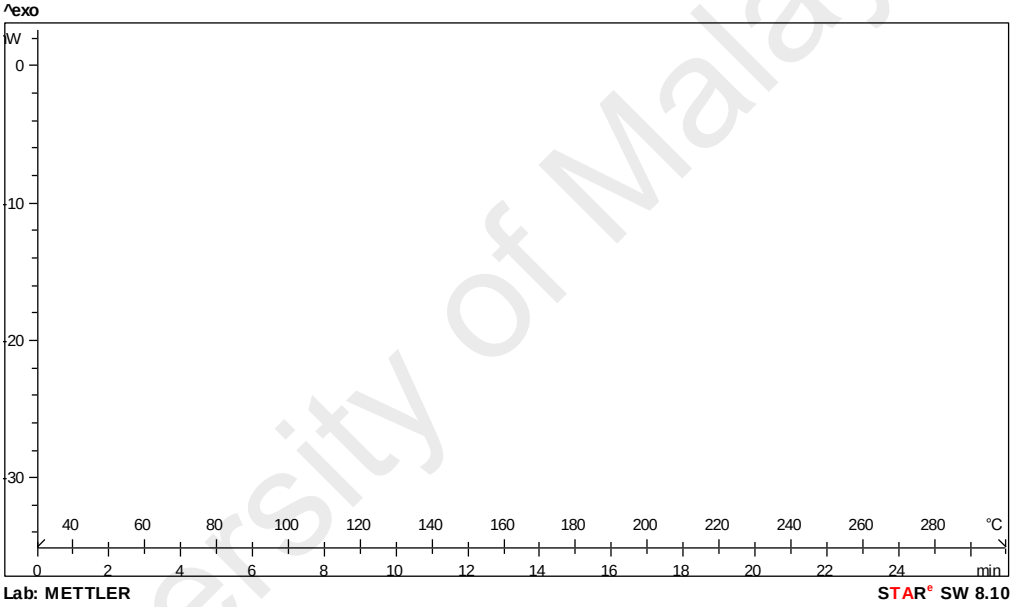

Figure 4.5 DSC scan of H_2L1

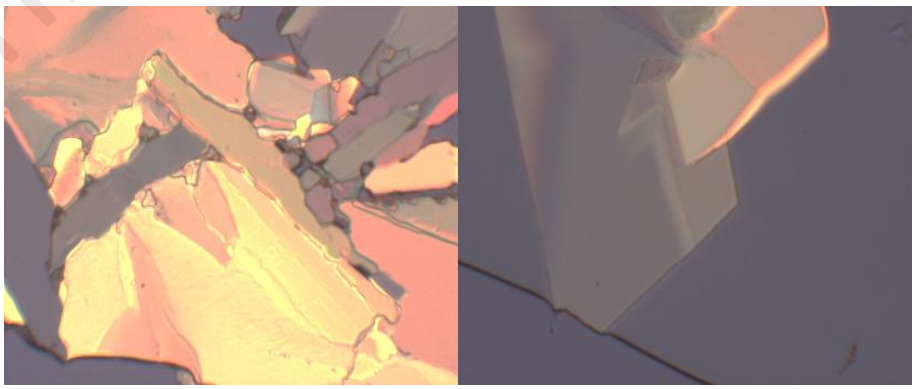

(a) (b)

Figure 4.6 Photomicrographs of H_2L1 at: (a) 77.9 °C (melting), and (b) 51.6 °C (crystallizing)

4.2.2 Synthesis of [M(CH$_3$(CH$_2$)$_{14}$COO)$_2$]

The starting complexes, [M(CH$_3$(CH$_2$)$_{14}$COO)$_2$], were synthesized by first reacting CH$_3$(CH$_2$)$_{14}$COOH with Na$_2$CO$_3$ to form CH$_3$(CH$_2$)$_{14}$COONa, and then reacting the CH$_3$(CH$_2$)$_{14}$COONa obtained with MCl$_2$ to form [M(CH$_3$(CH$_2$)$_{14}$COO)$_2$]. The reaction equations are shown below, and the data for all complexes are shown in **Table 4.3**.

$$CH_3(CH_2)_{14}COOH + Na_2CO_3 \longrightarrow CH_3(CH_2)_{14}COONa + CO_2 + H_2O$$

$$2\ CH_3(CH_2)_{14}COONa + MCl_2 \longrightarrow [M(CH_3(CH_2)_{14}COO)_2] + 2\ NaCl$$

Table 4.3 Synthetic data for [M(CH$_3$(CH$_2$)$_{14}$COO)$_2$]

Complex (Formula mass/g mol^{-1})	Yield (%)	Colour	Elemental Analysis Calculated (Found)	
			C	H
[Cu(CH$_3$(CH$_2$)$_{14}$COO)$_2$] (574.38)	43.0	Greenish blue	66.9 (66.1)	10.9 (11.0)
[Ni(CH$_3$(CH$_2$)$_{14}$COO)$_2$] (569.53)	35.2	Light green	67.4 (66.9)	10.9 (11.0)
[Co(CH$_3$(CH$_2$)$_{14}$COO)$_2$] (569.76)	46.8	Purple	67.5 (68.0)	11.0 (10.8)
[Fe(CH$_3$(CH$_2$)$_{14}$COO)$_2$(EtOH)] (612.75)	73.7	Light brown	66.6 (66.4)	11.2 (12.5)

4.2.3 Reaction of H$_2$L1 with [M(CH$_3$(CH$_2$)$_{14}$COO)$_2$]

(a) M = Cu

H$_2$L1 reacted with [Cu(CH$_3$(CH$_2$)$_{14}$COO)$_2$] to form a dark khaki-green powder in 92.0% yield.Recrystallization from ethanol yielded very small needle-like crystals. However, its crystal structure could not be deduced by single crystal X-ray crystallography due to poor diffraction. Based on the analytical data presented below, it is proposed that its chemical formula was [Cu(L1)]. Its structure (**Figure 4.7**) may be similar to [Cu(Sal-6)]$_2$ reported by Nathan [4], which is different from that proposed for Cu(II) complex of similar Schiff base as H$_2$L1, but with n = 9 [1].

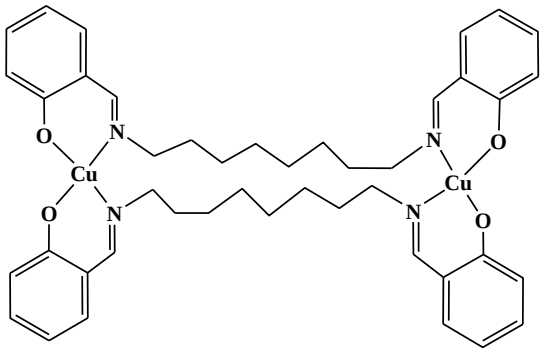

Figure 4.7 Proposed structural formula of $[Cu_2(L1)_2]$

The results from the **elemental analyses** (C, 63.2; H, 6.5; N, 6.8) were in good agreement with those calculated for the chemical formula $C_{22}H_{26}CuN_2O_2$ (C, 63.8; H, 6.3; N, 6.8; FW: 414 g mol^{-1}).

Its **FTIR spectrum** (**Figure 4.8**) shows two weak peaks at 2921 cm^{-1} and 2850 cm^{-1} and a strong peak at 1620 cm^{-1}. These peaks are similarly assigned as for H_2L1. It is noted that the imine peak was shifted to lower energy compared to H_2L1 (1633 cm^{-1}; **Table 4.2**), suggesting the coordination of both imine nitrogen atoms to Cu(II) centres [5]. Also observed are two new peaks at 578$cm^{-1}$and 471 cm^{-1}, which are assigned as the M-O and M-N bonds respectively [6-8].

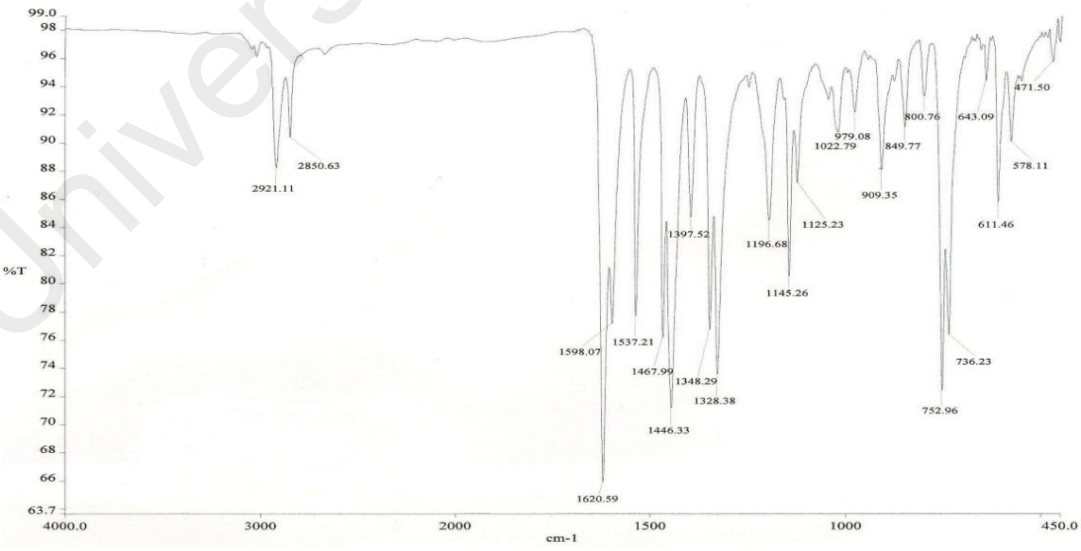

Figure 4.8. FTIR spectrum of [Cu(L1)]

The **UV-vis**spectrum of solid [Cu(L1)] (**Figure 4.9**(a)) shows a broad *d-d*band at about 585 nm. Accordingly, the geometry of the complex at Cu(II) may be square

planar [4]. Also observed is a strong band at 390 nm, assigned as phenoxide-to-Cu(II) charge transfer transition (LMCT). The spectrum for the complex dissolved in $CHCl_3$ (**Figure 4.9**(b)) shows a broad *d-d* band at 612 nm (ε_{max} = 271 $M^{-1}cm^{-1}$) [9]. Hence, it may be inferred that the complex maintained its planar geometry in this solution.

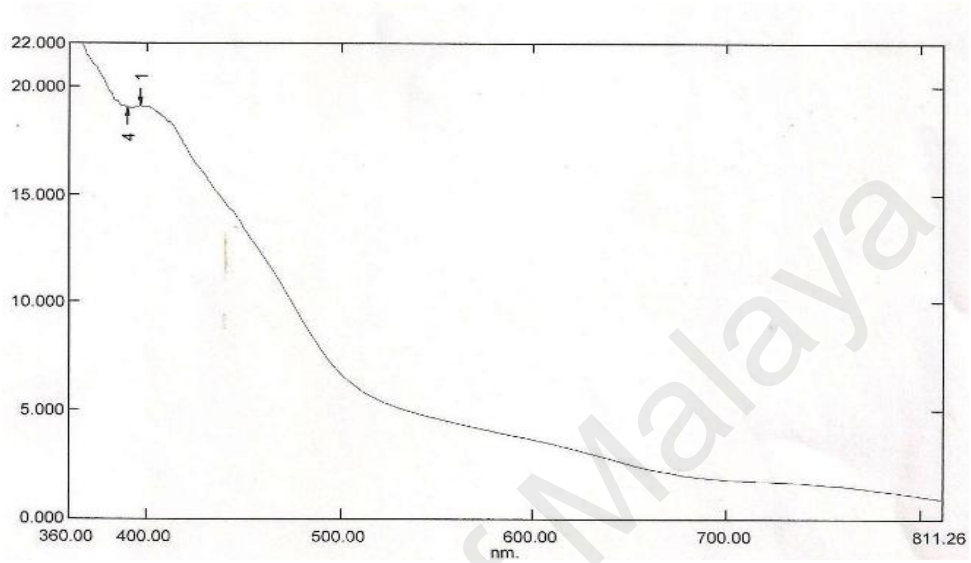

(a)

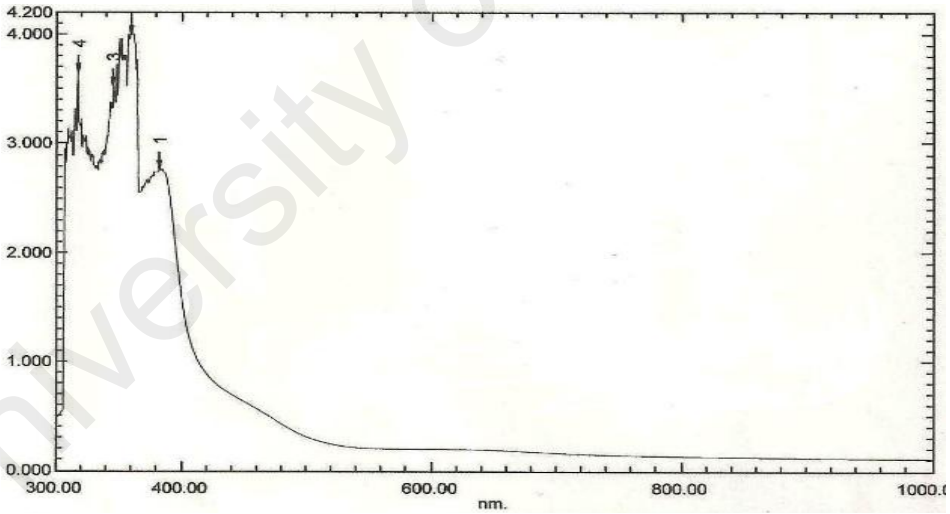

(b)

Figure 4.9 UV-vis spectra of [Cu(L1)] as a: (a) solid; and (b) solution in $CHCl_3$

The effective **magnetic moment** (μ_{eff}) of [Cu(L1)] was determined by the Guoy method at room temperature and using Equations 1 – 3.

$$\chi_m = \chi_g \,.Formula\ Weight \ldots\ldots\ldots\ldots \quad (1)$$

$$\chi_m^{corr} = \chi_m - \chi_{dia} \qquad \ldots\ldots\ldots\ldots \quad (2)$$

$$\mu_{eff} = 2.84\sqrt{\chi_m^{corr} T - N\alpha} \qquad \ldots\ldots\ldots\ldots \quad (3)$$

The μ_{eff} value, calculated for a monomeric formula and from the values of χ_g (3.71 x 10^{-6} cm^3 g^{-1}),χ_M (1.54 x $10^{-3}cm^3$ mol^{-1}), χ_{dia} (-2.16 x $10^{-4}cm^3$ mol^{-1}), χ_M^{corr} (1.75 x $10^{-3}cm^3$ mol^{-1}) and Nα (60 x 10^{-6} cm^3 mol^{-1}), was 1.97 B.M. at 300 K. This is slightly higher than the expected spin-only value of 1.73 B.M. for complexes of Cu(II) (valence electronic configuration $3d^9$; one unpaired electron) [10], suggesting slight distortion of the planar geometry of Cu(II). Additionally, if the complex adopted the dimericstructure as shown in**Figure 4.7**, the result suggests insignificant interaction between the two Cu(II) centres.

From its **TGA** trace, the complex started to lose 80.1% of its weight from 310 °C to 800 °C due to the decomposition of the ligand (expected, 80.8%). The amount of residue at temperatures above 800 °C was 19.9% (expected, 19.2%, assuming pure CuO [11]. The good agreement between the experimental and calculated values further supports the proposed chemical formula.

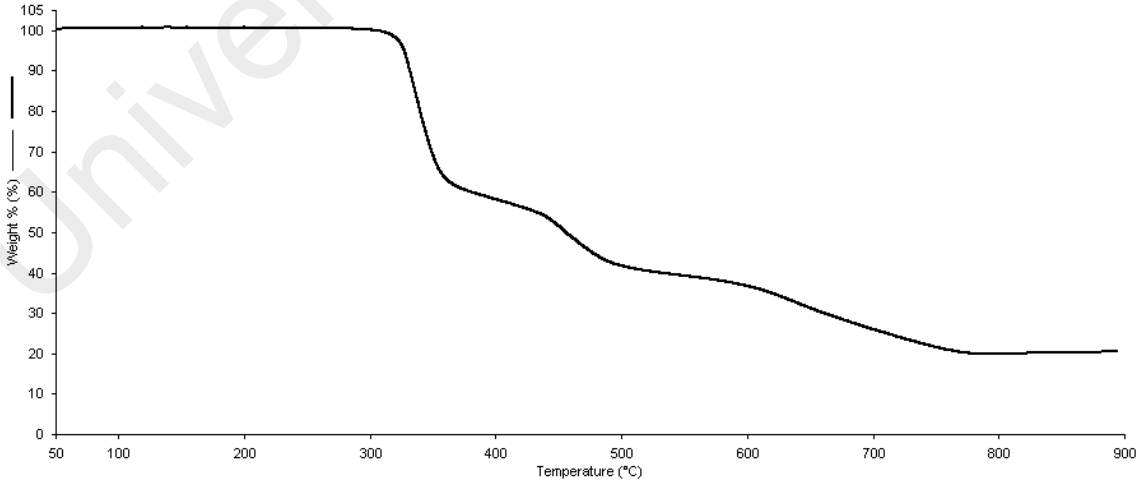

Figure 4.10 TGA trace of [Cu(L1)]

Its **DSC**, recorded in the temperature range 30 – 300 °C (**Figure 4.11**), shows an endothermic peak at 190.2 °C (ΔH = + 41.6 kJ mol^{-1}). When viewed under POM, the sample became fluid at 189 °C. However, no optical texture was observed on cooling

from 200 °C, and the sample remained fluid on further cooling to room temperature. Combining POM and DSC results, it may be suggested that on heating, the imine bond of the complex was hydrolysed to 1,8-diaminooctane and 2-hydroxybenzaldehyde (a liquid at room temperature). The presence of water in the sample, which was not apparent in its chemical formula, was likely due to atmospheric absorption.

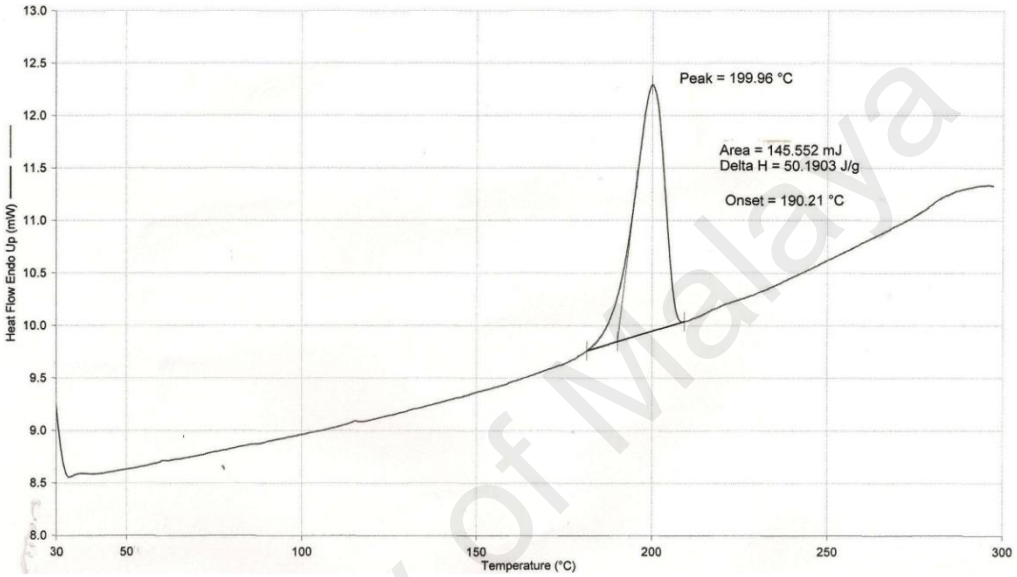

Figure 4.11DSC trace of [Cu(L1)]

(b) M = Ni

H_2L1 reacted with $[Ni(CH_3(CH_2)_{14}COO)_2]$ to form a pale khaki-green powder (yield:39.7%). Based on the instrumental data discussed below, the structural formula of the complex formed is [Ni(L1)], which is similar to the corresponding Cu(II) complex (**Section 4.2.3(a)**).

The results of the **elemental analyses**were in good agreement with the chemical formula calculated for $C_{22}H_{26}NiN_2O_2$ (FW: 409 g mol^{-1}): C, 64.6; H, 6.4; N, 6.9. Found: C, 64.8; H, 6.7; N, 6.8.

Its **FTIR spectrum** (**Figure 4.12, Table 4.2**) showssimilar peaks as found for the corresponding Cu(II) complex and may be similarly assigned.

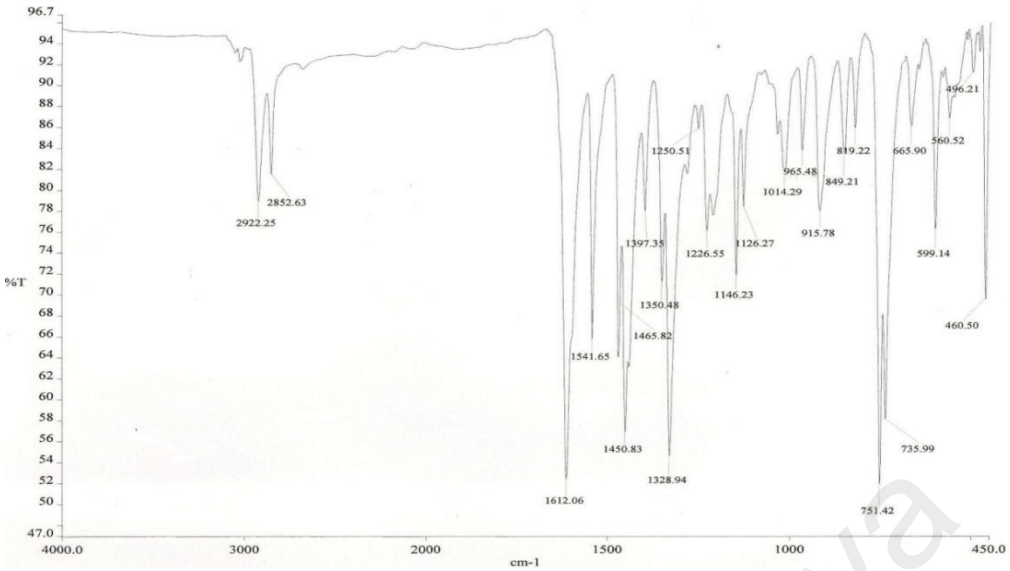

Figure 4.12 FTIR spectrum of [Ni(L1)]

The **UV-vis** spectrum of the solid sample (**Figure 4.13**(a)) shows a strong band at 422nm assigned to nickel(II)-to-phenoxide CT transition, and a weak band at 627nm for the *d-d*transition. These results suggest a square planar geometry at Ni(II) for the complex. The spectrum for a solution of the complex in chloroform (**Figure 4.13**(b)) shows a broad *d-d* band at 675 nm (ε_{max} = 80 cm^{-1} M^{-1}). Hence, there was a slight geometrical changewhen the solid dissolved in chloroform.

The χ_g value of [Ni(L1)],obtained by the Gouy method (**Section 4.2.3(a)**), was -8.0 x $10^{-8}cm^3$ g^{-1}. The negative value means that the complex was diamagnetic, hence Ni(II) was square planar. The magnetic result was in agreement with that of UV-vis spectroscopy.

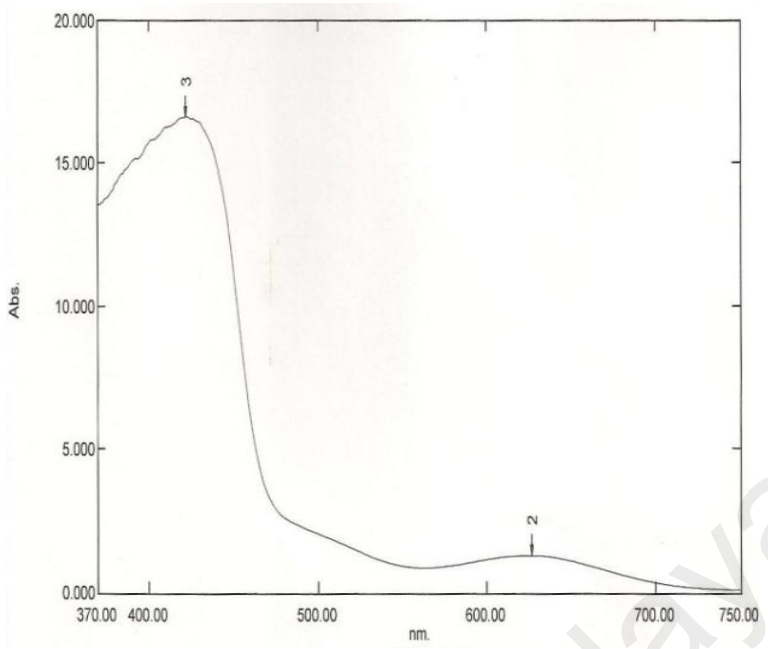

(a)

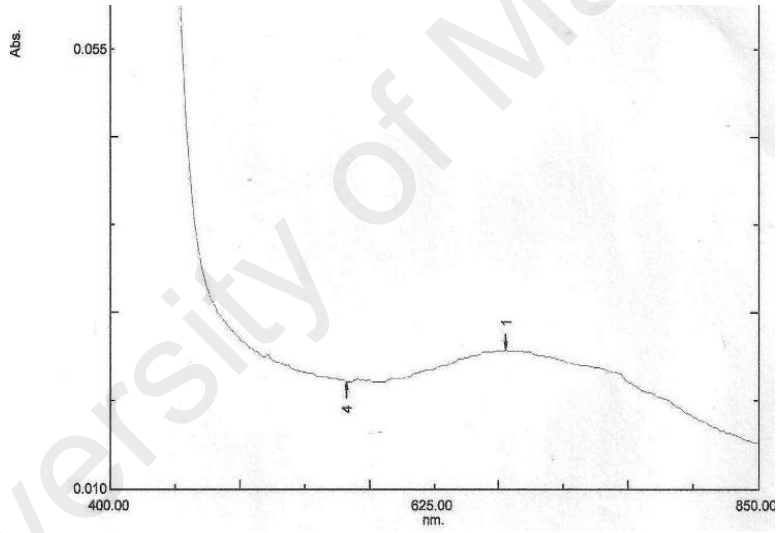

(b)

Figure 4.13UV-vis spectra of [Ni(L1)]: (a) solid; and (b) solution in $CHCl_3$

From the **TGA** scan, the complex started to lose 82.1% of its weight from 313 °C to 800 °C, due to the decomposition of the ligand (expected, 80.2%). The amount of residue at temperatures above 800 °C was 17.9% (expected, 19.8% assuming pure NiO). Hence, there was a good agreement between the experimental and calculated results.

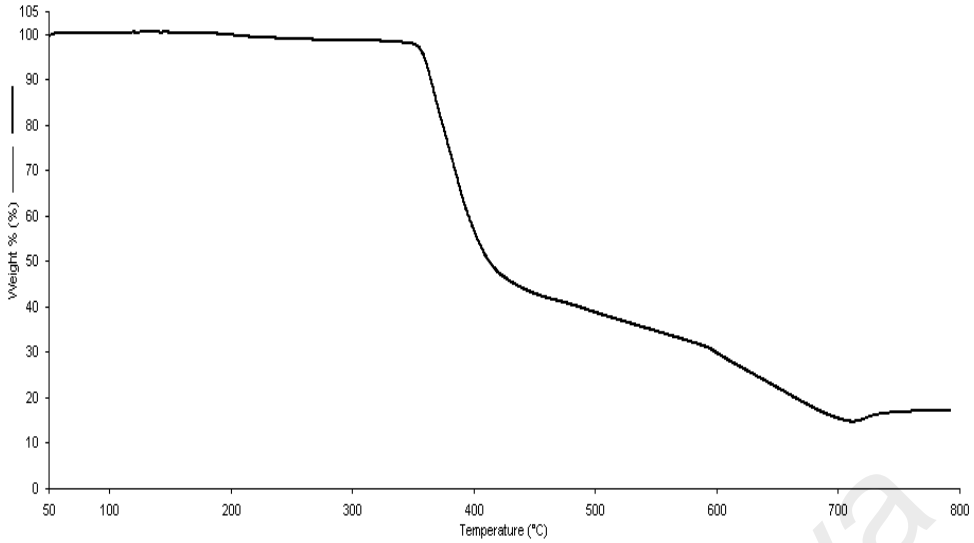

Figure 4.14 TGA thermogram of [Ni(L1)]

The **DSC**scan of the complex, recorded from 30 °C to 300 °C (**Figure 4.15**), shows an endothermic peak at 263.5 °C (ΔH = + 26.1 kJ mol^{-1}). Under POM, it was observed to be fluid at 253 °C. Upon cooling to room temperature, there was no optical texture and the sample remained fluid. This observation was similar to that for the corresponding Cu(II) complex, and may be similarly explained.

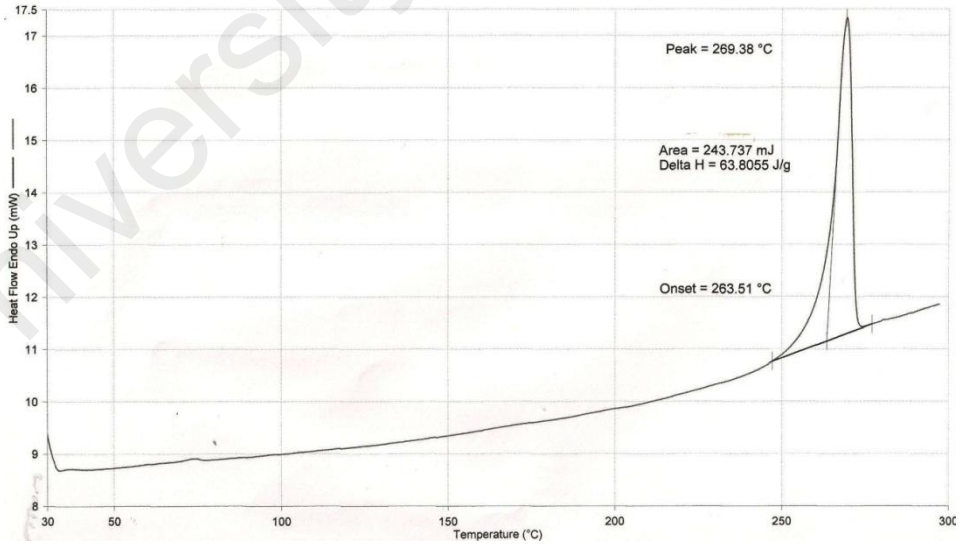

Figure 4.15 DSC trace of [Ni(L1)]

(c) M = Co

H_2L1 reacted with $[Co(CH_3(CH_2)_{14}COO)_2]$ to form a fine black solid (yield: 78.7%). However, attempted crystallization using ethanol was unsuccessful. Based on the

instrumental data presented below, it is proposed that the structural formula of the complex is [Co(L1)], which is similar to those of the corresponding Cu(II) and Ni(II) complexes.

The results ofthe **elemental analyses**were in good agreement with the chemical formula calculated for $C_{22}H_{26}CoN_2O_2$ (FW: 409.39 g mol^{-1}): C, 64.5; H, 6.4; N, 6.8. Found: C, 65.0; H, 6.5; N, 6.9

Its **FTIR spectrum** (**Figure 4.16**) is similar to those of the corresponding Cu(II) and Ni(II) complexes (**Section 4.2.3(a)** and **4.2.3(b)**).

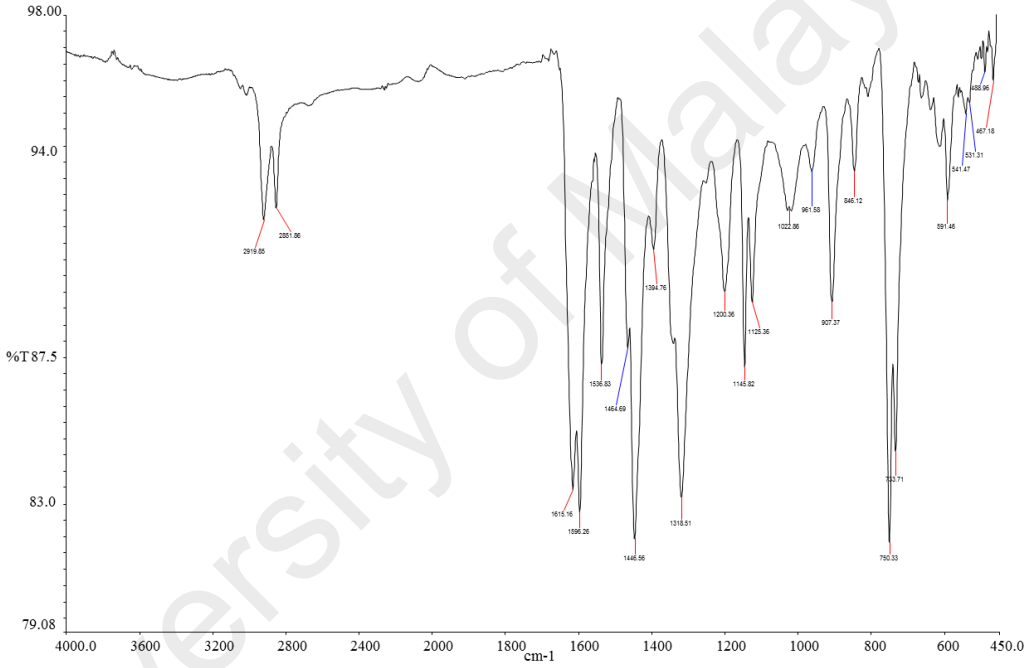

Figure 4.16 FTIR spectrum of [Co(L1)]

The **UV-vis** spectrum of solid [Co(L1)] (**Figure 4.17**(a)) shows an MLCT band at 467 nm, and a *d-d* band at 567 nm for $(t_{2g})^6(e_g)^1$ to $(t_{2g})^5(e_g)^2$ electronic transitions.This indicates the most probable geometry of Co(II) in the complex was square planar. In solution, the spectrum (**Figure 4.17**(b)) shows a MLCT band at 344 nm (ε = 3463 cm^{-1} M^{-1}) and a *d-d* band at 656 nm (ε = 682 cm^{-1} M^{-1}). Hence, the complex maintained its geometry at Co(II) in solution, as similarly observed for the corresponding Cu(II) and Ni(II) complexes.

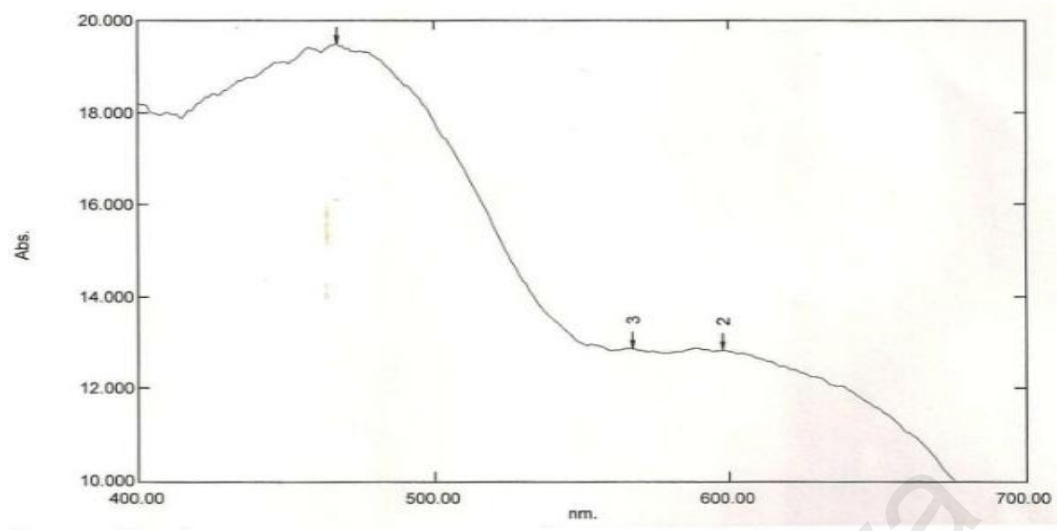

(a)

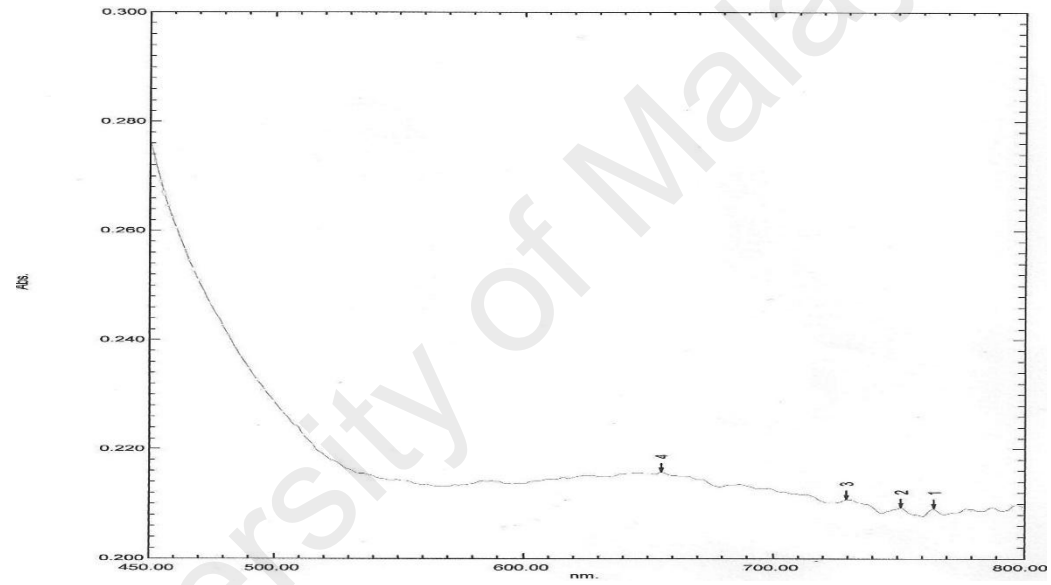

(b)

Figure 4.17 UV-vis spectra of [Co(L1)] (a) solid; and (b) solution in $CHCl_3$

The μ_{eff} of [Co(L1)], calculated as before from the values of χ_g (4.45×10^{-6}cm^3 g^{-1}), χ_M (1.82×10^{-3}cm^3 mol^{-1}), χ_{dia} (-2.16×10^{-4}cm^3 mol^{-1}), and χ_M^{corr} (2.04×10^{-3} cm^3 mol^{-1}), was 2.2 B.M. at 300 K. The expected spin-only value for a Co(II) complex ($3d^7$) with one unpaired electron is 1.73 B.M.The experimental value is within the range reported for many square planar Co(II) complexes[10,12].

A superconducting quantum interference device (**SQUID**) magnetometry was also used to probe the magnetic property of [Co(L1)]. The magnetic measurement was

recorded from 300 K to 2 K, and the magnetic field 1 Tesla. A plot of $\chi_M T$ vs. *T*is shown in **Figure 4.18**.

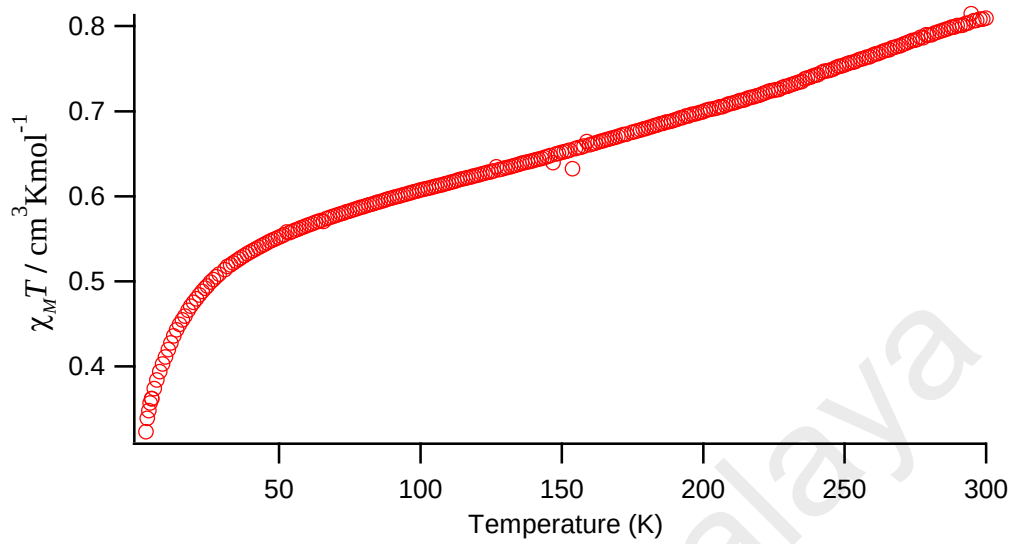

Figure 4.18$\chi_M T$ vs. *T* of [Co(L1)]o, experimental curve

From the graph, the $\chi_M T$value was 0.8 cm^3 K mol^{-1} at 300 K. On cooling, the value decreasedgradually to about 0.5 cm^3 K mol^{-1} at 30 K, and then rapidly until it was 0.3 cm^3 K mol^{-1}at 2 K. The μ_{eff}value at room temperature was 2.54 B.M, which is in a good agreement with the theoretical value of 1.73 B.M. for one unpaired electron, and the Néeltemperature (T_N), which is the temperature at which there is enough thermal energy to destroy the magnetic ordering of the material, was 30 K.Hence, it may be inferred that there exists an antiferomagetic interaction between the Co(II) centres in the complex.

From the **TGA** scan, the complex started to lose 91% of its weight from 90 °C to 800 °C, due to evaporation of water (2.3%) and decomposition of the ligand (expected, 85.6%).Unlike previous complexes, the percentage of the residue of this Co(II) cannot be determined as there is no distinct plateau in the thermogram. The sample started to lose weight at low temperature due to loss of water absorbed during storage [13].

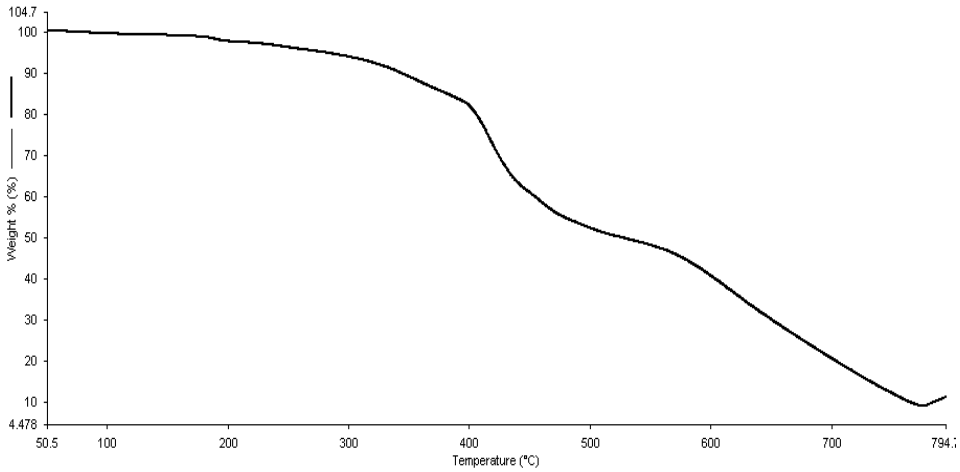

Figure 4.19 TGA thermogram of [Co(L1)]

The **DSC**, recorded in the temperature range 30 – 300 °C (**Figure 4.20**), shows broadoverlapping endotherms, starting at quite low temperature (about 50 °C). The result is consistent with dissociation of water molecules and hydrolysis of the complex.This is further supported by POM, which did not show any optical textures on cooling and the sample remained fluid at room temperature, as was similarly observed for the corresponding Cu(II) and Ni(II) complexes.

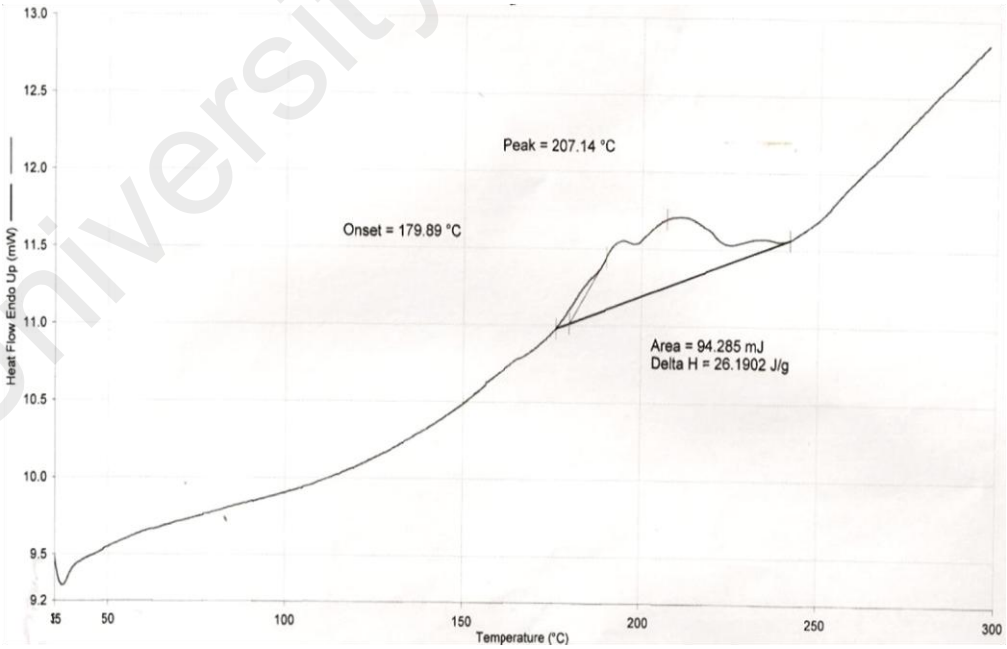

Figure 4.20DSC trace of [Co(L1)]

(d) M = Fe

H_2L1 reacted with $[Fe(CH_3(CH_2)_{14}COO)_2]$ to form a dark brown powder (Yield: 46.6%). Based on similar analytical data as for previously discussed complexes, the structural formula proposed for the product is $[Fe_2(CH_3(CH_2)_{14}COO)_2(L1)(H_2O)_4].2.5H_2O$ (**Figure 4.21**). Hence, unlike the corresponding Cu(II), Ni(II) and Co(II) complexes, Fe(II) complex was dinuclear and has two hexadecanoato ligands in addition to L1.

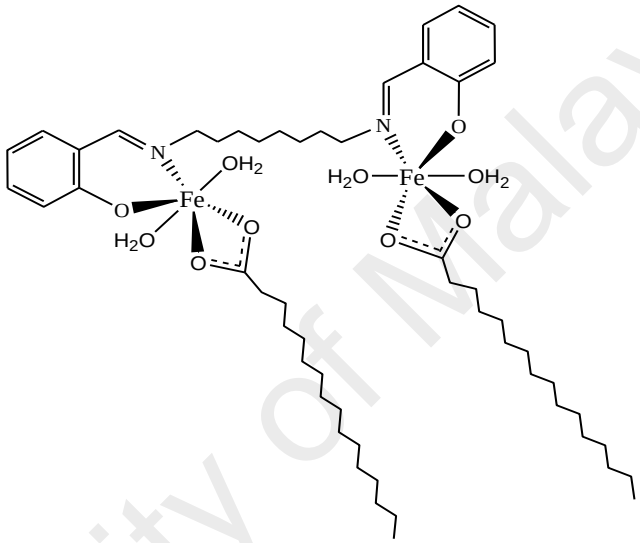

Figure 4.21 Proposed structural formula of $[Fe_2(CH_3(CH_2)_{14}COO)_2(L1)(H_2O)_4].2.5H_2O$

The results of the **elemental analyses**were in good agreement with the chemical formula calculated for $C_{54}H_{102}Fe_2N_2O_{13}$ (FW: 1090.6 g mol^{-1}):C, 59.5; H, 9.2; N, 2.5. Found: C, 59.1; H, 8.6; N, 2.9.

Its **FTIR spectrum** (**Figure 4.22**) shows a broad peak at 3396 cm^{-1} for coordinated H_2O, two strong peaks at 2917 cm^{-1} and 2849 cm^{-1} for $\bar{\upsilon}_{asym}CH_2and\bar{\upsilon}_{sym}CH_2$respectively, a weak peak at 1612 cm^{-1} for $\bar{\upsilon}$C=N, a strong peak at 1574 cm^{-1} for $\bar{\upsilon}_{asym}$COO, and a peak at 1446 cm^{-1} for $\bar{\upsilon}_{sym}$COO. From the latter peaks, the Δ value was 128 cm^{-1}, suggesting a chelating binding mode for $CH_3(CH_2)_{14}COO$ ligand [6, 14].

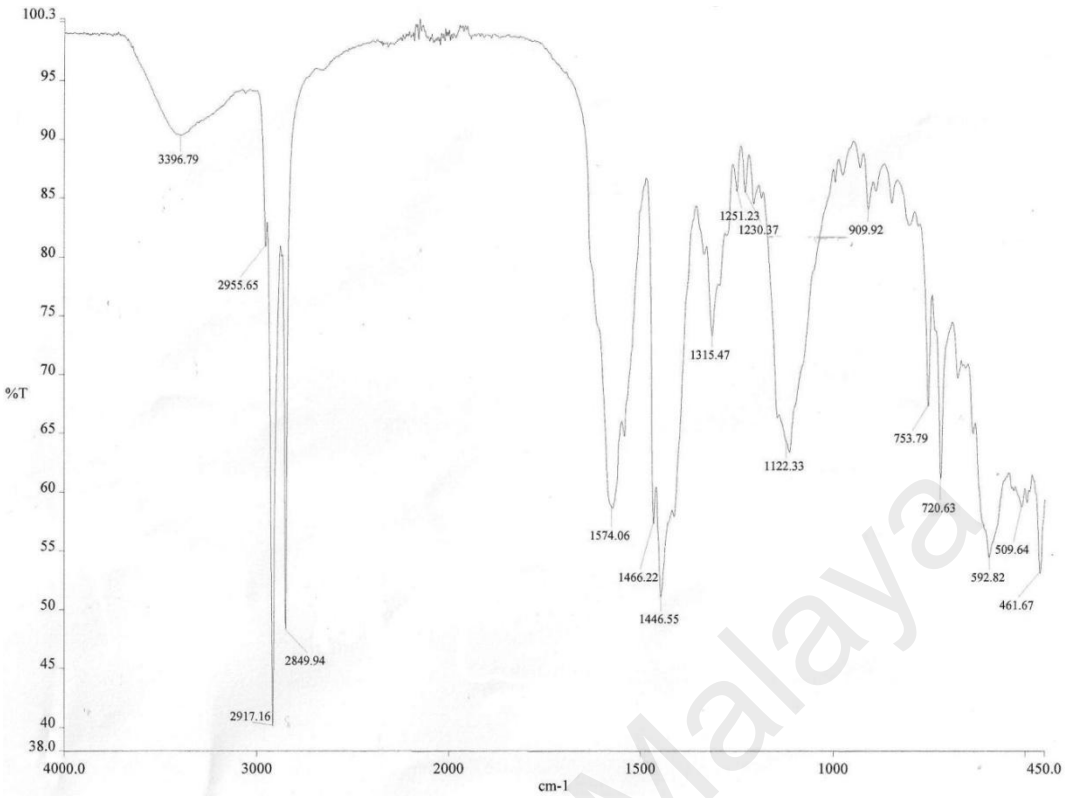

Figure 4.22 FTIR spectrum of $[Fe_2(CH_3(CH_2)_{14}COO)_2(L1)(H_2O)_4].2.5H_2O$

The **UV-vis** spectrum of solid$[Fe_2(CH_3(CH_2)_{14}COO)_2(L1)(H_2O)_4].2.5H_2O$ (**Figure 4.23 (a)**) shows a band at about 479 nm which may be assigned to the $^1A_{1g} \rightarrow {}^1T_{1g}$ transition.The spectrum of the complex dissolved in chloroform shows two overlapping bands at 468 nm (ε_{max} = 114.3 M^{-1} cm^{-1}) assigned to n → π* electronic, and at 510 nm (ε_{max} = 63.5 M^{-1} cm^{-1}) assigned to $^1A_{1g} \rightarrow {}^1T_{1g}$ electronic transition for LS Fe(II).

The μ_{eff}value of the complex, calculated as before from the values of χ_g (1.22 x 10^{-5} cm^3 g^{-1}), χ_M (1.33 x 10^{-2} cm^3 mol^{-1}), χ_{dia} (-6.96 x 10^{-4} cm^3 mol^{-1}), and χ_M^{corr} (1.26 x 10^{-2} cm^3 mol^{-1}), was 5.79 B. M. The expected value for a two HS Fe(II) complex (four unpaired electrons each) is 8.94 B.M., assuming perfect octahedral geometry at both Fe(II) centres. Since LS Fe(II) is diamagnetic (μ_{eff}= 0 B.M.), it may be inferred that the complex was made up of 64.7% HS Fe(II) and 35.3% LS Fe(II) atoms [15].

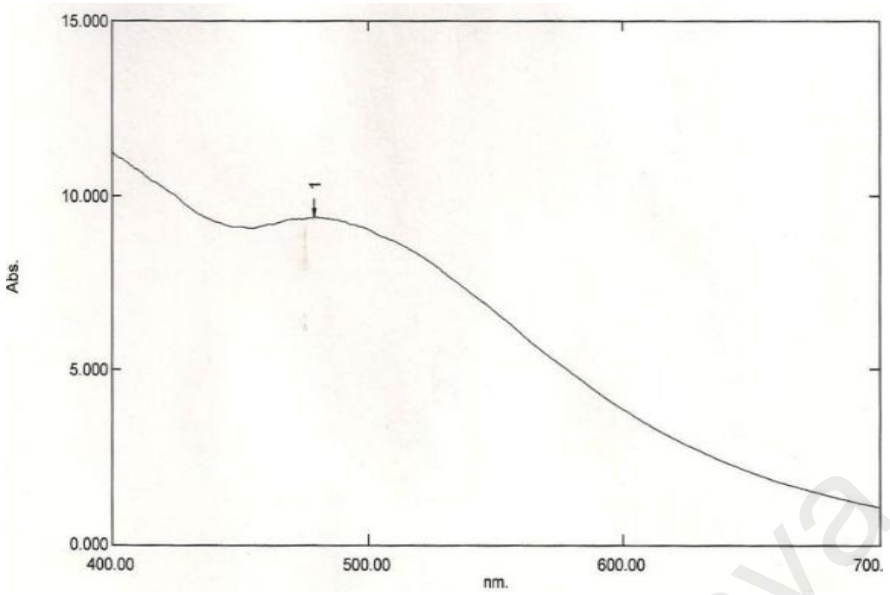

(a)

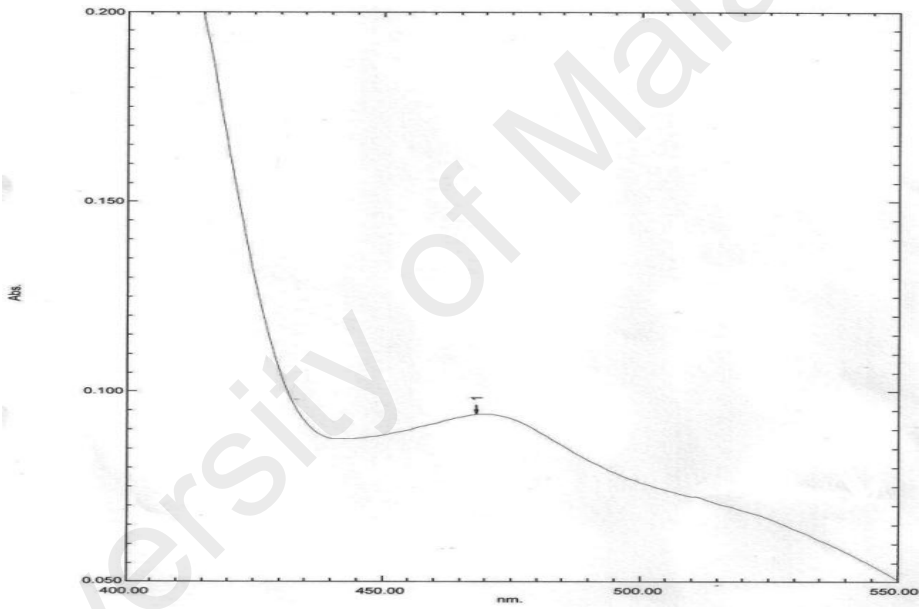

(b)

Figure 4.23 UV-vis spectra of $[Fe_2(CH_3(CH_2)_{14}COO)_2(L1)(H_2O)_4].2.5H_2O$: (a) solid sample; and (b) solution in $CHCl_3$

The temperature dependence of the **magnetic susceptibility** was measured in the form of $\chi_M T$ versus T using the SQUID magnetometer (**Figure 4.24**). It is observed that the experimental curve shows a good fit with the theoretical curve obtained using the formula for a symmetrical dinuclear complex [16], and inserting the values of g= 1.3 and J = - 28.4 cm^{-1} into the formula.

$$\chi_m = \frac{Ng^2\beta^2}{3kT}\frac{\sum_S S(S+1)(2S+1)\exp[-\frac{E(S)}{kT}]}{\sum_S (2S+1)\exp[-\frac{S}{kT}]}$$

$$E(S) = -J/2\, S(S+1)$$

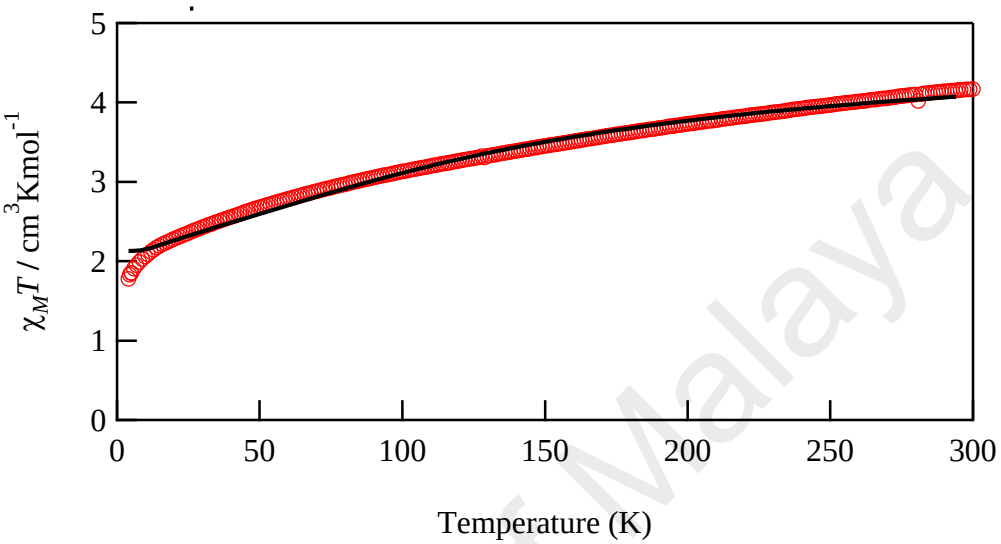

Figure 4.24 Plot of$\chi_M T$ vs. T for[$Fe_2(CH_3(CH_2)_{14}COO)_2(L1)(H_2O)_4$].2.5$H_2O$; o, experimental curve, - fitting curve.

From the graph, the $\chi_M T$ values decreased gradually from 4.15 cm^3 K mol^{-1} at 294 K to 2.03 cm^3K mol^{-1} at 8.8 K, and then rapidly to about 1.78 cm^3 K mol^{-1} at 4 K as a result of zero-field splitting. It is also noted that the *g* value was significantly lower than the theoretical value (2.0023), suggesting a highly distorted octahedral environment, expected for HS Fe(II) atoms due to the weaker Fe-L bonds. The calculated *J* value means that there was a weak antiferromagnetic interactionbetween the two Fe(II) centres, which may occur through H-bonds between the coordinated and lattice H_2O.

From the **TGA** trace, the complex started to lose 82.1% of its weight from 198 °C to 800 °C, due to the decomposition of the ligand (expected, 85.3%). The amount of residue at temperatures above800 °C was 17.9% (expected, 14.7%; assuming pure Fe_2O_3 [11]. Hence, there was a good agreement between the experimental and calculated results.

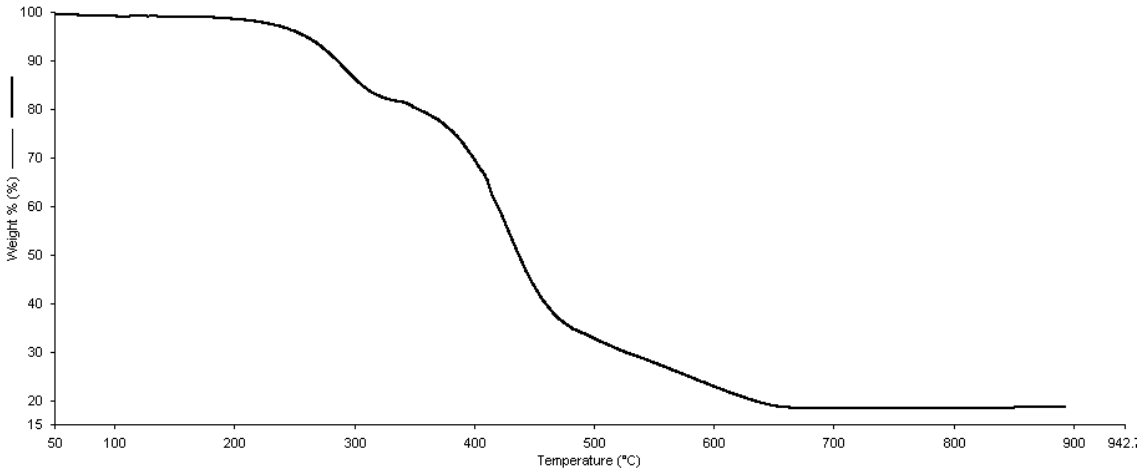

Figure 4.25 TGA thermogram of $[Fe_2(CH_3(CH_2)_{14}COO)_2(L1)(H_2O)_4].2.5H_2O$

The **DSC**scan shows two overlapping endotherms on heating at 77°C ($\Delta H_{combined}$ = + 48 kJ mol^{-1}), assigned to the breaking of H-bonds in the complex. When observed under OPM, the sample became fluid at 104 °C, but there were no optical textures upon cooling from 180 °C. This is similar to the corresponding complexes, and may be similarly explained.

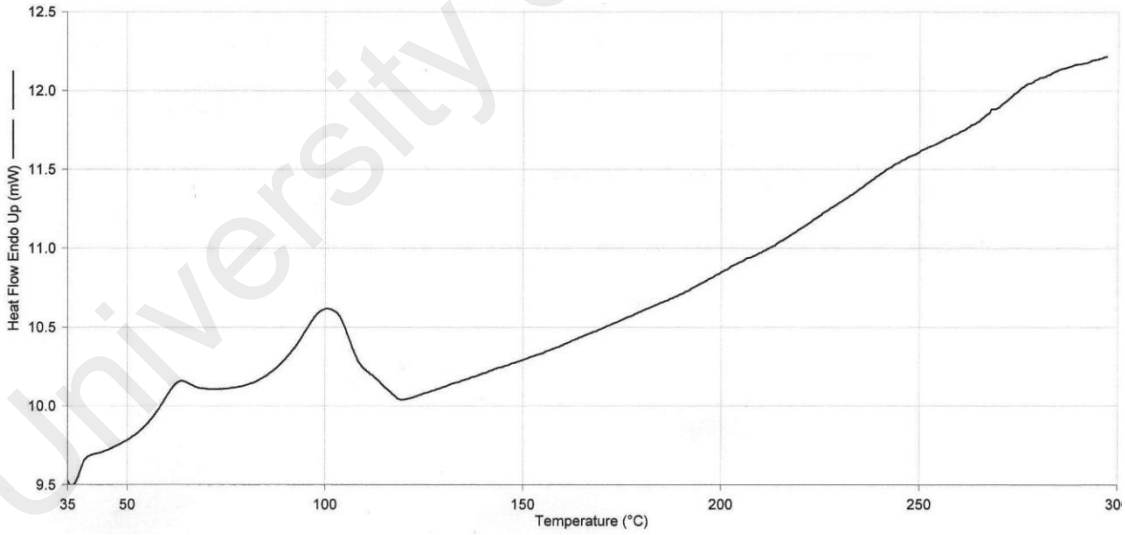

Figure 4.26 DSC trace of $[Fe_2(CH_3(CH_2)_{14}COO)_2(L1)(H_2O)_4].2.5H_2O$

4.2.4 Summary

To summarise,L1 formed mononuclear complexes with Cu(II), Ni(II) and Co(II)with general formula [M(L1)], and formed dinuclearoctahedral complex with Fe(II) with the structural formula, $[Fe_2(CH_3(CH_2)_{14}COO)_2(L1)(H_2O)_4].2.5H_2O$. The Ni(II) complex was diamagnetic, while the other complexes were paramagnetic. All complexes were hydrolysed by water on heating, and hence did not exhibit any mesophases.

4.3 Synthesis, Structural Deduction and Characterisation of Complexes of H_2L2

The second phase of this research was to synthesis H_2L2, which is an analog of H_2L1 but with longer alkyl chains, and to similarly ascertain its structure by elemental analyses, FTIR spectroscopy and ^{1}H-NMR spectroscopy. This was followed by reacting $H_2L2$with $[M(CH_3(CH_2)_{14}COO)_2]$ (M = Cu, Ni, Co, Fe), and the complexes formed analysed as before by elemental analyses, FTIR spectroscopy, UV-vis spectroscopy, magnetic susceptibility, TGA, DSC, and OPM.

4.3.1 Synthesis and characterization of H_2L2

H_2L2 was obtained as yellow small crystals from the reaction of 1,10-diaminodecane and 2-hydroxybenzaldehyde (mole ratio = 2:1). The solvent used was ethanol and the yield was 74.2%.However, its structure could not be determined by single crystal X-ray crystallography due to poor diffraction. Hence, its structural formula was ascertained from instrumental data.

The results of the **elemental analyses** (75.5% C, 8.8% H, 7.3% N) were in good agreement with the chemical formula $C_{12}H_{16}NO$ (75.8% C, 8.5% H, 8.4% N). Its structure was further supported by ^{1}H-NMR spectrum (**Figure 4.27)** and peak assignments (**Table 4.4)**.

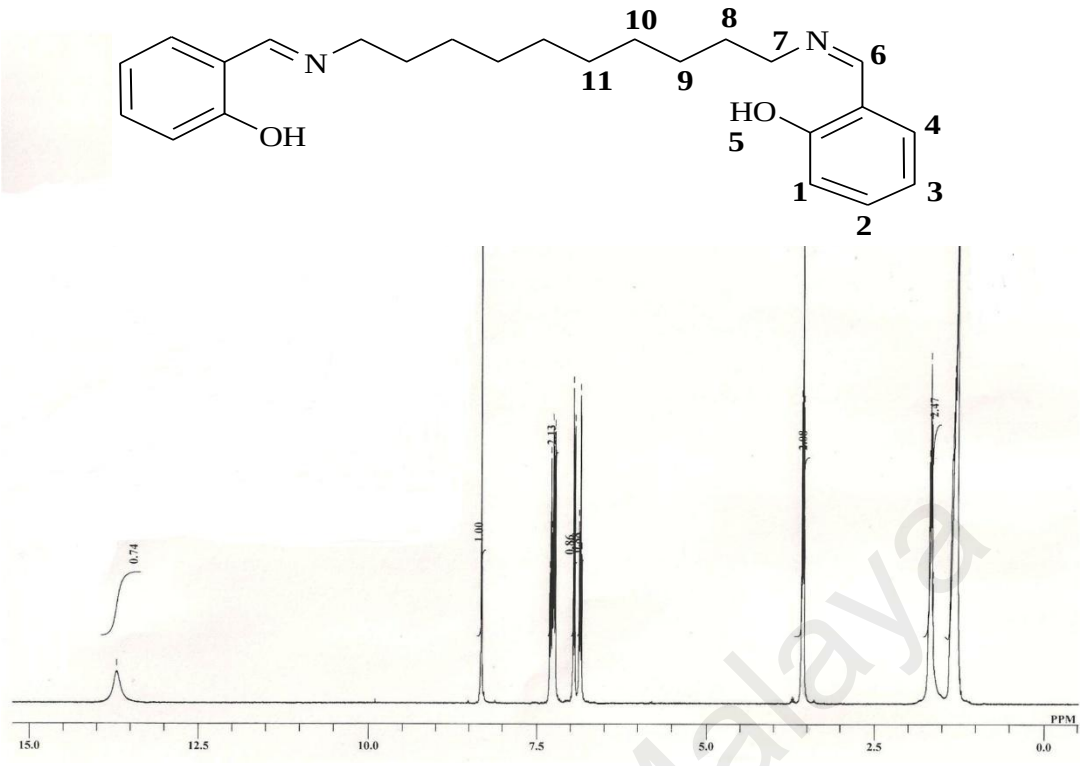

Figure 4.27 ^{1}H-NMR spectrum of H_2L2

Table 4.4 The ^{1}H-NMR data and assignment for H_2L2

Chemical Shift (ppm)	Integral	Multiplicity	Assignment
1.3 – 1.7	8.5	multiplet	H-8, H-9, H-10, H-11
3.5	2.0	triplet	H-7
6.8	0.8	triplet	H-3
6.9	0.8	doublet	H-4
7.2	1.05	triplet	H-2
7.3	1.05	doublet	H-1
8.3	1.0	singlet	H-6
13.7	0.74	singlet	H-5

Its **FTIR**spectrum (**Figure 4.28**) and data (**Table 4.5)**,which also includes the data for the corresponding complexes for later discussion) showthe expected peaks as previously discussed for H_2L1.

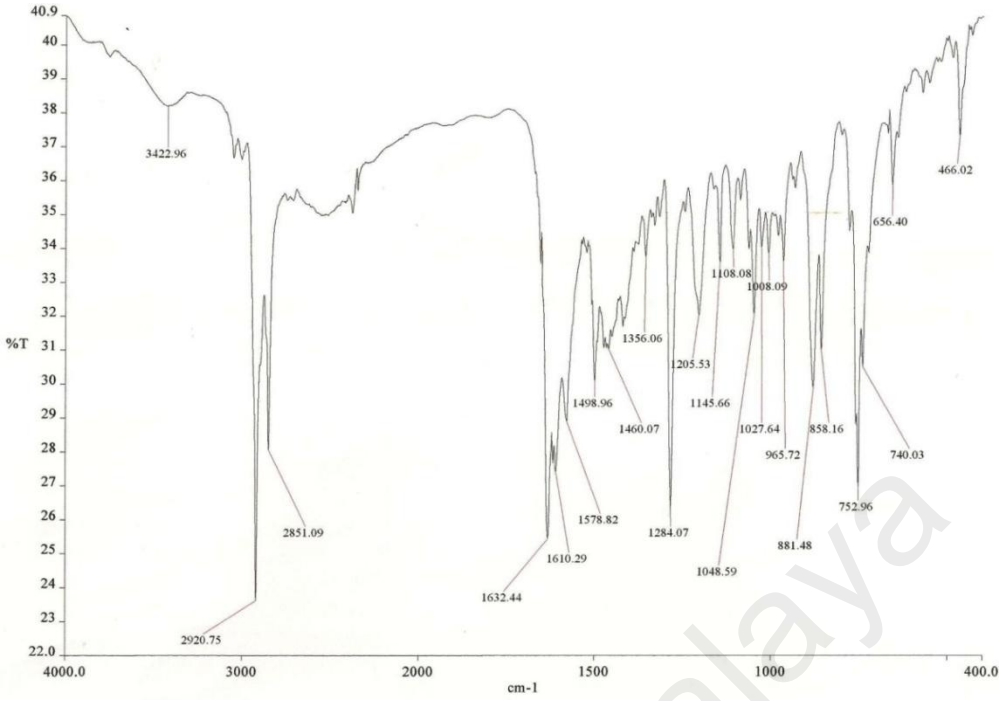

Figure 4.28IR spectrum of H_2L2

Table 4.5 The FTIR data for H_2L2 and its metal complexes; R = $CH_3(CH_2)_{14}COO$

Compound	Assignment/$\bar{\upsilon}$ (cm^{-1})					
	OH	CH_2 (asym)	CH_2 (sym)	C=N	M-O	M-N
H_2L2	3422	2920	2851	1632	-	-
[Cu(L2)]	-	2919	2849	1616	578	492
[Ni(L2)].EtOH	3300	2916	2849	1613	561	461
$[Co_2(L2)(HL2)_2(EtOH)_4]$	3100 - 3400	2918	2850	1617	591	461
$[Fe_2(R)(L2)(HL2)_2(H_2O)_2].H_2O$	3375	2921	2851	1618	520	450

TGA (**Figure 4.29**) shows that H_2L2 started to lose 99.2% of its mass in the temperature range of 233 – 840 °C. The **DSC** trace (**Figure 4.30**) shows one endothermic peak at onset temperature of 63.8 °C (ΔH = + 53.4 kJ mol^{-1}), assigned as its melting temperature. Observed under **OPM**, the sample melted at 60.2 °C and cleared to an isotropic liquid (I) at 67.0 °C. Upon cooling from I, it showed an optical texture corresponding to crystallization at 37.0 °C (**Figure 4.31**).

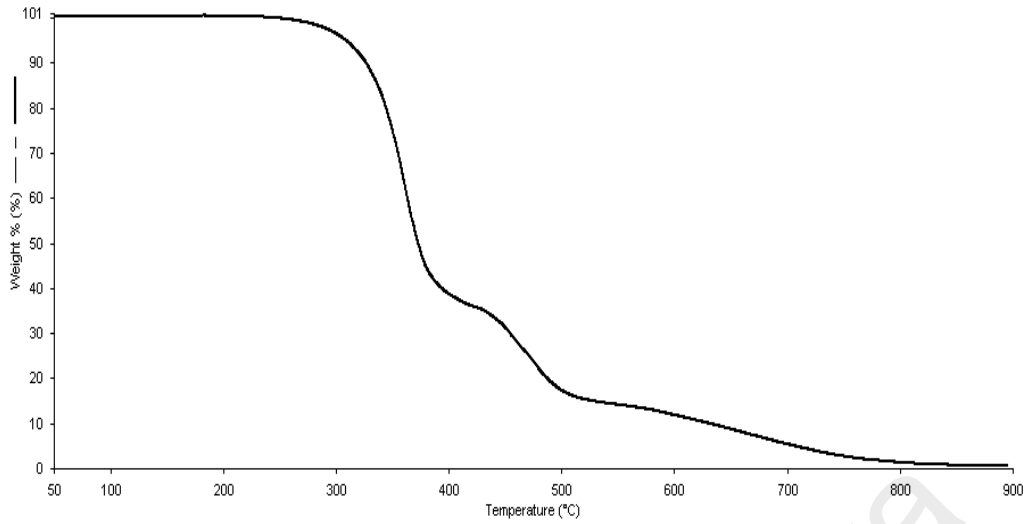

Figure 4.29TGA trace of H_2L2

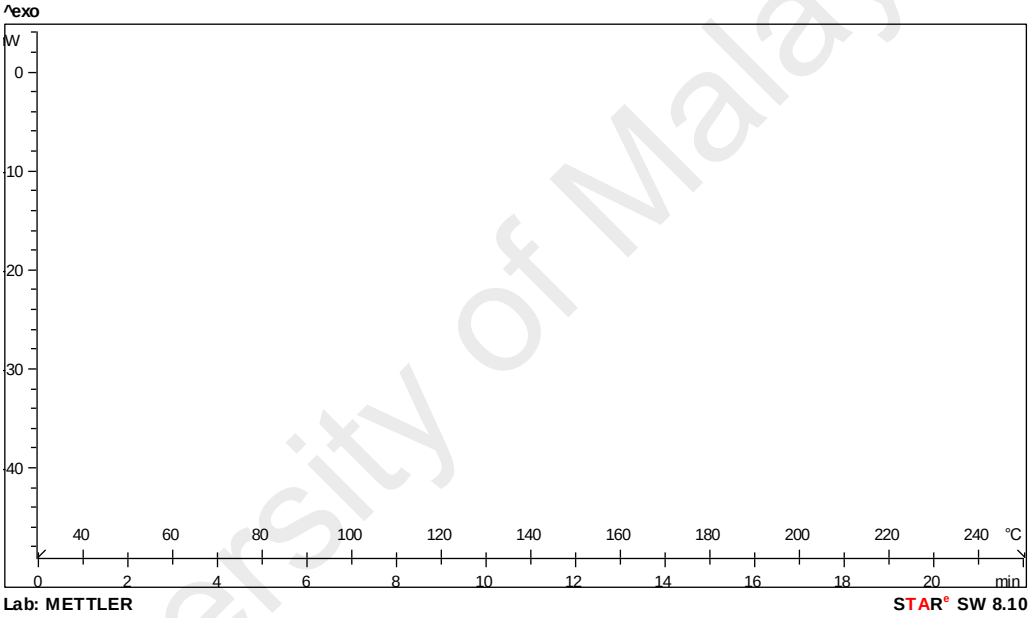

Figure 4.30DSC trace of H_2L2

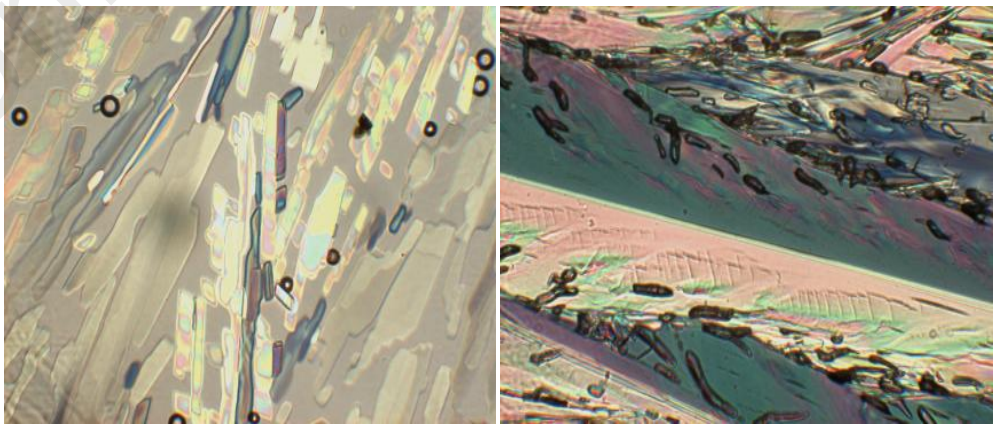

(a) (b)

Figure 4.31 Photomicrographs of H_2L2 at: (a) 62.0 °C (melting), and (b) 37.0 °C (crystallizing)

4.3.2 Metal complexes of H_2L2

Two methods were used to prepare metal(II) complexes of H_2L2, namely step-wise and one-pot reactions. The main objective was to see if the reaction products were method-dependence, especially since complexes obtained from H_2L1 differed from the expected products from the reaction of their analog (n = 9) [1].

(a) Step-wise method

The step-wise reaction was the method used to prepare metal(II) complexes of H_2L1 (**Section 4.2.3**).

(i) Copper(II) complex of H_2L2

H_2L2 reacted with $[Cu(CH_3(CH_2)_{14}COO)_2]$ to form a khaki green powder in 67.9% yield. Based on the analytical data presented below, it is proposed that its chemical formula was [Cu(L2)], which is similar to copper(II) complex of H_2L1, and is proposed to have similar dimeric structure (**Figure 4.32**)[4].

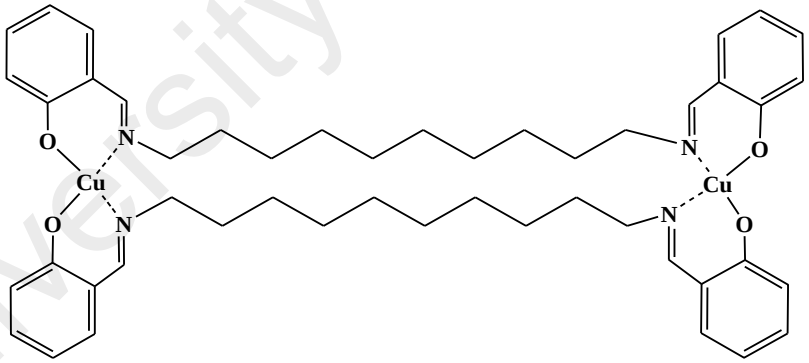

Figure 4.32 Proposed structural formula of $[Cu_2(L2)_2]$

The results of the **elemental analyses** were in good agreement with the chemical formula calculated for $C_{24}H_{30}CuN_2O_2$ (FW: 442 g mol^{-1}): C, 65.2; H, 6.8; N, 6.3%.Found: C, 65.9; H, 7.0; N, 6.2%.

Its **FTIR spectrum** (**Figure 4.33**) is similar to that of [Cu(L1)], and may be similarly assigned.

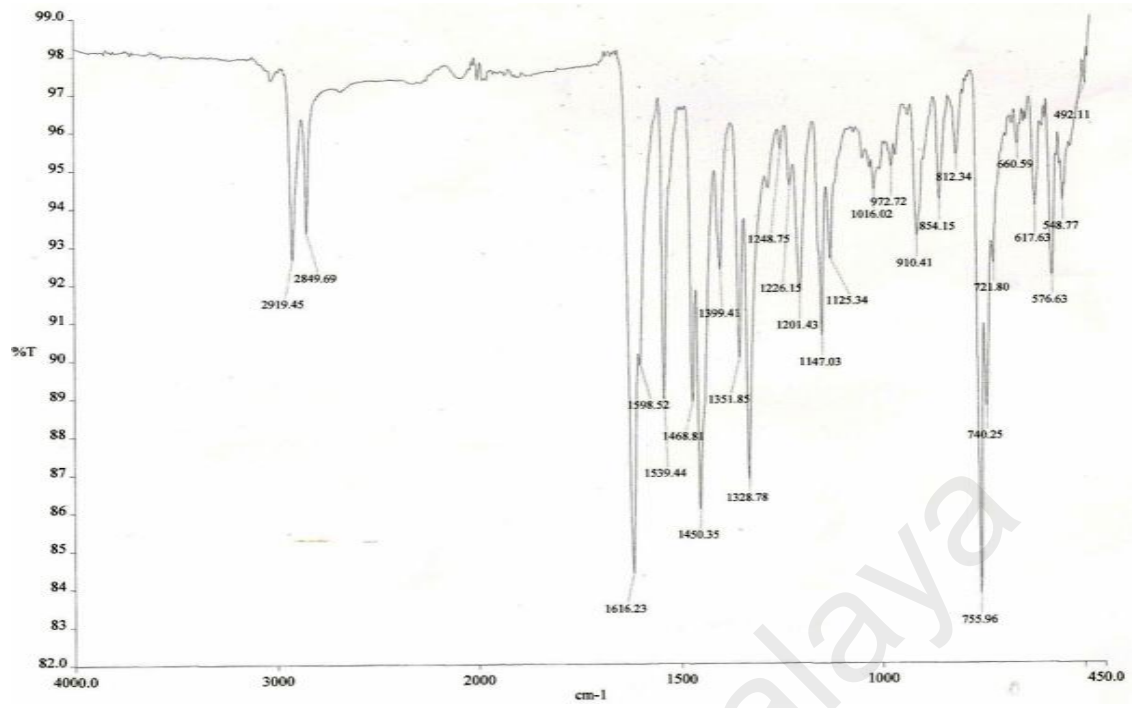

Figure 4.33FTIR spectrum of [Cu(L2)]

The **UV-vis**spectrum of [Cu(L2)] dissolved in $CHCl_3$ (**Figure 4.34**) shows a weak *d-d* bands at 599 nm (ε_{max}= 129.6 cm^{-1} M^{-1}). Hence, the geometry at Cu(II) is square planar. Also observed is a strong shoulder at 385 nmfor LMCT transition. It is noted that the geometry at Cu(II) for [Cu(L2)] is less distorted than [Cu(L1)], possibly due to the longer alkyl chain of L2 for the former complex.

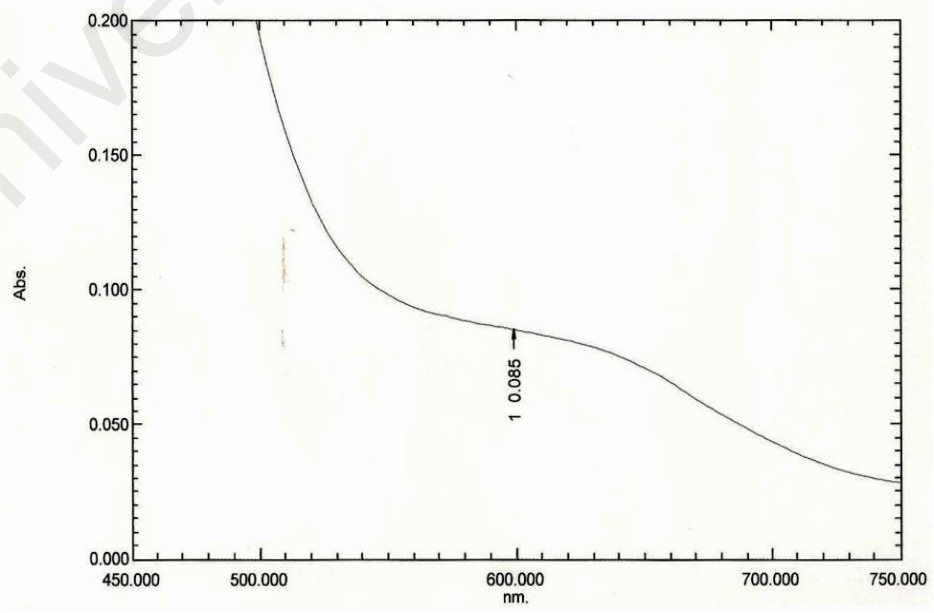

Figure 4.34 UV-vis spectrum of [Cu(L2)] in $CHCl_3$

The value of μ_{eff}, calculated as before from the values of χ_g (3.3 x 10^{-6}cm^3 g^{-1}), χ_M (1.46 x 10^{-3}cm^3 mol^{-1}), χ_{dia} (-2.28 x 10^{-4}cm^3 mol^{-1}) and χ_M^{corr} (1.69 x 10^{-3}cm^3 mol^{-1}), was 2.0 B.M. at 300 K. The value was similar found for [Cu(L1)] (μ_{eff} = 1.97 B.M.). Hence, the magnetic properties of the Cu(II) complexes is not affected by the difference length of the alkyl chain.

From **TGA** trace, [Cu(L2)] lost 85.4% of its weight on heating from 304 °C to 850 °C, due to the decomposition of the ligand (expected, 82.0%). Hence, the thermal decomposition is similar to the [Cu(L1)]. The amount of residue at temperatures above 850 °C was 14.6% (expected, 18.0%, assuming pure CuO).

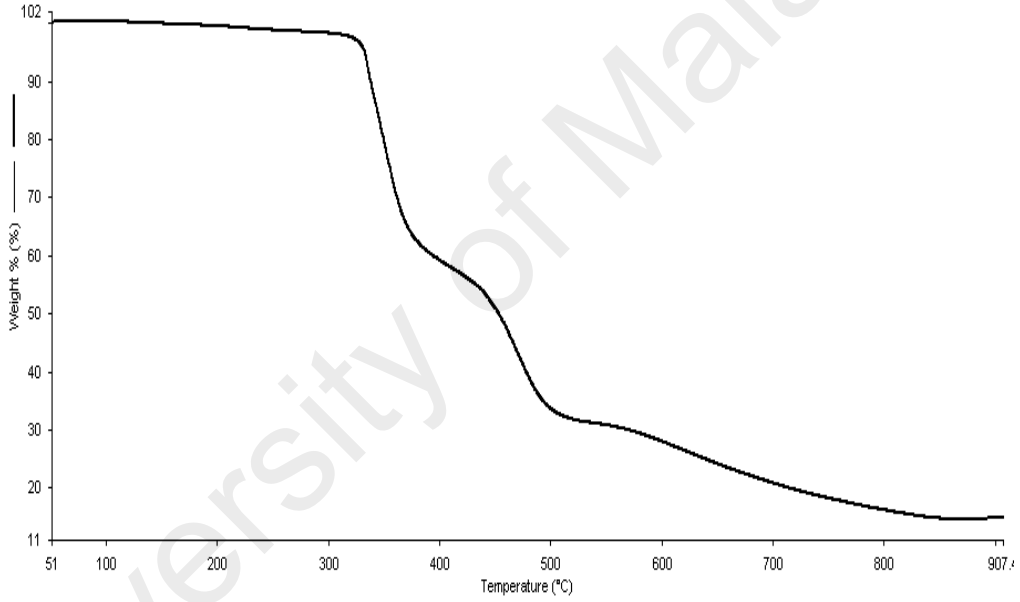

Figure 4.35 TGA trace of [Cu(L2)]

(ii) Ni(II) complex of H_2L2

H_2L2 reacted with [Ni($CH_3(CH_2)_{14}COO)_2$] to form a light khaki green powder (yield:68.3%). Based on the instrumental data discussed below, its proposed chemical formula is [Ni(L2)].CH_3CH_2OH.

The results of the **elemental analyses** were in good agreement with the chemical formula calculated for $C_{22}H_{26}NiN_2O_2$ (FW: 483.2 g mol^{-1}):C, 64.6; H, 7.5; N, 5.8%. Found: C, 65.0; H, 7.7; N, 5.5%.

Its **FTIR spectrum**(**Figure 4.36**, **Table 4.5**) shows a weak peak for the hydroxyl group at 3300 cm^{-1} as well peaks similarly found for the corresponding Cu(II) complex.

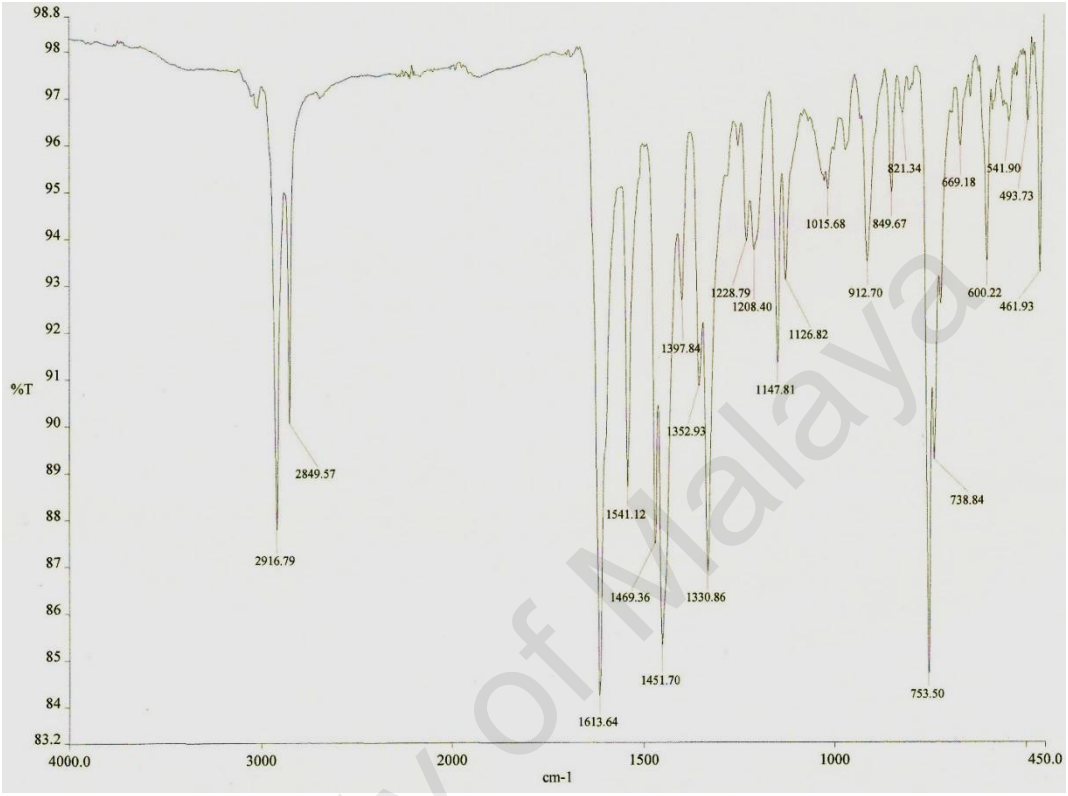

Figure 4.36IR of [Ni(L2)].CH_3CH_2OH

The **UV-vis**spectrum of the solid [Ni(L2)].CH_3CH_2OH (**Figure 4.37**) shows a *d-d* band at 630. These results suggest a square planar geometry at Ni(II) for the complex, which is similar to [Ni(L1)][17]. The spectrum for sample in solution could not be measured due to insolubility in most common solvents.

The χ_g value of [Ni(L2)].CH_3CH_2OH, determined as before by the Gouy method (**Section 4.2.3(a)**), was -7.0 x 10^{-7} cm^3 g^{-1}. The negative value means that the complex was diamagnetic, thus confirming its geometry is square planar as deduced from UV-vis spectroscopy.

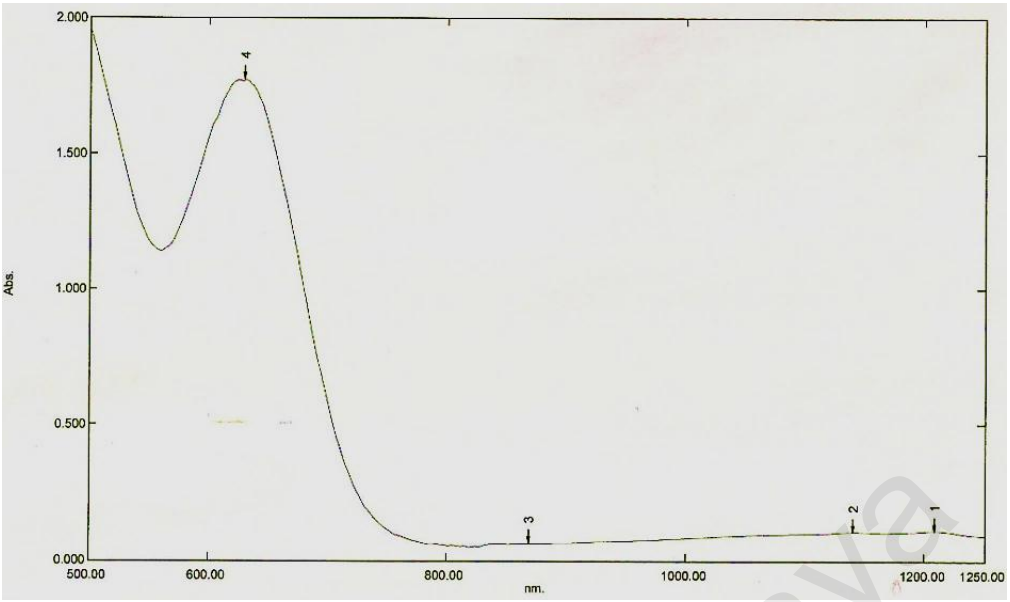

Figure 4.37 UV-vis spectrum of [Ni(L2)].CH_3CH_2OH

From **TGA**, the complex started to lose 5.0% of its weight at 70 °C due loss of solvated EtOH (expected, 9.5%), and 77.3% at 316 °C due to decomposition of L2 (expected, 75%) on further heating to 600 °C. The amount of residue at temperatures above 600 °C was 17.7% (expected, 15.5% assuming NiO). Hence, there was a good agreement between the experimental and calculated results.

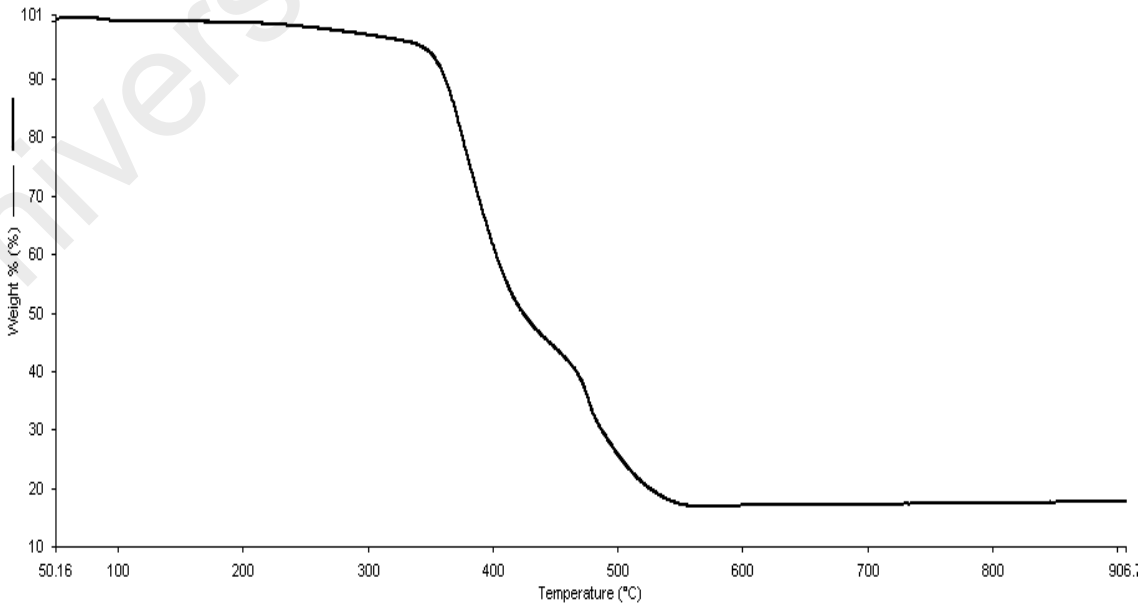

Figure 4.38 TGA thermogram of [Ni(L2)].CH_3CH_2OH

(iii) Co(II) complex of H_2L2

H_2L2 reacted with $[Co(CH_3(CH_2)_{14}COO)_2]$ to form a fine black solid (yield: 25%). Hence, based on the instrumental data presented below, it is proposed that the structural formula of the complex is $[Co_2(L2)(HL2)_2(EtOH)_4]$, which differ significant from the corresponding Cu(II) and Ni(II) complexes.

The results of the **elemental analyses**were in good agreement with the chemical formula calculated for $C_{40}H_{58}CoN_3O_5$(FW: 1438.74 g mol^{-1}): C, 66.8; H, 8.1; N,5.8%. Found: C, 66.8; H, 7.6; N, 5.8%.

Its **FTIR spectrum** (**Figure 4.39**) is similar to those of the corresponding Ni(II) complexes (**Section 4.3.2(a)(ii)**) and **Table 4.5**)

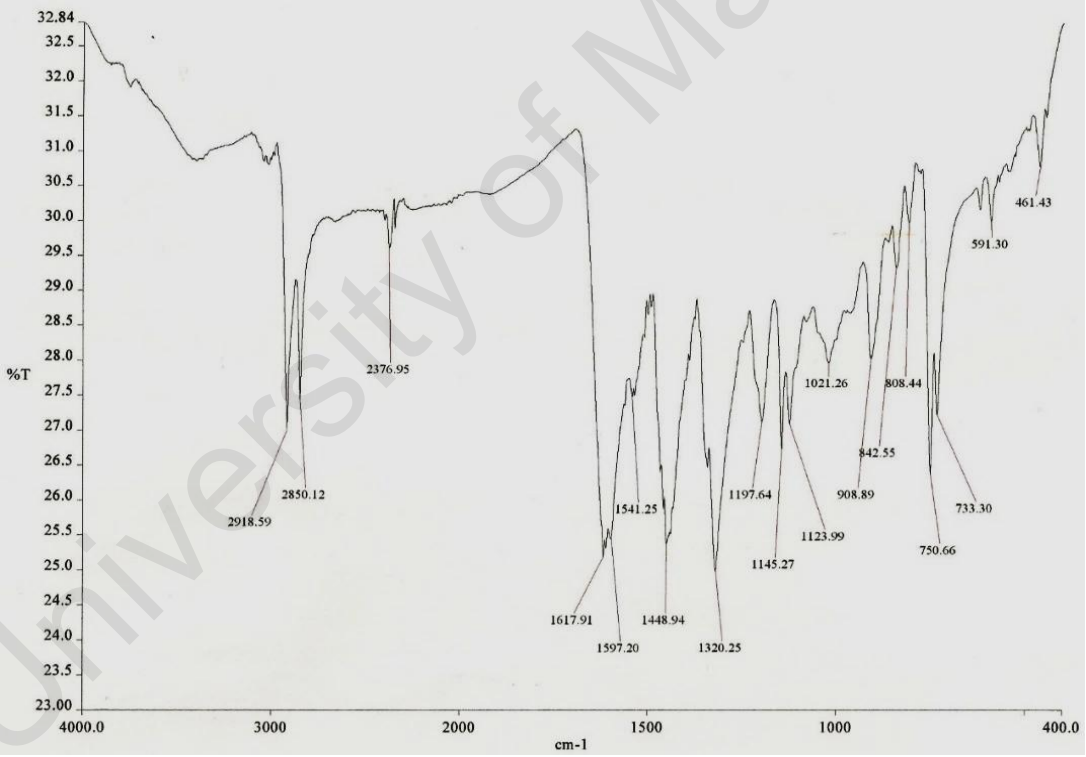

Figure 4.39 FTIR spectrum of $[Co_2(L2)(HL2)_2(EtOH)_4]$

The **UV-vis** spectrum of solid $[Co_2(L2)(HL2)_2(EtOH)_4]$(**Figure 4.40**(a)) shows a*d-d* band, which appears as a shoulder at 590 nm to a strong MLCT band at 460 nm. The *d-d* band may be assigned to $t_{2g}^5e_g^2 \rightarrow t_{2g}^4e_g^3$ electronic transition. The **UV-vis** spectrum of the sample in $CHCl_3$ (**Figure 4.40**(b)) shows a weak *d-d* band at 572 nm

(ε_{max} = 122.3 $M^{-1}cm^{-1}$) and the MLCT band shifted to 364 nm. These imply an octahedral geometry for the high-spin Co(II) centres [18, 19].

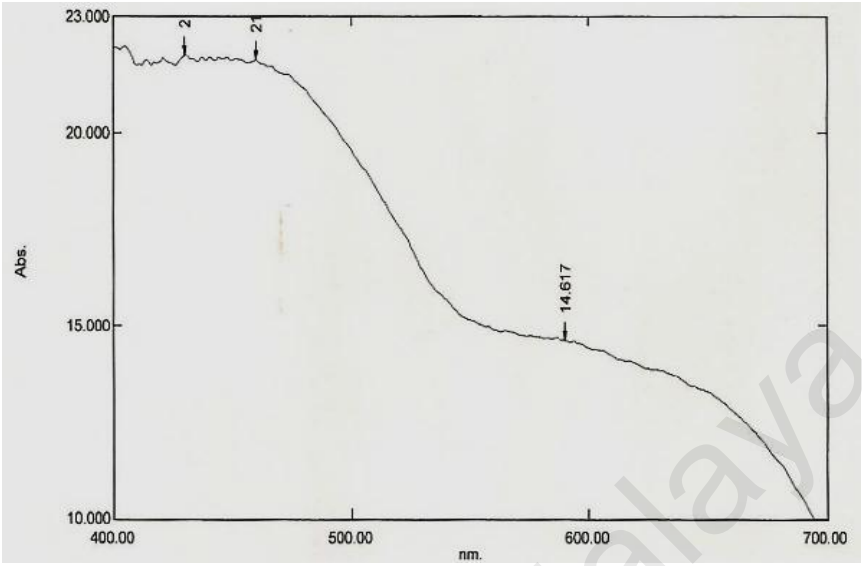

(a)

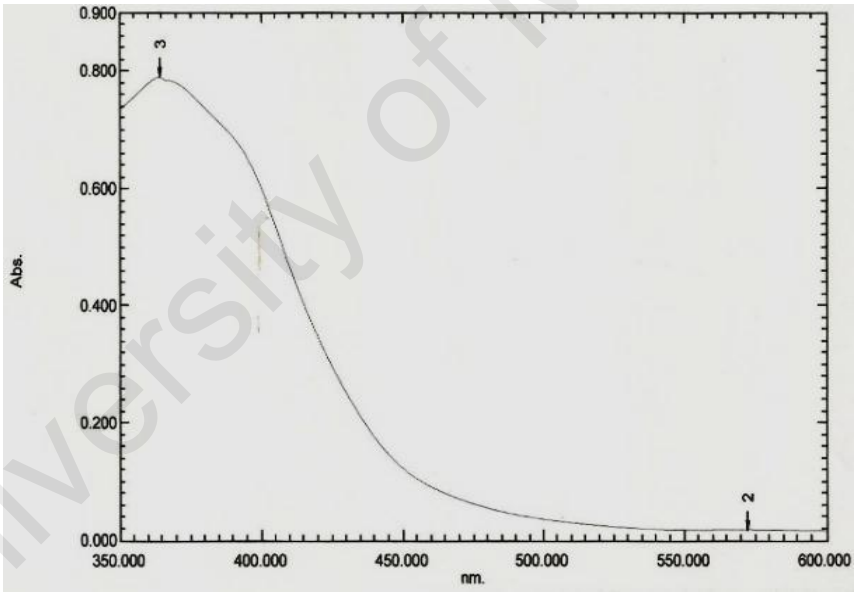

(b)

Figure 4.40 UV-vis spectra of $[Co_2(L2)(HL2)_2(EtOH)_4]$: (a) solid sample; and (b) solution in $CHCl_3$

The μ_{eff} value, calculated as before from the values of χ_g (6.84 x 10^{-6} cm^3 g^{-1}), χ_M (9.84 x 10^{-3} cm^3 mol^{-1}), χ_{dia} (-8.80 x 10^{-4} cm^3 mol^{-1}), and χ_M^{corr} (1.07 x 10^{-2}), was 5.06 B.M. or at 300 K, ($\chi_M T$= 3.2 cm^3 K mol^{-1}).This indicates quartet state in an

octahedral arrangement around the metal which is within range for d^7 system with three unpaired electrons [20].

A plot of $\chi_M T$ vs. T, from **SQUID** magnetometric measurements (**Figure 4.41**) shows a value of $\chi_M T$ = 2.94 cm^3 K mol^{-1} 300 K, which is in good agreement with the value obtained by the Gouy method. This is in agreement with the proposed structure which contained two Co(II) centers with S = 3/2 ($\chi_M T$= 3.752 cm^3 K mol^{-1}). Using the symmetrical dinuclear complexes stated previously, the calculated curve was not a good fit with the experimental curve. Hence, the two Co(II) atoms were not geometrically equivalent. Nevertheless, it can still be inferred that the Co(II) has antiferromagnetic interaction based on the $\chi_M T$ plot [21].

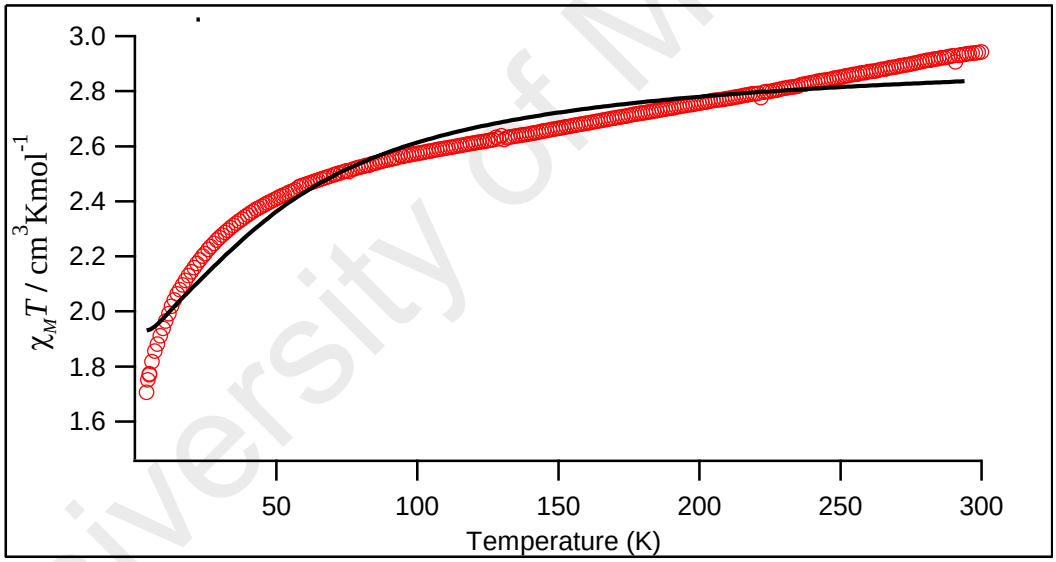

Figure 4.41 $\chi_M T$ vs. T of $[Co_2(L2)(HL2)_2(EtOH)_4]$ o, experimental curve, - fitting curve

From **TGA**, $[Co_2(L2)(HL2)_2(EtOH)_4]$ lose 85.3% of its weight from 70 °C to 750 °C, due to the loss of EtOH and the decomposition of the L2 and HL2 (expected, 86.0%). However, the amount of residue for this complex could not be determined as there was no distinct plateau in the thermogram.

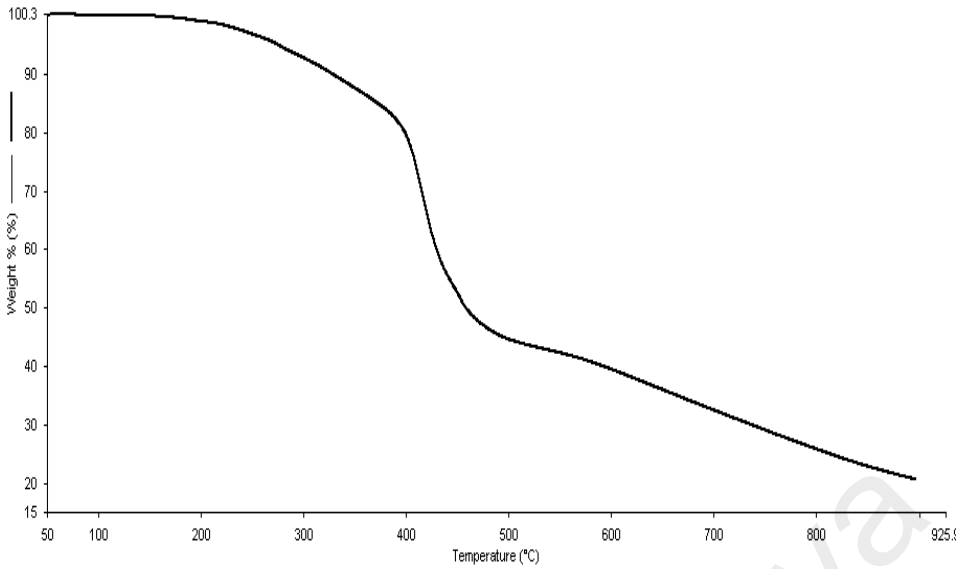

Figure 4.42TGA thermogram of $[Co_2(L2)(HL2)_2(EtOH)_4]$

(iv) Fe(II) complex of H_2L2

H_2L2 reacted with $[Fe(CH_3(CH_2)_{14}COO)_2]$ to form a black gummy solid (yield: 40.4%). As was similarly done before, it is proposed that the structural formula of the complex formed is $[Fe^{II}Fe^{III}(CH_3(CH_2)_{14}COO)(L2)(HL2)_2(H_2O)_2].H_2O$

The results of the **elemental analyses (**C, 67.8; H, 8.3; N, 5.4%)were in good agreement with the chemical formula calculated for $C_{88}H_{129}Fe_2N_6O_{11}$(FW: 1558.69 $gmol^{-1}$):C, 67.6; H, 7.9; N, 5.5%.

The **FTIR** spectrum (**Figure 4.43, Table 4.5**) of the complex shows a broad peak at 3375 cm^{-1} for OH group, two strong peaks at 2921 cm^{-1} and 2851 cm^{-1} for $\bar{\upsilon}_{asym}$ and $\bar{\upsilon}_{sym}$of CH_2 group of $CH_3(CH_2)_{14}COO$ ligand, weak overlapping peaks at 1596 cm^{-1} for –COO ($\bar{\upsilon}_{asym}$) and 1449 cm^{-1} for –COO ($\bar{\upsilon}_{sym}$), a peak at 1147 cm^{-1} for C-O phenolic group, and other expected peaks for L2 as previously discussed for the corresponding Cu(II), Ni(II) and Co(II) complexes. The Δ value is 147 cm^{-1}, indicating abridging binding mode of the carboxylato ligand.

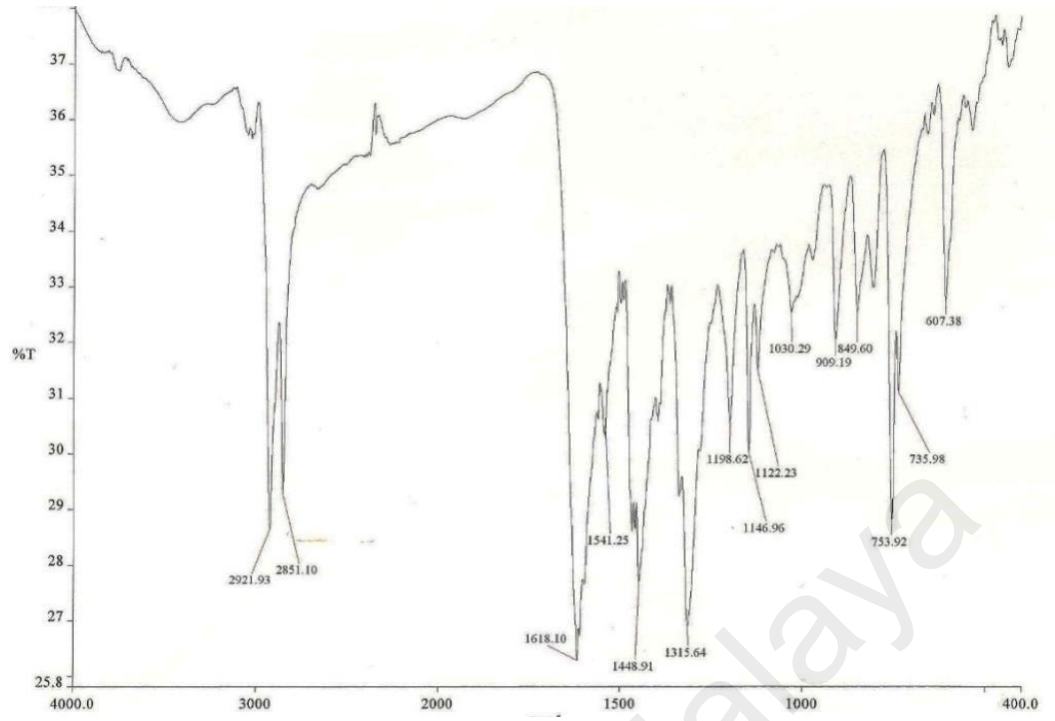

Figure 4.43 FTIR spectrum of $[Fe^{II}Fe^{III}(CH_3(CH_2)_{14}COO)(L2)(HL2)_2(H_2O)_2].H_2O$

The **UV-vis** spectrum of $[Fe^{II}Fe^{III}(CH_3(CH_2)_{14}COO)(L2)(HL2)_2(H_2O)_2].H_2O$ in $CHCl_3$ shows a band at 471 nm (ε = 7212 cm^{-1} M^{-1}) which is assigned to $t_{2g} \rightarrow \pi^*$ electronic transition [22] which is in evidence of a LS Fe(II).

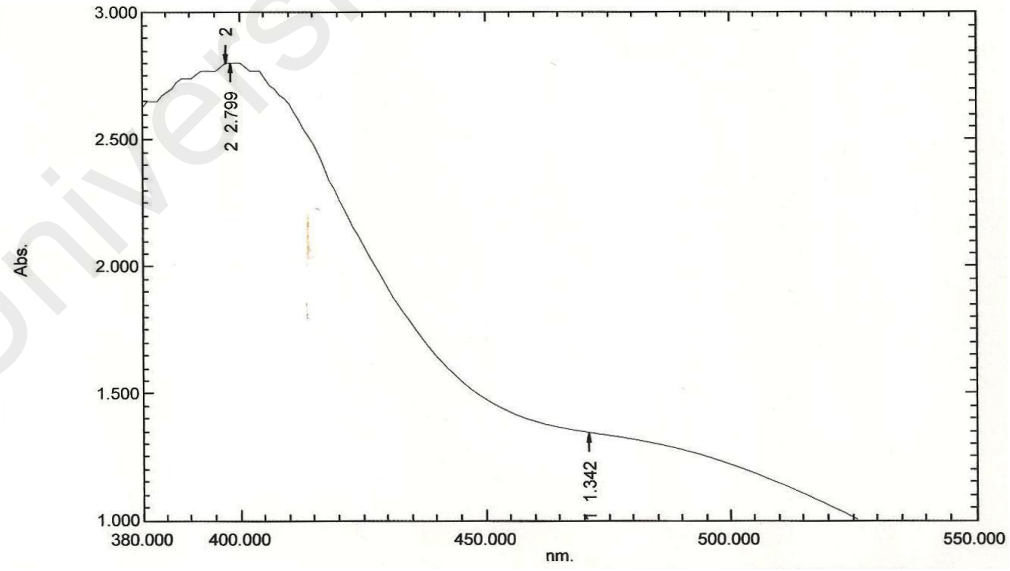

Figure 4.44 UV-vis spectrum of $[Fe^{II}Fe^{III}(CH_3(CH_2)_{14}COO)(L2)(HL2)_2(H_2O)_2].H_2O$in $CHCl_3$

The value of χ_g could not be determined for this complex by the Gouy method as it was a gummy solid at room temperature. However using **SQUID** magnetometer, a

graph of $\chi_M T$ vs. T (**Figure 4.45**) shows a value of 7.32 cm^3 K mol^{-1} for $\chi_M T$ at 300 K. This is in good agreement with the expected value of 7.38cm^3 K mol^{-1} for a $Fe^{II}Fe^{III}$ complex (S = 2 for HS Fe(II) and S = 5/2for HS Fe(III). The values then gradually decreased with temperature until at 18 K, and then decreased more rapidly. However, the complex remained paramagnetic even at 2 K ($\chi_M T$ = 5.10 cm^3 K mol^{-1}). It is noted that the experimental data show a good fit with those calculated using the equation for symmetrical dinuclear complex (**Section4.2.3(d)**), using J= -33 cm^{-1} and g = 1.15. The J value suggests weak antiferromagnetic interaction between Fe(II) and Fe(III) centres.

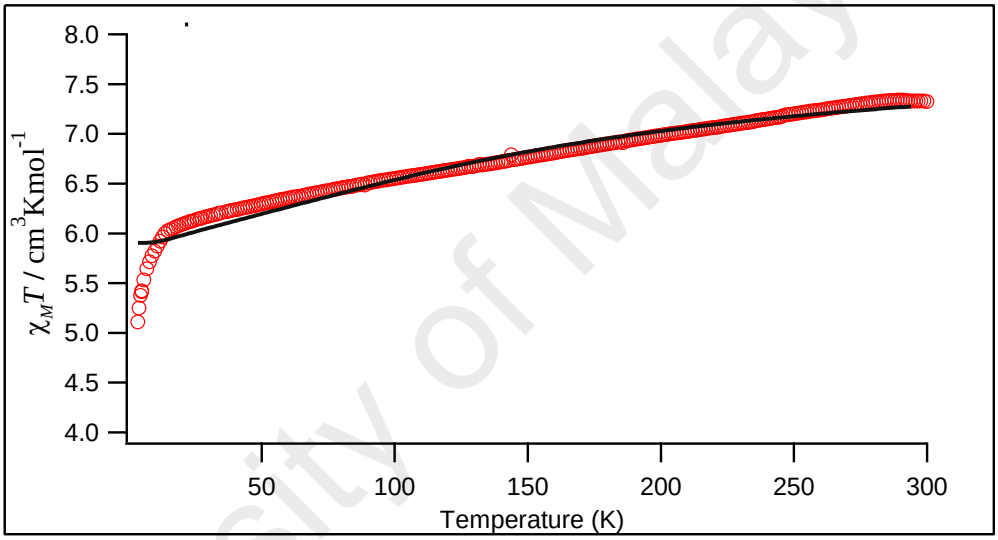

Figure 4.45 $\chi_M T$ vs. T for $[Fe^{II}Fe^{III}(CH_3(CH_2)_{14}COO)(L2)(HL2)_2(H_2O)_2].H_2O$
o, experimental curve, - fitting curve

From **TGA,** the complex started to lose 6.3% of its weight from 73 °C to 130 °C, due to the evaporation of water (expected 3.5%). It then suffered a total of 80.9% weight loss (expected, 86.3%) from 263 °C to 750 °C, due to the decomposition of all organic ligands. The amount of residue at temperatures above 750 °C was 12.8% (expected, 10.2% assuming that it was pure Fe_2O_3) [11]. Hence, there was a good agreement between the experimental and calculated results, further supporting the proposed chemical formula for the complex.

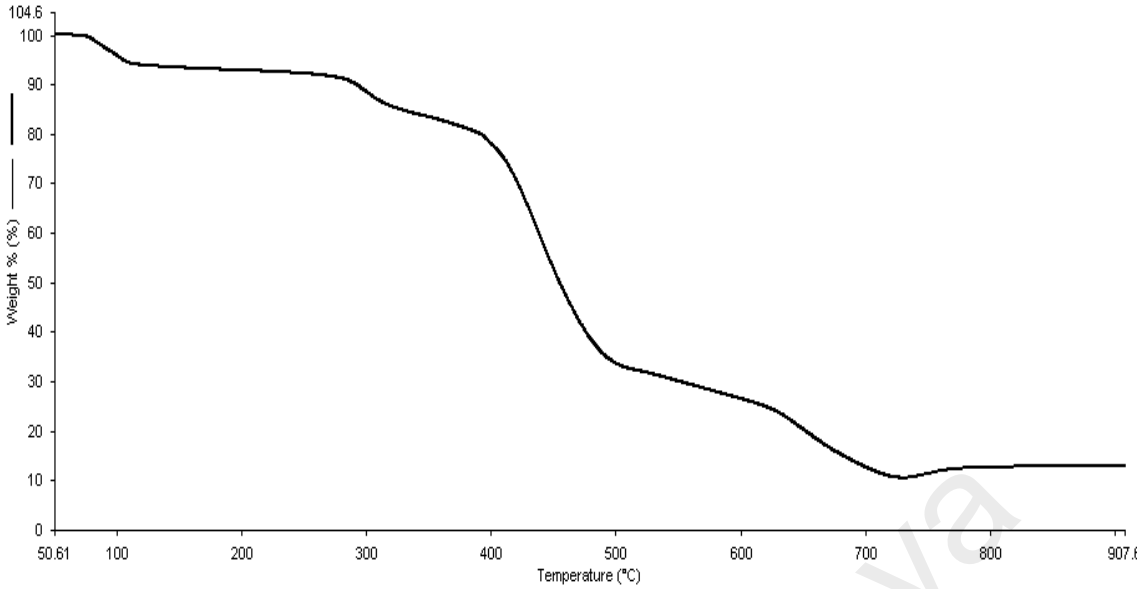

Figure 4.46TGA trace of $[Fe^{II}Fe^{III}(CH_3(CH_2)_{14}COO)(L2)(HL2)_2(H_2O)_2].H_2O$

(b) One-pot reaction

One-pot method involved refluxing 1,10-diaminodecane, 2-hydroxybenzaldehyde and $[M(CH_3(CH_2)_{14}COO)_2]$ (M = Cu(II), Ni(II), Co(II) and Fe(II)) in ethanol.

(i) M = Cu

The product obtained from the reaction was a khaki green powder (yield: 90.1%). Based on the instrumental data as previously done, its structural formula was [Cu(L2)], which is the same as the complex obtained by the step-wise method.

The results for the **elemental analyses (**C, 66.5; H,7.1; N,6.3%)was in good agreement with those calculated for $C_{24}H_{30}CuN_2O_2$ (FW: 442.06 g mol^{-1}):C, 65.2; H, 6.8; N, 6.3%.Its **FTIR spectrum (Figure 4.47, Table 4.6)** is also similar the Cu(II) complex obtained by the step-wise method.

Table 4.6 FTIR data for complexes of H_2L2 obtained by the one-pot method (R = $CH_3(CH_2)_{14}COO$

Compound	Assignment ($\bar{\upsilon}$ / cm^{-1})					
	OH	CH_2(asym)	CH_2 (sym)	C=N	M-O	M-N
H_2L2	3422	2920	2851	1632	-	-
[Cu(L2)]	-	2923	2850	1618	576	471
$[Ni_2(L2)(HL2)_2].H_2O$	3200 - 3400	2923	2851	1614	600	461
[Co(L2)(HL2)]	3380	2921	2851	1618	540	464
$[Fe^{II}Fe^{III}(R)(L2)(HL2)_2(EtOH)_2].2EtOH$	3193	2920	2851	1615	535	464

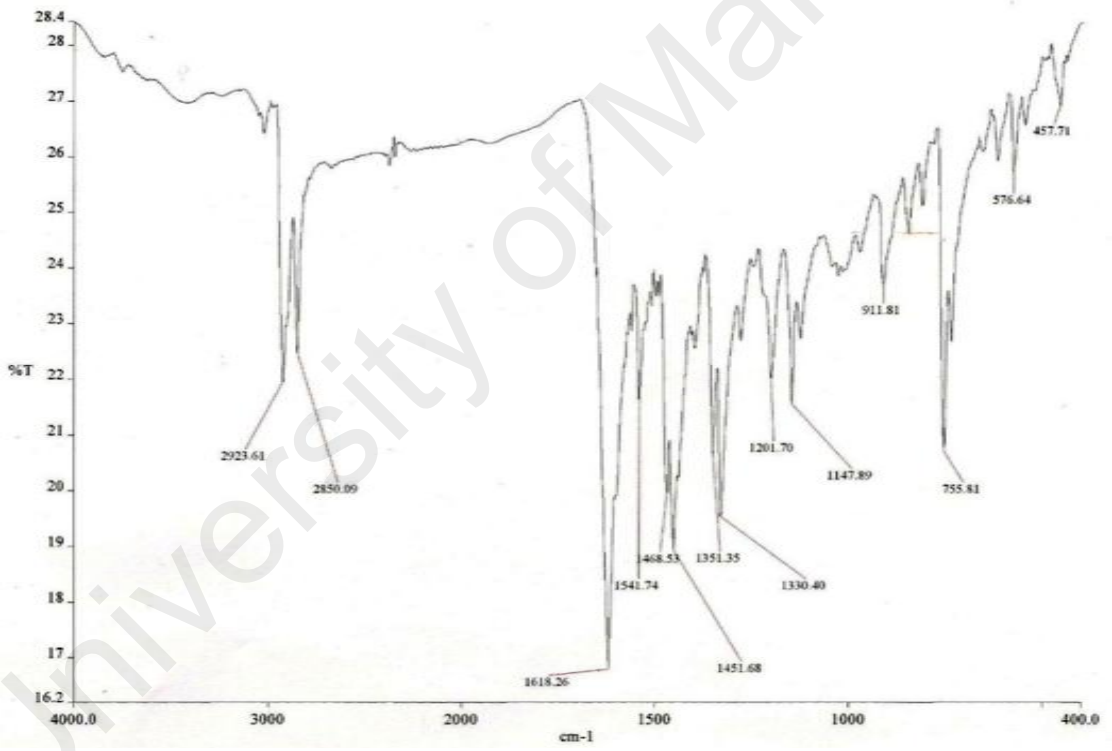

Figure 4.47FTIR spectrum of [Cu(L2)]

The **UV-vis** spectrum of [Cu(L2)] dissolved in $CHCl_3$ (**Figure 4.48**) shows a weak *d-d* band (appearing as a shoulder) at 589 nm (ε_{max} = 158 $M^{-1}cm^{-1}$) and a strong MLCTband at 390 nm. It is noted that the spectrum is the same as [Cu(L2)] obtained from the step-wise method (**Section 4.3.2 (a)(i)**).

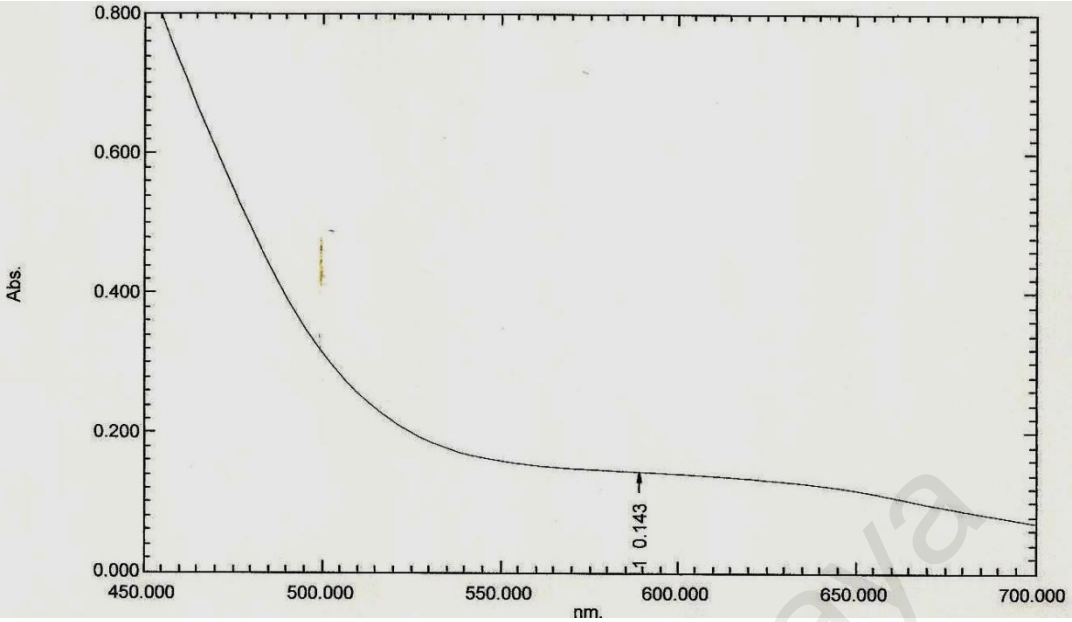

Figure 4.48 UV-vis spectrum of [Cu(L2)]in $CHCl_3$

The μ_{eff} value, calculated as before from the values of χ_g (3.16 x $10^{-6}$$cm^3$ g^{-1}), χ_M (1.40 x $10^{-3}$$cm^3$ mol^{-1}), χ_{dia} (-2.28 x $10^{-4}$$cm^3$ mol^{-1}) and χ_M^{corr} (1.62 x $10^{-3}$$cm^3$ mol^{-1}), was 1.97 B.M. at 300 K. Comparing with the [Cu(L2)] (μ_{eff} = 2.0 B.M.)obtained from the step-wise method, there is no difference in the magnetic properties of the complexes thus proving the presence of square planar geometry around the Cu(II) ion [23].

From **TGA**, the complex started to lose 79.0% of its weight at 309 °C, assigned as the decomposition of L2 (expected 85.6%). Hence, the decomposition temperatures of both Cu(II) complexes obtained from the step-wise and one-pot methods are almost the same(**Figure 4.35**and **Figure 4.49**).

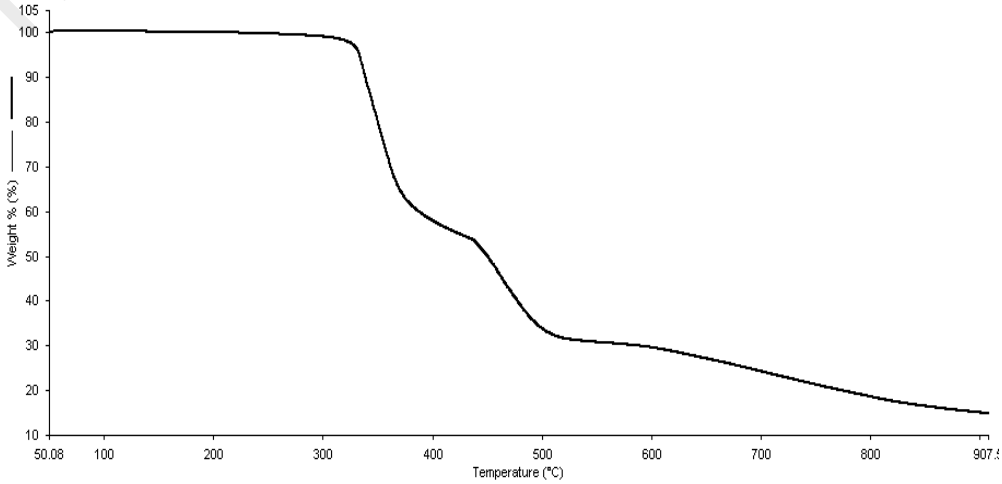

Figure 4.49 TGA of [Cu(L2)]

(ii) M = Ni

The product from the reaction was a pale khaki-green powder (yield: 87.7%). As before, its proposed structural formula is $[Ni_2(L2)(HL2)_2].H_2O$, which is different from the step-wise method ($[Ni(L2)].CH_3CH_2OH$).

The results for the **elemental analyses** was in good agreement with the calculated values for the chemical formula $C_{72}H_{94}N_6Ni_2O_7$ (FW: 1272.9 g mol^{-1}): C, 67.9; H, 7.4; N, 6.6%. Found: C, 67.2; H, 7.1; N, 6.4%.

Its **FTIR spectrum** (**Figure 4.50**) shows all of the expected functional groups at almost similar wavenumbers as for the Ni(II) complex prepared by the step-wise (**Table 4.5**).

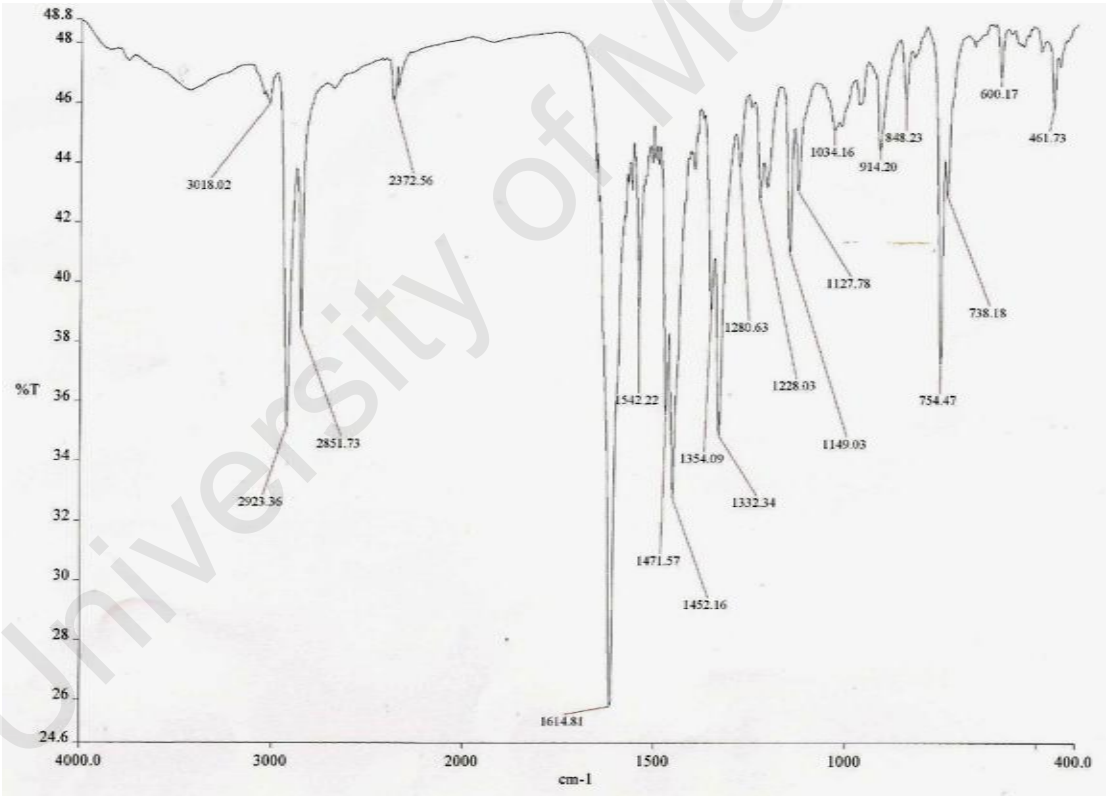

Figure 4.50FTIR spectrum of $[Ni_2(L2)(HL2)_2].H_2O$

The **UV-vis** spectrum of solid of $[Ni_2(L2)(HL2)_2].H_2O$ (**Figure 4.51)** shows a *d-d* band at 627 nm which is similar to Ni(II) complex obtained from the step-wise method (630 nm). The spectrum in solution for the complex could not be recorded as it was insoluble in most available solvents.

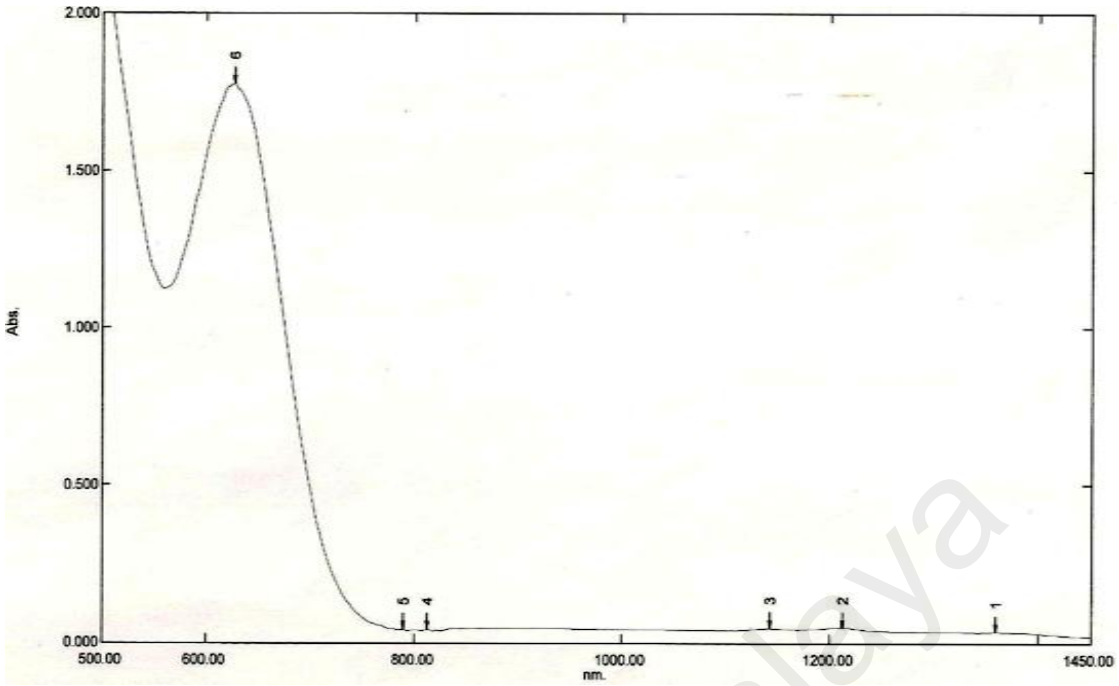

Figure 4.51 UV-vis spectrum of $[Ni_2(L2)(HL2)_2].H_2O$

The χ_g value of $[Ni_2(L2)(HL2)_2].H_2O$, obtained by the Gouy method, was -2.4 x $10^{-7}cm^3\ g^{-1}$. The negative value means that the complex was diamagnetic, thus confirming its geometry as square planar deduced from UV-vis spectroscopy. The result is similar to Ni(II) complex obtained by the step-wise method.

From the **TGA** scan, the complex started to lose 85.4% of its weight from 260 °C to 780 °C due to evaporation of water and decomposition of L2 and HL2 (expected, 88.3%). The amount of residue at temperatures above 800 °C was 14.6% (expected, 11.7%). Hence, the decomposition temperature of Ni(II) from the one-pot method is higher than the product obtained from step-wise method. (**Figure 4.38** and **Figure 4.52**)

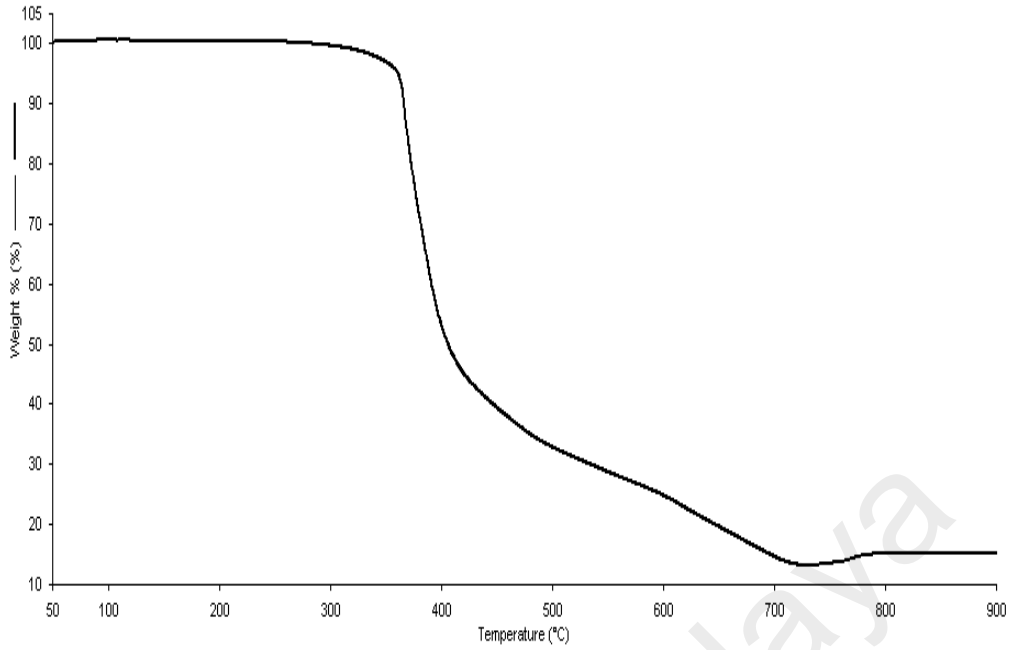

Figure 4.52 TGA thermogram of $[Ni_2(L2)(HL2)_2].H_2O$

(iii) M = Co

The product from the reaction was ablack gummy solid (yield: 32.8%). Based on the instrumental data presented below, it is proposed that the structural formula of the complex is [Co(L2)(HL2)]. The complex is suggested to contain Co(III) and this will be explained by the results below.

The results of the **elemental analyses**were in good agreement with the chemical formula calculated for $C_{48}H_{61}CoN_4O_4$ (FW: 816.9 g mol^{-1}): C, 70.6; H, 7.5; N, 6.8% Found:C, 70.1; H,7.6; N,6.7%.

Its **FTIR spectrum** (**Figure 4.53, Table 4.6**) shows all of the expected functional groups with similar wavenumber to the spectrum of $[Co_2(L2)(HL2)_2(EtOH)_4]$ obtained from the step-wise method.

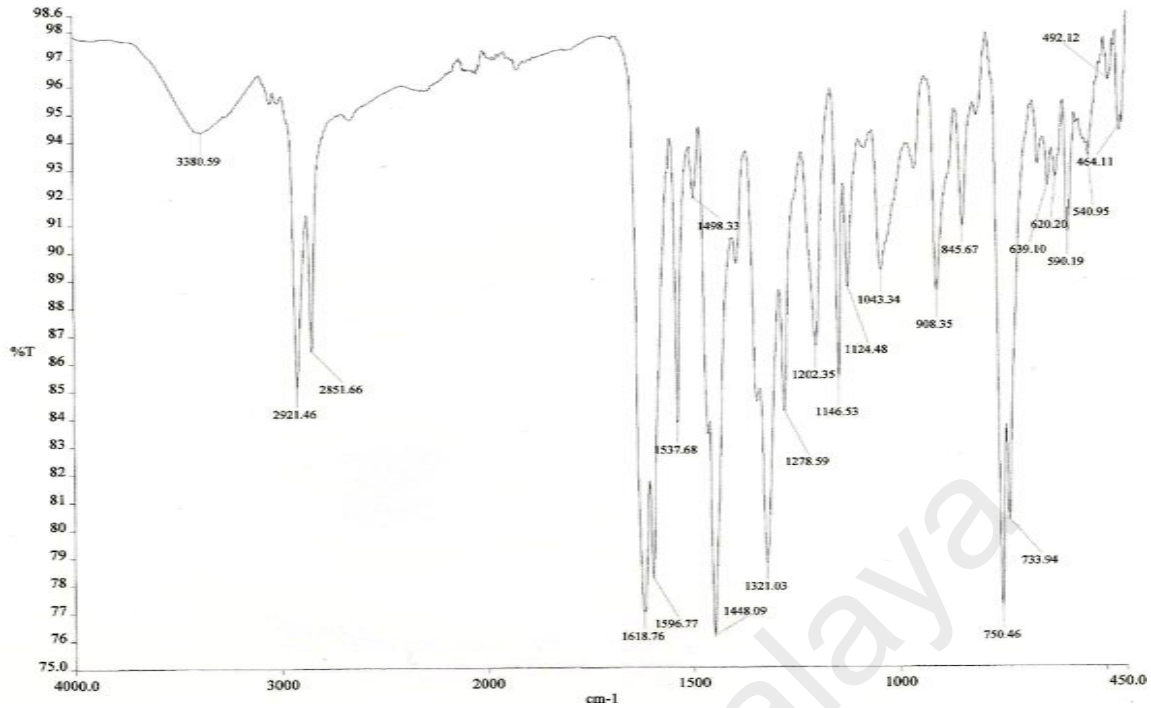

Figure 4.53 FTIR spectrum of [Co(L2)(HL2)]

The **UV-vis** spectrum of solid [Co(L2)(HL2)] (**Figure 4.54**(a)), a band at 633 nm was assigned as the *d-d* band of $t_{2g}^{6} \rightarrow t_{2g}^{5} e_g^{1}$ for a low spin Co(III). Another band was observed at 380 nm can be assigned as the MLCT of the cobalt to the phenoxide. The **UV-vis** in solution (**Figure 4.54**(b)) gave rise to a band at 618 nm (ε_{max}= 134.0 cm^{-1} M^{-1}) which is assigned as the *d-d* transition for the cobalt. The MLCT was shifted to 392 nm in the presence of solution.

Magnetic measurement could not be performed on [Co(L2)(HL2)] by the Gouy method as the sample was a semisolid. However, a plot of $\chi_M T$ vs. T, from **SQUID** magnetometric measurements (**Figure 4.55**) shows a value $\chi_M T$ = 0.079 cm^3 K mol^{-1} at 300 K. This value indicates a LS Co(III) complex, which should be diamagnetic. A possible explanation for the value at room temperature can be the result of the presence of a LS Co(II) which exist as a resonance form [12]. On decreasing the temperature, the $\chi_M T$ value decreased to almost zero, indicating complete electron pairing. Hence, it seems that during this reaction, Co(II) was oxidized to Co(III). Similar occurrence was reported in several journals. An example is $[Co^{III}_2(bhnq)(tpa)_2](PF_6)_4$ which was oxidized from $[Co^{II}_2(bhnq)(Metpa)_2](ClO_4)_2$[24].

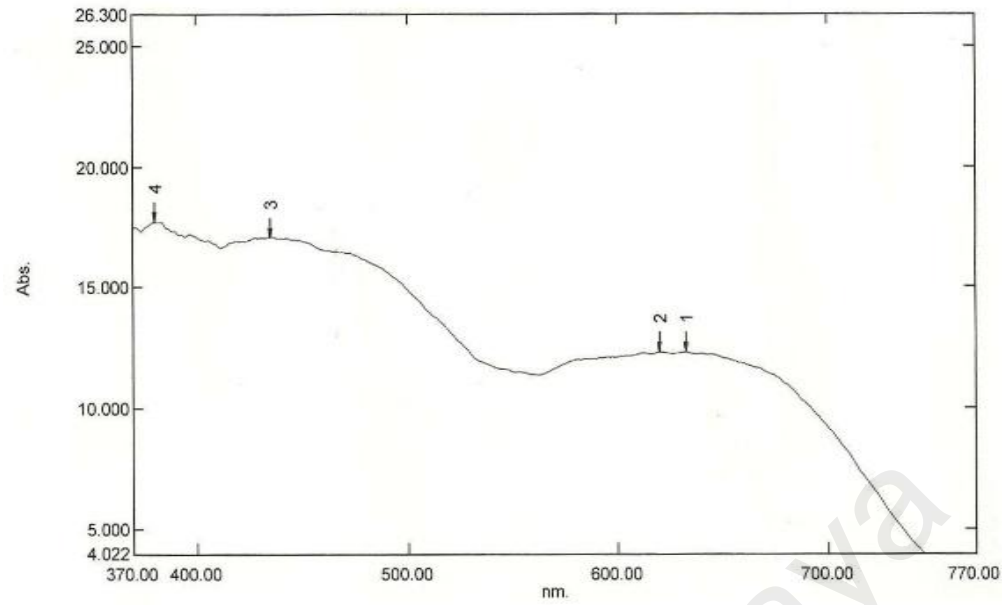

(a)

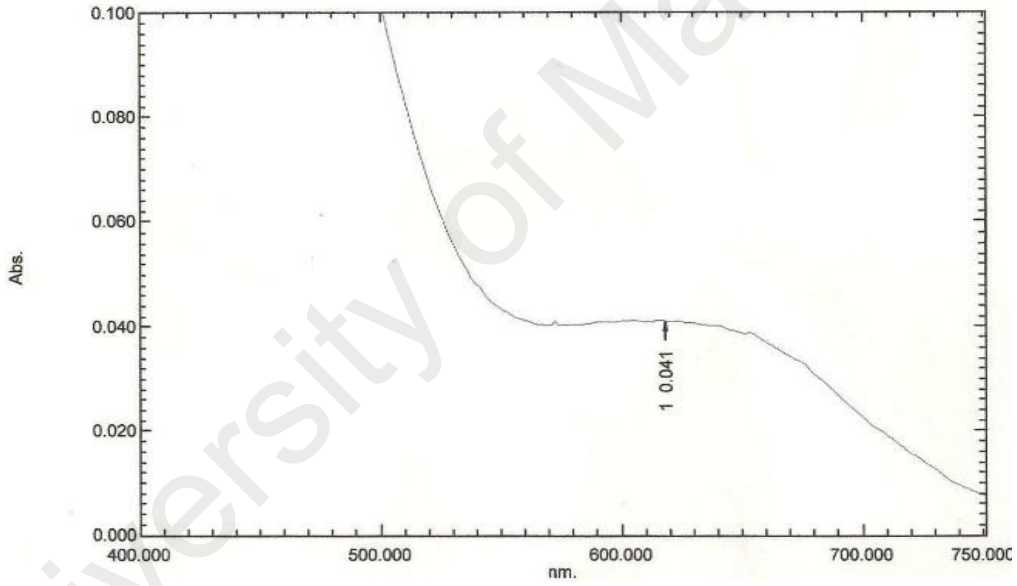

(b)

Figure 4.54 UV-visspectra of [Co(L2)(HL2)] (a) solid; and (b) solution in $CHCl_3$

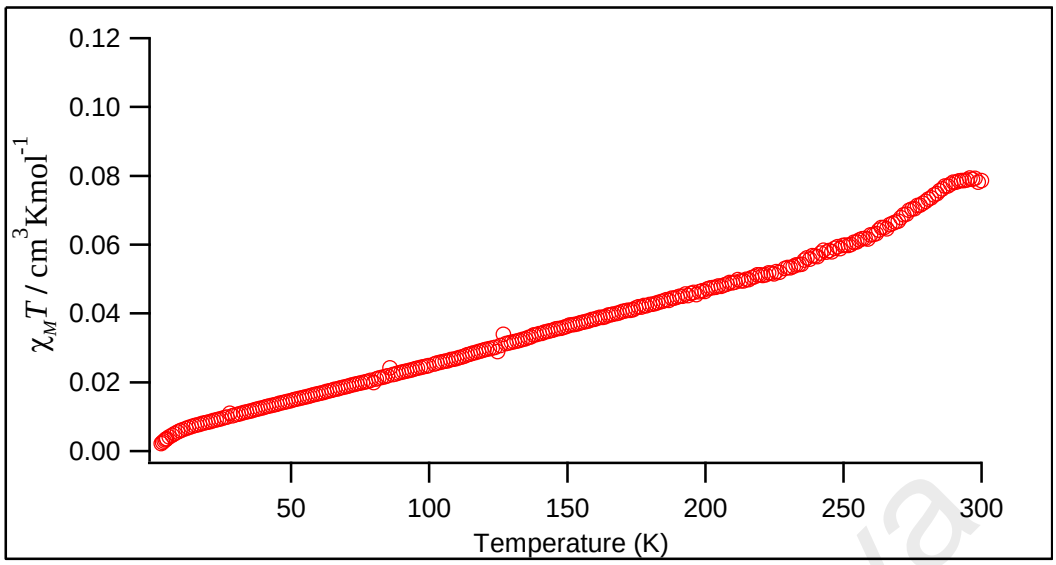

Figure 4.55 Graph of $\chi_M T$ vs. *T*for [Co(L2)(HL2)]o, experimental curve

From **TGA**, [Co(L2)(HL2)] lost 88.0% of its weight from 220 °C to 550 °C due to the decomposition of L2 and HL2 (expected, 79.7%). The amount of residues at temperatures above 600 °C is 12.0% (expected, 20.3%). The lower percentage of the residue may be due to the formation of volatile complex.

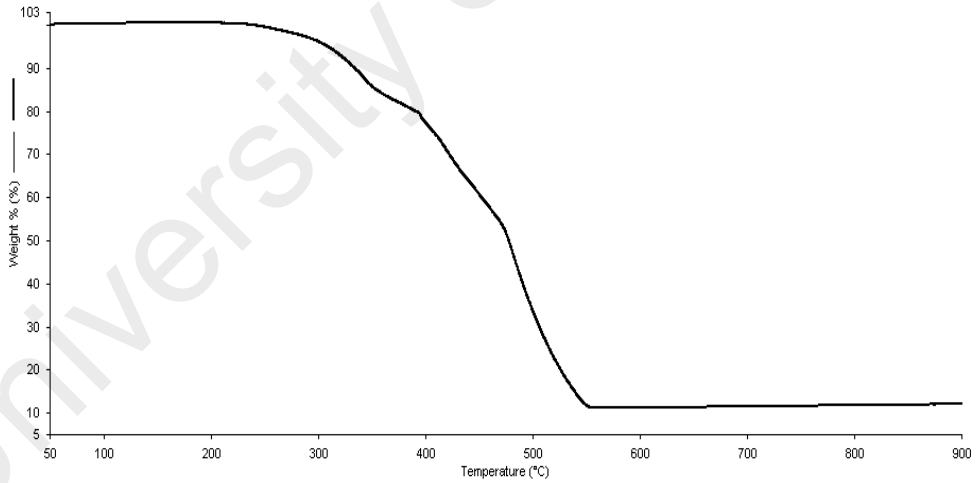

Figure 4.56TGA of [Co(L2)(HL2)]

(iv) M = Fe

The product obtained from the reaction was black gummy solid (yield: 47.9%). From instrumental data obtained, it is proposed that the structural formula for the complex is $[Fe^{II}Fe^{III}(CH_3(CH_2)_{14}COO)(L2)(HL2)_2(EtOH)_2].2EtOH$. Except for coordinated and

non-coordinated solvent molecules, the structure is similar to the iron complex obtained from the step-wise method ($[Fe^{II}Fe^{III}(CH_3(CH_2)_{14}COO)(L2)(HL2)_2(H_2O)_2].H_2O$).

The results of the **elemental analyses** were in good agreement with the chemical formula calculated for $C_{96}H_{147}Fe_2N_6O_{11}$ (FW: 1688.9 $gmol^{-1}$): C, 68.2; H, 8.8; N, 4.9%.Found: C, 68.0; H, 8.6; N, 4.7%.

Its **FTIR** spectrum (**Figure 4.57**) is similar to the corresponding complex obtained by the step-wise reaction.

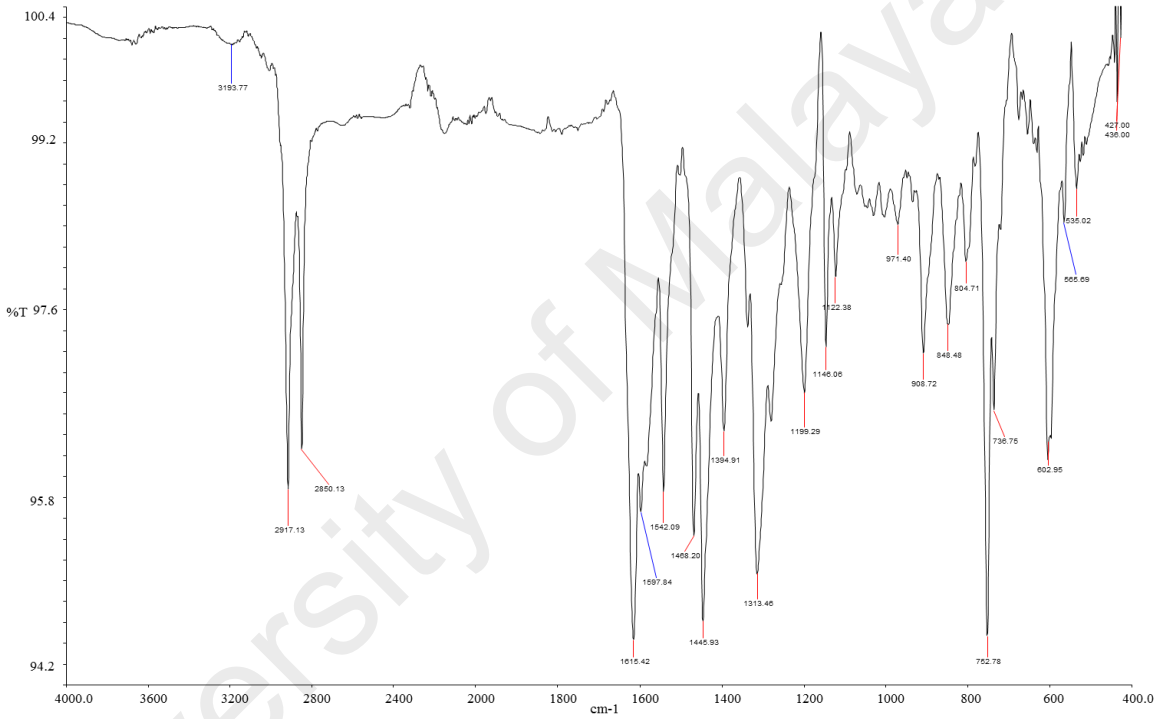

Figure 4.57FTIR spectrum of $[Fe^{II}Fe^{III}(CH_3(CH_2)_{14}COO)(L2)(HL2)_2(EtOH)_2].2EtOH$

The **UV-vis**spectrum of $[Fe^{II}Fe^{III}(CH_3(CH_2)_{14}COO)(L2)(HL2)_2(EtOH)_2].2EtOH$ in $CHCl_3$ shows a band at 476 nm (ε = 1538 cm^{-1} $M^{-1)}$. It can be assigned as the assigned to $t_{2g} \rightarrow \pi^*$ electronic transition. This is similar compared with the spectrum of the $Fe^{II}Fe^{III}$ complex obtained from step-wise method.

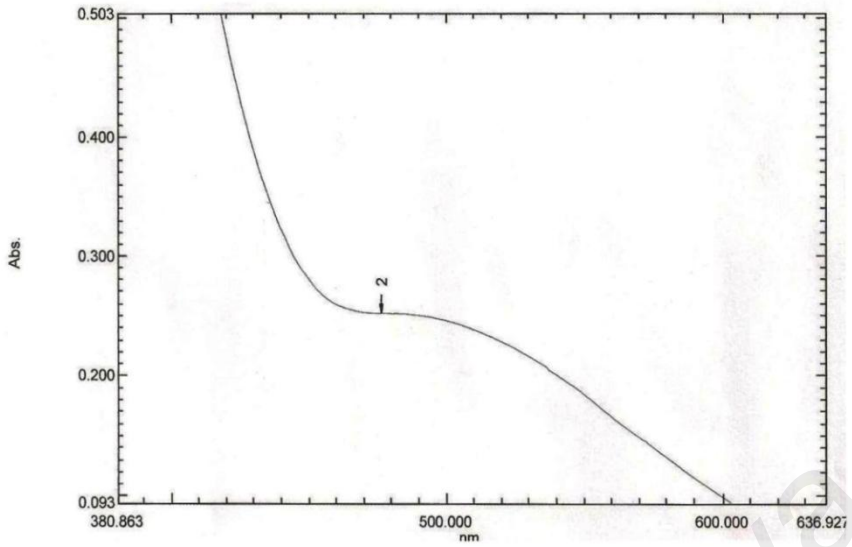

Figure 4.58 UV-visspectrum of $Fe^{II}Fe^{III}(CH_3(CH_2)_{14}COO)(L2)(HL2)_2(EtOH)_2].2EtOH$ in CH_2Cl_2

Magnetic measurement could not be performed on the complex by the Gouy method as the sample was a semisolid.However using **SQUID** magnetometer, a graph of $\chi_M T$ vs. T (**Figure 4.59**) shows a value7.74 cm^3 K mol^{-1} at room temperature which is higher than theoretical value of 7.377 cm^3 K $mol^{-1}$for a $Fe^{II}Fe^{III}$ centers with a combination of*S*= 2 and *S* = 5/2. Upon cooling at 25 K, the complex $\chi_M T$started to decrease rapidly until it reaches 2 K with $\chi_M T$ value of 5.15 cm^3 K mol^{-1}. This suggests that there is interaction in the form of charge distribution between the iron centres through the ligands. The calculated curve has a good fit with experimental curve from 300 K to 60 K. The *J* value obtained from calculation using the equation for symmetrical dinuclear complex is -41 cm^{-1} (g = 1.39). This indicates that the complex has antiferromagnetic interaction between both iron centres. The complex is believed to be a mixed valence which is similar to the previous iron complex.

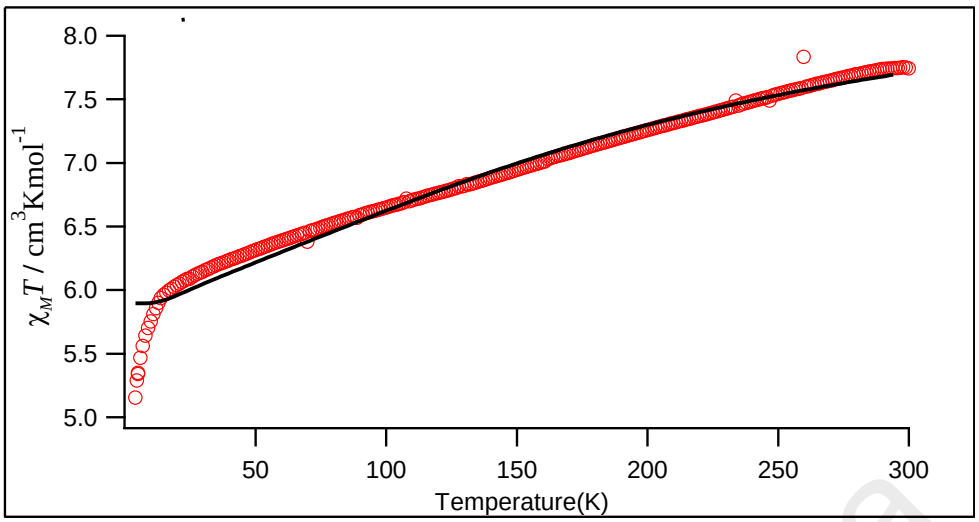

Figure 4.59 $\chi_M T$ vs. T of $[Fe^{II}Fe^{III}(CH_3(CH_2)_{14}COO)(L2)(HL2)_2(EtOH)_2].2EtOH$.
o, experimental curve, - fitting curve

From the **TGA** trace the sample started to lose 90.6% of its weight from60 °Cuntil 600 °C.The weight loss was due to evaporation of ethanol which started at 60 °C (expected 10.9%), followed by the hexadecanoate chain at 305 °C (expected 14.8%) and lastly the ligand (expected 65.3%). Assumption were made that the residue of 9.4% is Fe_2O_3(expected 9.0%) which is in good agreement with the proposed structural formula.

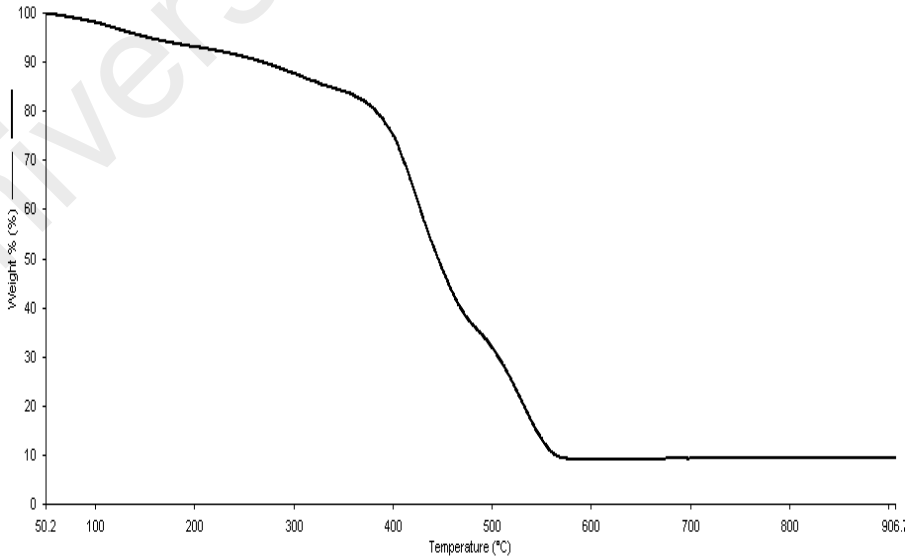

Figure 4.60TGA scan of $[Fe^{II}Fe^{III}(CH_3(CH_2)_{14}COO)(L2)(HL2)_2(EtOH)_2].2EtOH$

4.3.3 Summary

The data for the metal complexes of H2L2, obtained both by the one-pot and step-wise methods, are shown in **Table 4.7.**

Table 4.7 The summary data for metal complexes of H_2L2;R = $CH_3(CH_2)_{14}COO$

Complexes	Cu(II) Step-wise	Cu(II) One-pot	Ni(II) Step-wise	Ni(II) One-pot	Co(II) Step-wise	Co(III) One-pot	Fe(II)Fe(III) Step-wise	Fe(II)Fe(III) One-pot
Colour	Khaki green	Khaki green	Light khaki green	Pale khaki green	black	black	Black gummy	Black gummy
Yield (%)	67.9	90.1	68.3	87.7	25	32.8	40.4	47.9
Chemical Formula	[Cu(L2)]	[Cu(L2)]	[Ni(L2)].EtOH	$[Ni_2(L2)(HL2)_2].H_2O$	$[Co_2(L2)(HL2)_2(EtOH)_4]$	[Co(L2)(HL2)]	$[Fe^{II}Fe^{III}(R)(L2)(HL2)_2(H_2O)_2].H_2O$	$[Fe^{II}Fe^{III}(R)(L2)(HL2)_2(EtOH)_2].2EtOH$
Geometry	Square planar	Square planar	Square planar	Square planar	octahedral	octahedral	octahedral	octahedral
Magnetic susceptibility (B.M)	2.0	1.97	diamagnetic	diamagnetic	5.06	diamagnetic	7.65	7.87
Thermal Decompostion, T_{dec} (°C)	304	309	316	260	205	220	263	305

From **Table 4.7**, a comparison of the step-wise and one-pot methods is made. For Cu(II), both methods gave the same product, [Cu(L2)]. However, the one-pot method gave higher yield.

For Ni(II), both methods gave different Ni(II) complexes. The step-wise method formed a mononuclear complex, $[Ni(L2)].CH_3CH_2OH$, while the one-pot method formed dinuclear Ni(II) complex, $[Ni_2(L2)(HL2)_2].H_2O$, and in higher yield. For both complexes, Ni(II) centres were in a square planar geometry. Additionally, the mononuclear complex has a higher thermal stability than the dinuclear complex.

For Co(II), the step-wise method formed a dinuclearCo(II) complex, $[Co_2(L2)(HL2)_2(EtOH)_4]$, while one-pot method formed a mononuclear Co(III) complex, [Co(L2)(HL2)]. Both complexes were obtained in low yields. The thermal stability of both complexes were comparable and the geometry of Co(II) and Co(III) were octahedral. However, the dinuclear complex was paramagnetic while the mononuclear complex was diamagnetic.

For Fe(II), both methods formed dinuclear mixed valence complexes in good yields. The difference for both productswas the presence of coordinated and non-coordinated solvent, and the magnetic susceptibility and thermal stability for the product formed from the one-pot method were slightly higher than that from the step-wise method.

From the above findings, it can be concluded that the step-wise method was a better choice as it formed M(II) complexes for all metal ions studies. The one-pot method, which even though gave higher yields, resulted in the oxidation of Co(II) to Co(III).

4.4 Synthesis, Structural Deduction and Characterisation of Complexes of H_2L3

The last phase of this research involved step-wise syntheses of complexes of H_2L3, a Schiff base with a branched and shorter alkyl chain compared to H_2L1 and H_2L2. This part of the research arose from a literature report that this ligand reacted with Cu(II) acetate to form a trinuclear complex involving acetate bridging [25]. Hence, it was of interest to see if similar multinuclear complexes may formed from its reactions with $[M(CH_3(CH_2)_{14}COO)_2]$, which may function as linear chain molecular magnetic materials.

4.4.1 Synthesis and characterization of H_2L3

H_2L3 was obtained as a viscous yellow liquid from the reaction between 1,3-diaminopentane and 2-hydroxybenzaldehyde (mol ratio = 2:1).The solvent used was ethanol and the yield was 84.8 %. Its structural formula was ascertained from the following instrumental data.

The results of the **elemental analyses** (72.8% C, 7.0% H, 8.8% N) were in good agreement with the chemical formula $C_{19}H_{22}N_2O_2$ (73.5% C, 7.1% H, 9.0% N). Its structural formula was supported by ^{1}H-NMR spectroscopy (**Figure 4.61**; **Table 4.8**).

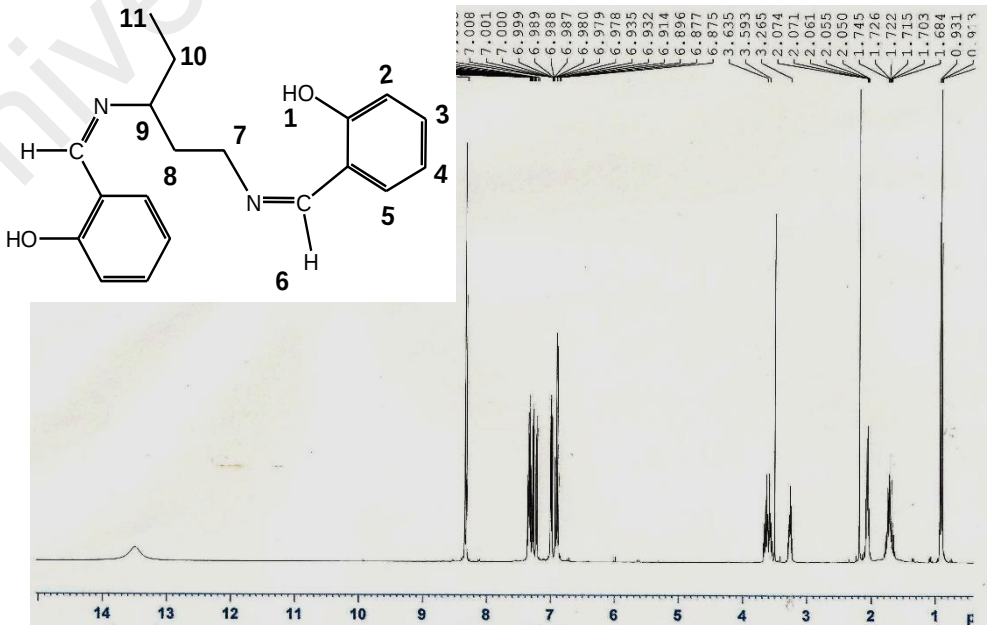

Figure 4.61 ^{1}H-NMR spectrum of H_2L3

Table 4.8 The ^{1}H-NMR peak assignment for H_2L3

Chemical Shift (ppm)	Ratio	Multiplicity	Assignment
0.8 – 0.9	1.8	triplet	H-11
1.6 – 1.7	1.5	triplet	H-10
2.0	1.2	triplet	H-8
3.2	0.6	singlet	H-9
3.5	1.2	doublet	H-7
6.8	1.2	triplet	H-4
6.9	1.2	doublet	H-5
7.2	1.3	triplet	H-3
7.3	1.2	doublet	H-2
8.3	1.2	singlet	H-6
13.5	1.0	singlet	H-1

Its **FTIR** spectrum and data, which also includes those of its complexes, are shown in **Figure 4.62** and **Table 4.9**, respectively. The spectrum shows a very broad peak centered at 3556 $cm^{-1}$for OH group, two weak peaks at 2923 cm^{-1} and 2851 cm^{-1} for the asymmetric and symmetric vibrations of CH_2 group respectively, a strong peak at 1627 cm^{-1} for the C=N (imine) bond.

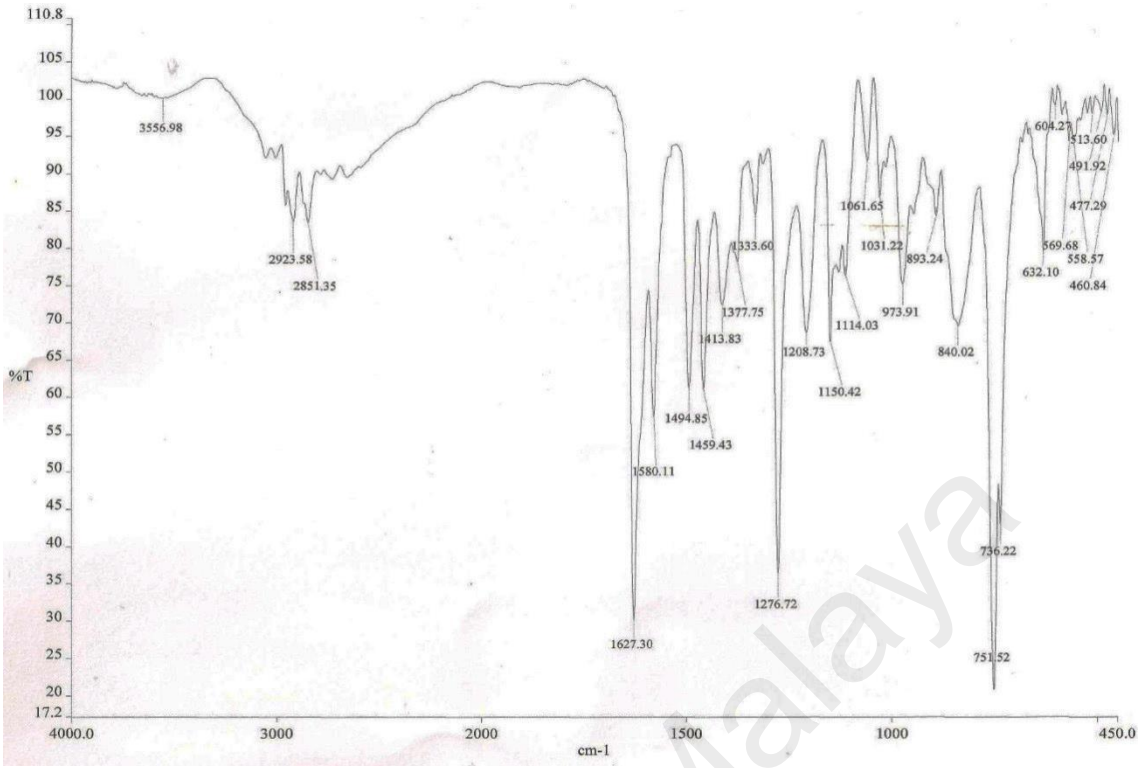

Figure 4.62 FTIR spectrum of H_2L3

Table 4.9 The FTIR data for H_2L3 and its metal complexes;R = $CH_3(CH_2)_{14}COO$

Compound	Assignment/$\bar{\upsilon}$ (cm^{-1})					
	OH	CH_2 (asym)	CH_2 (sym)	C=N	M-O	M-N
H_2L3	3406	2921	2850	1633	-	-
$[Cu_2(R)(L3)(HL_3)]$	-	2915	2848	1611	557	455
$[Ni(R)(HL3)_2]$	-	2917	2849	1612	541	461
[Co(R)(HL3)]	-	2917	2850	1618	548	465
$[Fe(R)_2(HL3)]$	-	2917	2849	1612	598	462

TGA trace (**Figure 4.63**) shows that H_2L3 lost 99.7% of its mass in the temperature range of 155 - 900 °C. From this, it may be inferred that its decomposition temperature was 155 °C.

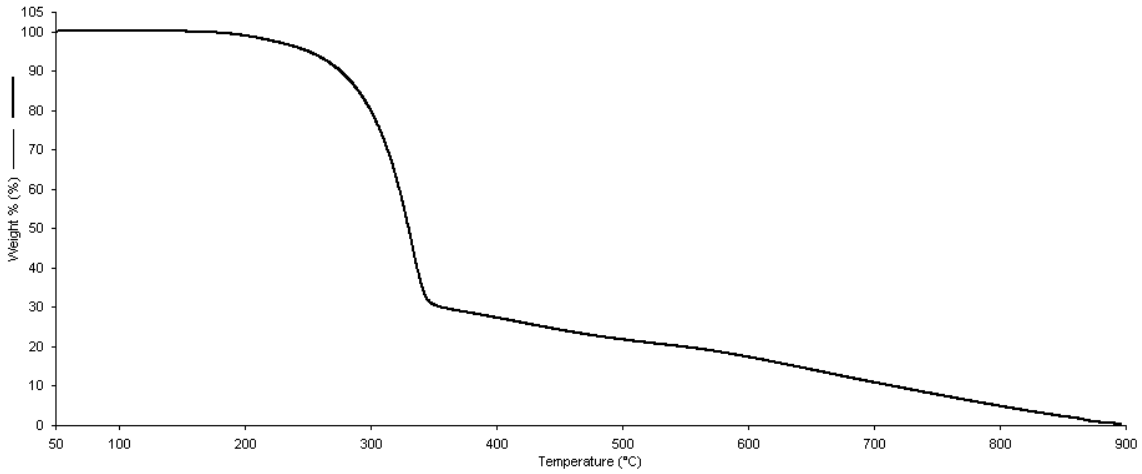

Figure 4.63TGA trace of H_2L3

4.4.2 Reaction of H_2L3 with $[M(CH_3(CH_2)_{14}COO)_2]$

(a) M = Cu

H_2L3 reacted with $[Cu(CH_3(CH_2)_{14}COO)_2]$ to form a dark khaki-green powder (yield: 64.8 %). Based on the analytical data presented below, it is proposed that its structural formula is $[Cu_2(CH_3(CH_2)_{14}COO)(L3)(HL_3)]$. Hence, the complex is dinuclear, which is unlike previous Cu(II) complexes which are mononuclear or trinuclear as reported in literature [25].

The results of the **elemental analyses (**C,64.5; H, 7.5; N, 5.8%) were in good agreement with the chemical formula calculated for $C_{54}H_{73}Cu_2N_4O_6$ (FW: 1001.3 g mol^{-1}; **(**C, 64.7; H, 7.4; N, 5.6%).

Its **FTIR spectrum** (**Figure 4.64**) shows two peaks at 2916 cm^{-1} and 2849 cm^{-1} for $\bar{\upsilon}_{sym}$ and $\bar{\upsilon}_{asym}$ of CH_2 group respectively, a strong peak at 1610 $cm^{-1}$for C=N,a weak peak at 1587 cm^{-1} for –COO (ν_{asym}), at 1446 $cm^{-1}$for –COO (ν_{sym}), (Δ = 141 cm^{-1}), and a weak peak at 1701 cm^{-1} for C=O. The latter peaks suggest bridging and monodentate binding modes for $CH_3(CH_2)_{14}COO^-$ ligand.

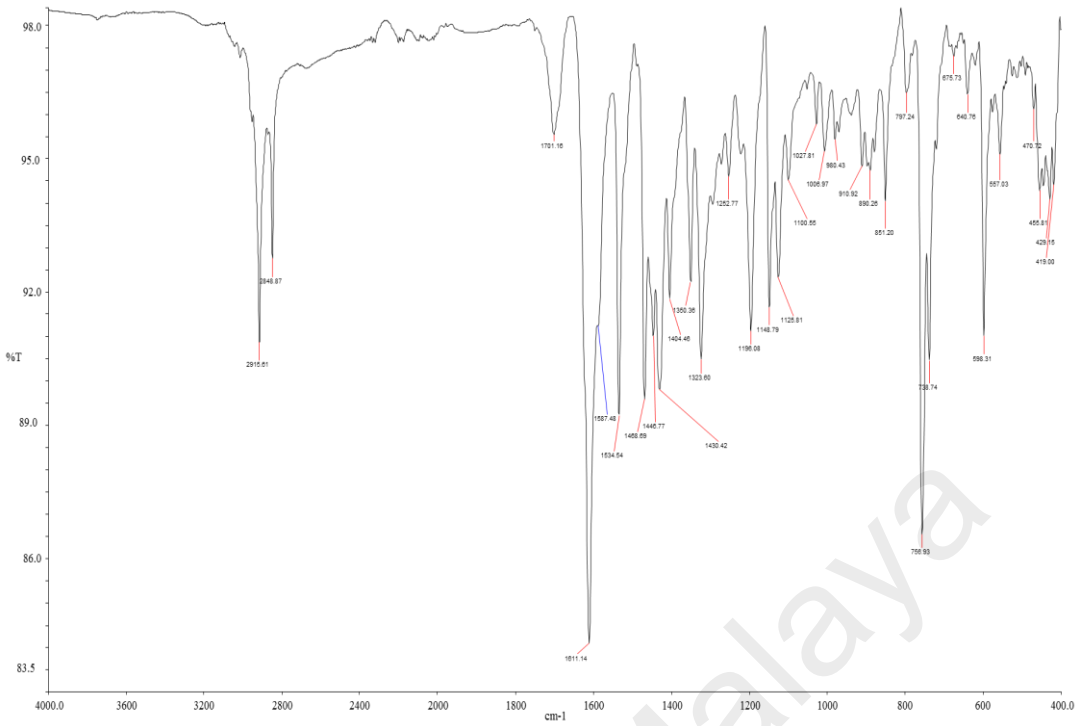

Figure 4.64 FTIR spectrum of $[Cu_2(CH_3(CH_2)_{14}COO)(L3)(HL_3)]$

Its **UV-vis** spectrum in $CHCl_3$ (**Figure 4.65**) shows a weak *d-d* band at 604 nm (ε_{max} = 367 $M^{-1}cm^{-1}$). This suggests a square planar geometry at Cu(II) in solution.

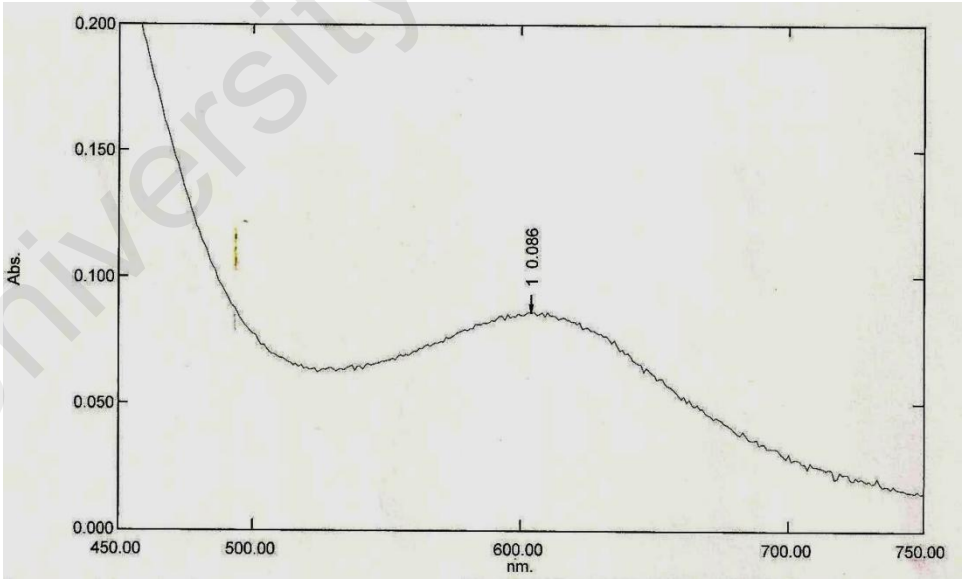

Figure 4.65 UV-visspectrum of $[Cu_2(CH_3(CH_2)_{14}COO)(L3)(HL_3)]$ in $CHCl_3$

The $\boldsymbol{\mu_{eff}}$value, calculated as before from the values of χ_g (2.39 x $10^{-6}cm^3$ g^1), χ_M (3.18 x $10^{-3}cm^3$ mol^{-1}), χ_{dia} (-5.78 x $10^{-4}cm^3$ mol^{-1}), χ_M^{corr} (3.68 x $10^{-3}cm^3$ mol^{-1}) and

Nα (60 x 10^{-6} cm^3 mol^{-1}), was 2.66 B.M. at 300 K. This is lower than expected spin-only value of 2.83 for a dinuclear Cu(II) complex , suggesting a weak antiferromagnetic interaction between the two metal(II) centres.

From its **TGA** trace, the complex lost86.5% of its weight from 142 °C to 900 °C, due to the decomposition of ($CH_3(CH_2)_{14}COO$), (L3) and (HL_3) (expected, 87.3%). It is noted that it was less thermally stable compared to Cu(II) complexes of H_2L1 (T_{dec} = 310 °C) and of H_2L2 (T_{dec} = 304 °C).

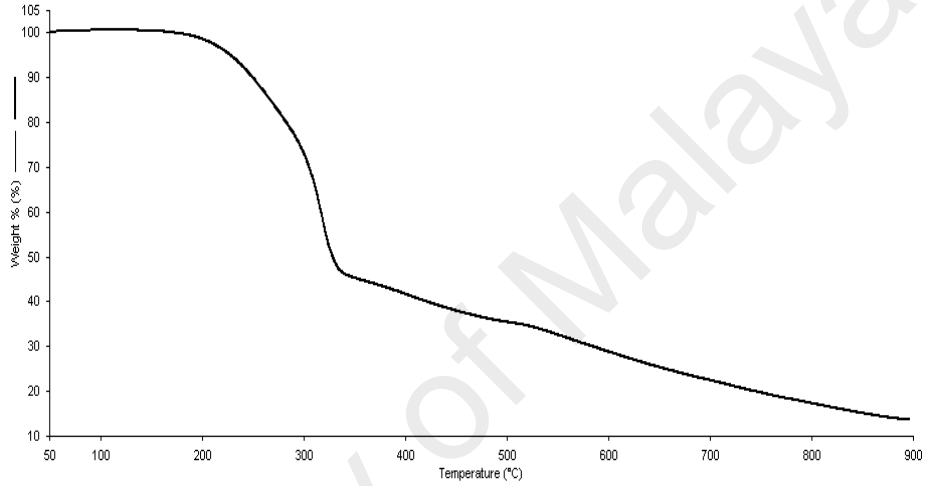

Figure 4.66 TGA trace of [$Cu_2(CH_3(CH_2)_{14}COO)(L3)(HL_3)$]

(b) M = Ni

H_2L1 reacted with [$Ni(CH_3(CH_2)_{14}COO)_2$] to forma dark green gummy solid (yield: 77.2%). As previously done, the proposed structural formula of the complex is [$Ni(CH_3(CH_2)_{14}COO)(HL3)_2$] which contain Ni(III). Hence, it is different from the Ni(II) complexes of H_2L1 and H_2L2 (step-wise method) and as reported by literature [26].

The results of the **elemental analyses (**69.5; H, 8.1; N, 5.9%)were in good agreement with the chemical formula calculated for $C_{54}H_{73}NiN_4O_6$ (FW: 934.89 g mol^{-1}; C, C, 70.2; H, 8.4; N, 5.9%).

Its **FTIR spectrum** (**Figure 4.67**) is similar to the corresponding copper(II) complex (**Table 4.9**), and may be similarly assigned.

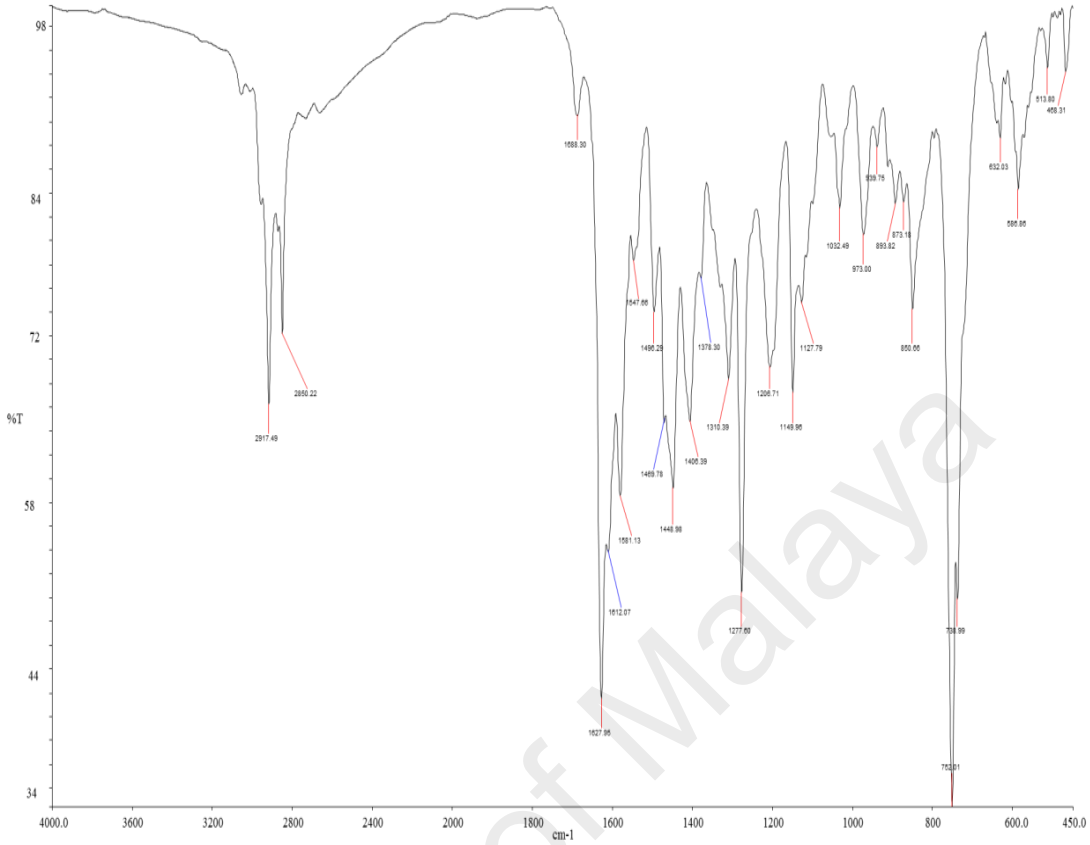

Figure 4.67 FTIR spectrum of $[Ni(CH_3(CH_2)_{14}COO)(HL3)_2]$

Its **UV-vis** spectrum(**Figure 4.68**) shows a peak observed at 598 nm (ε_{max} = 114$M^{-1}cm^{-1}$) which is assigned as the *d-d* transition of $^3A_2 \rightarrow {}^3T_2$. This indicates the geometry of the complex is most probably an octahedral which is consistent for a Ni(III) (d^7).

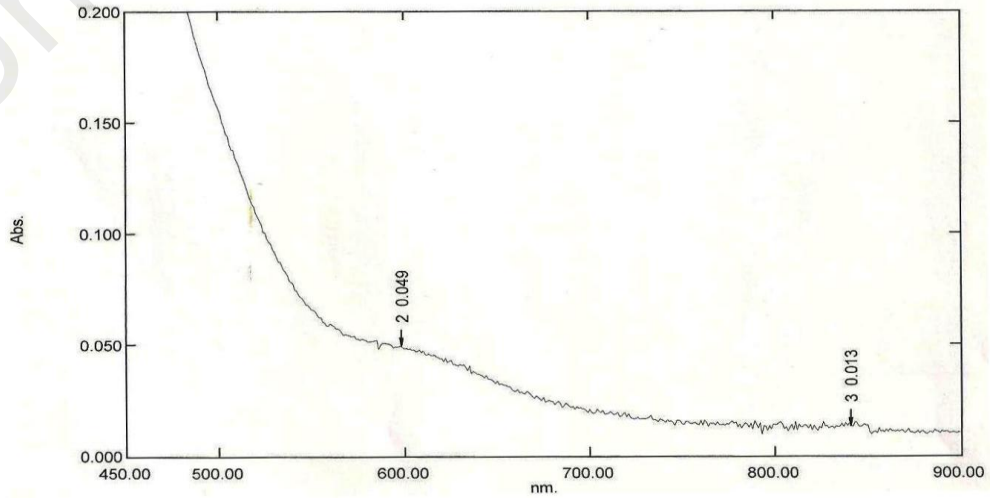

Figure 4.68 UV-vis spectrum of $[Ni(CH_3(CH_2)_{14}COO)(HL3)_2]$in $CHCl_3$

Its magnetic property could not be deduced by the Gouy method as the sample was a semisolid. However, its ^{1}H-NMR shows broadened peaks, indicating that the complex was paramagnetic.

From the **TGA** trace, the complex lost 93.4% of its weight from 163 °C to 800 °C (expected, 92.1%). The amount of residue at temperatures above 800 °C was 6.6% (expected, 7.9% assuming Ni_2O_3). Hence, there was a good agreement between the experimental and calculated results.

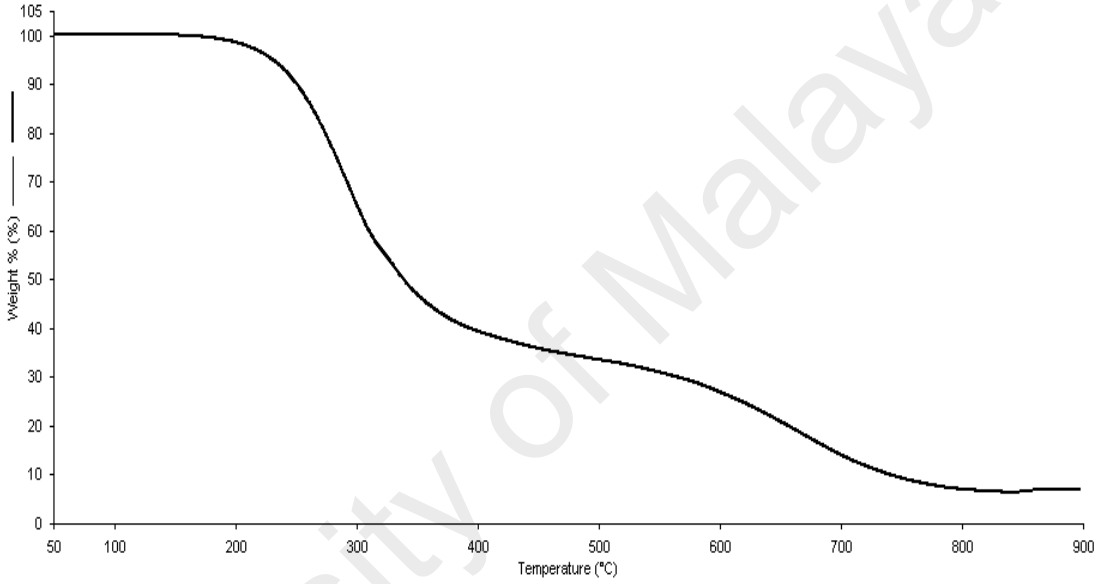

Figure 4.69TGA trace of $[Ni(CH_3(CH_2)_{14}COO)(HL3)_2]$

(c) M = Co

H_2L3 reacted with $[Co(CH_3(CH_2)_{14}COO)_2]$ to form a fine black solid (yield: 80.3%). As previously done, it is proposed that its structural formula is $[Co(CH_3(CH_2)_{14}COO)(HL3)]$.

The results of the **elemental analyses (**C, 67.5; H, 8.3; N, 4.5%) were in good agreement with the chemical formula calculated for $C_{35}H_{51}CoN_2O_4$ (FW: 623.7 g mol^{-1};C, 67.5; H, 9.9; N, 4.5%).

Its **FTIR spectrum** and data (**Figure 4.70**, **Table 4.9**) are similar to the corresponding Cu(II) and Ni(III) complexes, and may be similarly assigned.

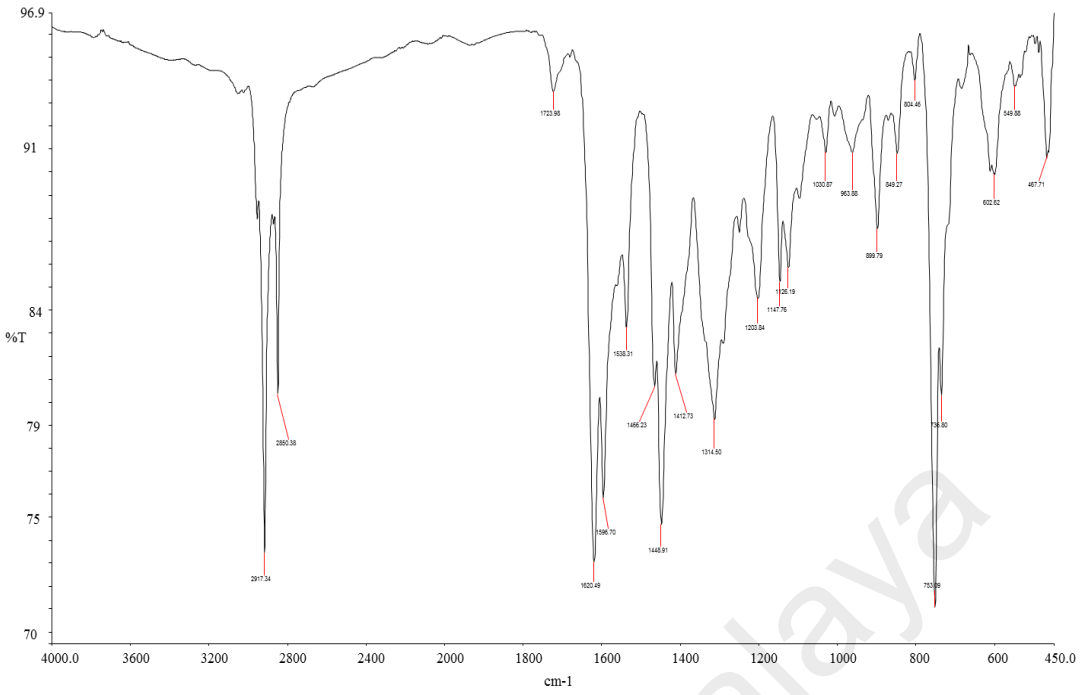

Figure 4.70 FTIR spectrum of [Co($CH_3(CH_2)_{14}COO$)(HL3)]

Its **UV-vis** spectrum in $CHCl_3$ shows a *d-d*band at 608 nm (ε_{max} = 233 $M^{-1}cm^{-1}$), assigned to $^4A_2 \rightarrow {}^4T_1$electronic transition, and another cobalt(II)-to-phenoxide CT band at 391 nm (ε_{max} = 233 $M^{-1}cm^{-1}$).This suggests a square planar geometry at the Co(II) centre.

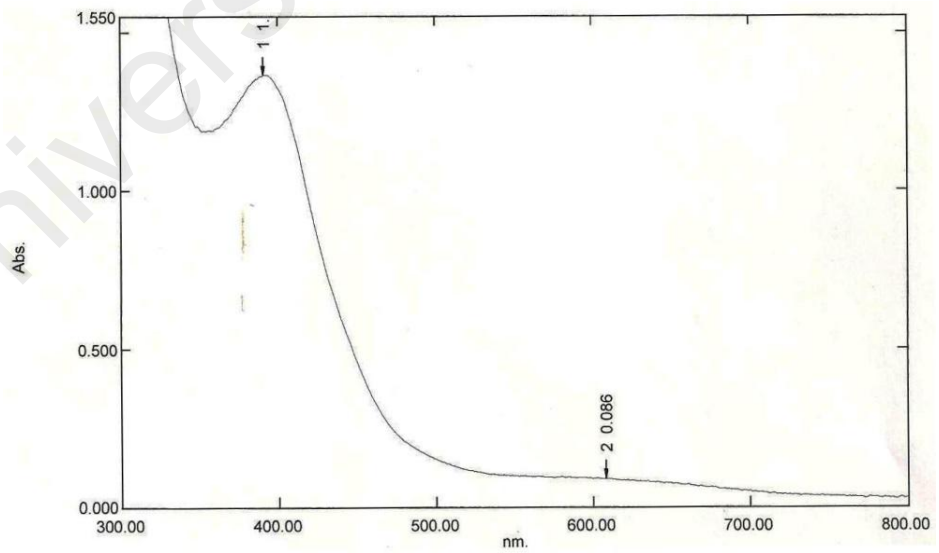

Figure 4.71 UV-vis spectrum of [Co($CH_3(CH_2)_{14}COO$)(HL3)]in $CHCl_3$

Its μ_{eff} value, calculated from the values of χ_g (4.10 x 10^{-7} cm^3 g^1), χ_M (2.55 x 10^{-4} cm^3 mol^{-1}), χ_{dia} (-3.76 x 10^{-4} cm^3 mol^{-1}), and χ_M^{corr} (6.32 x 10^{-4} cm^3 mol^{-1}), was 1.23 B.M. at 300 K. The expected spin-only value for a Co(II) complex ($3d^7$) with one unpaired electron is 1.73 B.M.However, the experimental value is within the range reported for many square planar Co(II) complexes[10].

From **TGA**, the complex lost89.7% of its weight from 144 °C to 670 °C due to loss of $CH_3(CH_2)_{14}COO$ and HL3 (expected, 90.6%). The amount of residue at temperatures above 670 °C was 10.3% (expected 9.4%, assuming CoO). As previous TGA results of corresponding Cu and Ni complexes, the thermal stability is lower than Co(II) complexes of H_2L1 (T_{dec} = 185 °C) and of H_2L2 (T_{dec} = 205 °C).

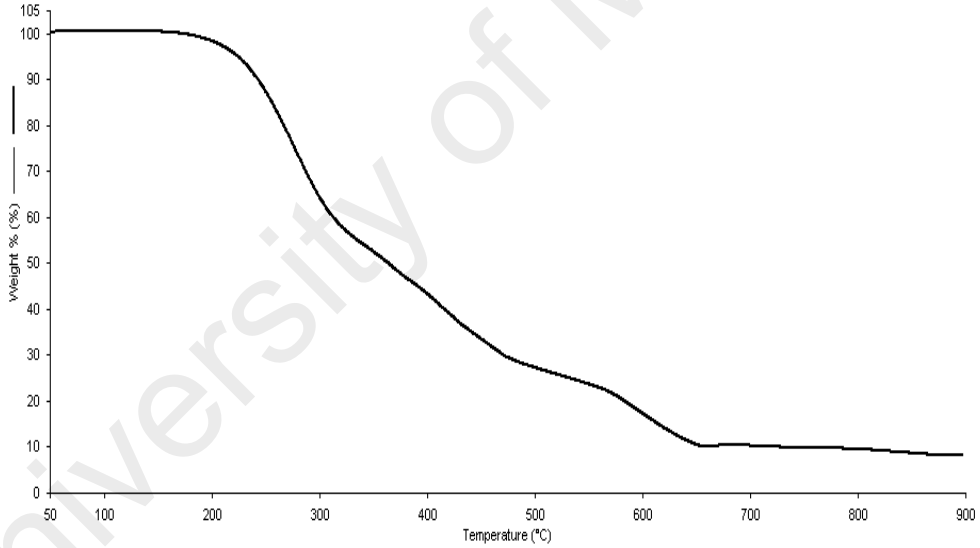

Figure 4.72 TGA trace of $[Co(CH_3(CH_2)_{14}COO)(HL3)]$

(d) M = Fe

H_2L3 reacted with $[Fe(CH_3(CH_2)_{14}COO)_2]$ to forma dark brown gummy solid (yield: 19.1%). As previously done, its proposed structural formula is $[Fe(CH_3(CH_2)_{14}COO)_2(HL3)]$. Hence, the complex is mononuclear Fe(III) , unlike those of H_2L1 ($[Fe_2(CH_3(CH_2)_{14}COO)_2(L1)(H_2O)_4].2.5H_2O$) which is dinuclear and H_2L2 ($[Fe^{II}Fe^{III}(CH_3(CH_2)_{14}COO)(L2)(HL2)_2(H_2O)_2].H_2O$).

The results of the **elemental analyses (**C, 70.0; H, 10.3; N, 4.3%) were in good agreement with the chemical formula calculated for $C_{51}H_{83}FeN_2O_2$ (FW: 876.06 g mol^{-1}; C, 69.9; H, 9.55; N, 3.2%)

Its **FTIR** spectrum and data (**Figure 4.73**; **Table 4.9**) are similar to the corresponding Cu, Ni and Co complexes, and may be similarly assigned [27].

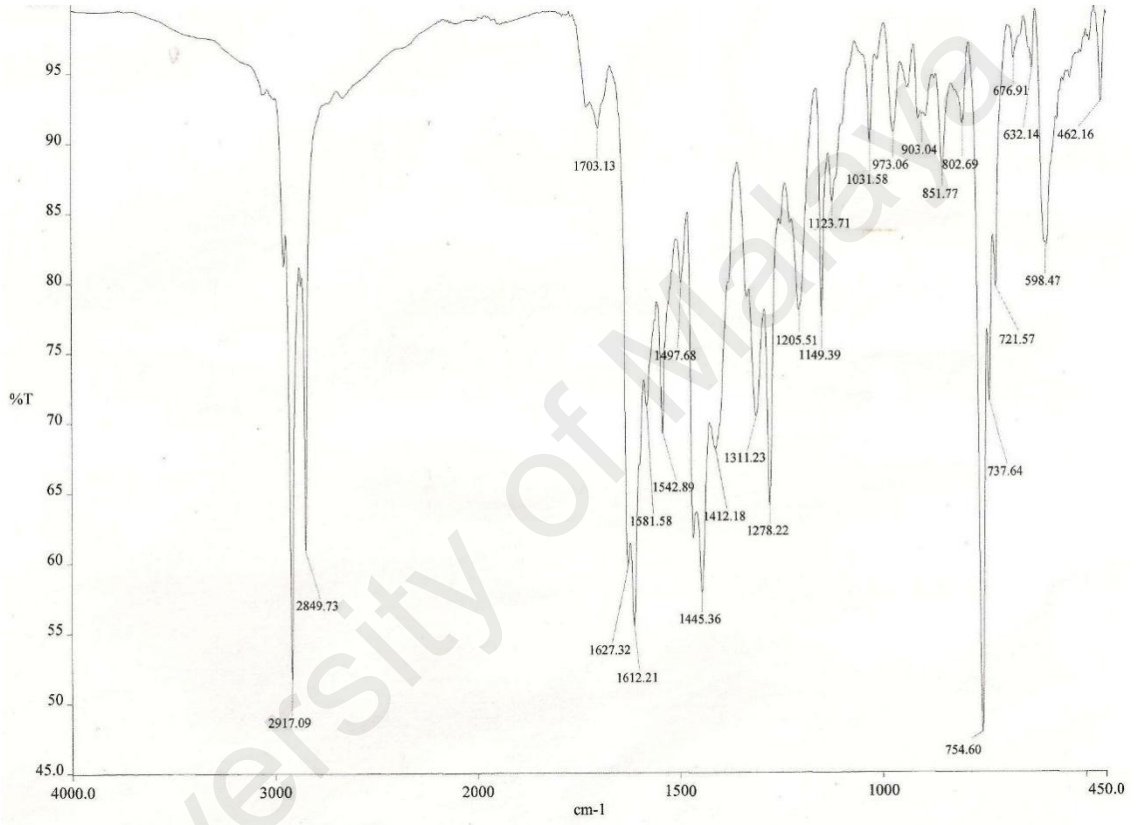

Figure 4.73 FTIR spectrum of $[Fe(CH_3(CH_2)_{14}COO)_2(HL3)]$

Its **UV-vis spectrum** in CH_3Cl shows a band at 509 nm (ε_{max}= 2633 $M^{-1}cm^{-1}$), which is assigned to $t_{2g} \rightarrow \pi^*$ electronic transition of the Fe(III) atom in an octahedral complex.The *d-d* transition for HS Fe(III) is spin forbidden hence weak band was observed [28]. A strong MLCT band was also observed at 429 nm (ε_{max} = 1977 $M^{-1}cm^{-1}$).

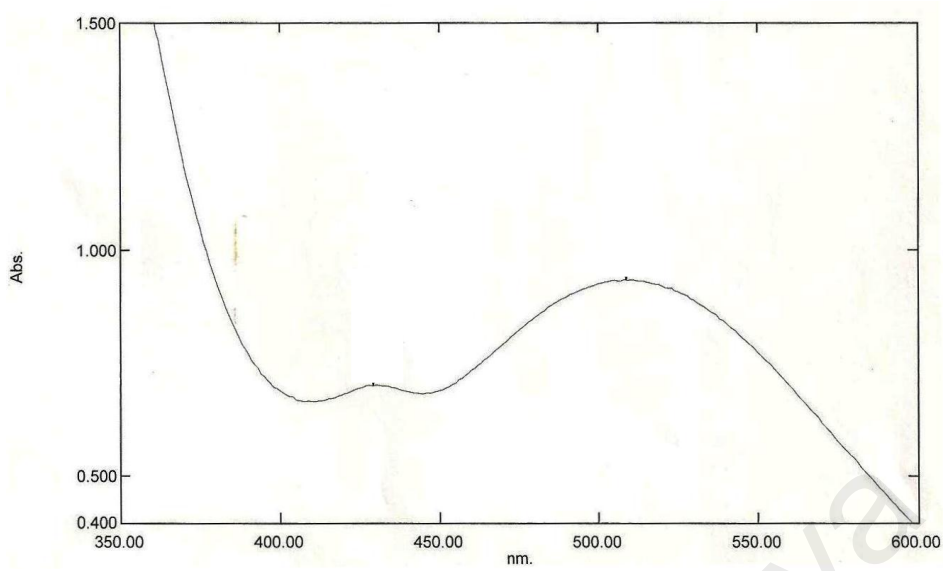

Figure 4.74 UV-vis spectrum of $[Fe(CH_3(CH_2)_{14}COO)_2(HL3)]$ in $CHCl_3$

Its μ_{eff} value could not be calculated by the Guoy balance as the sample was a gummy solid. However, its ^{1}H-NMR spectrum shows broad peaks, indicating a paramagnetic complex.

From **TGA**, the complex lost 93.5% of its weight from 209 °C to 750 °C due to the decomposition of all of its ligands (expected, 91.8%). The amount of residues at temperatures above 750 °C was 6.5% (expected 8.2%, assuming Fe_2O_3). Hence, there was a good agreement between the experimental and calculated results.

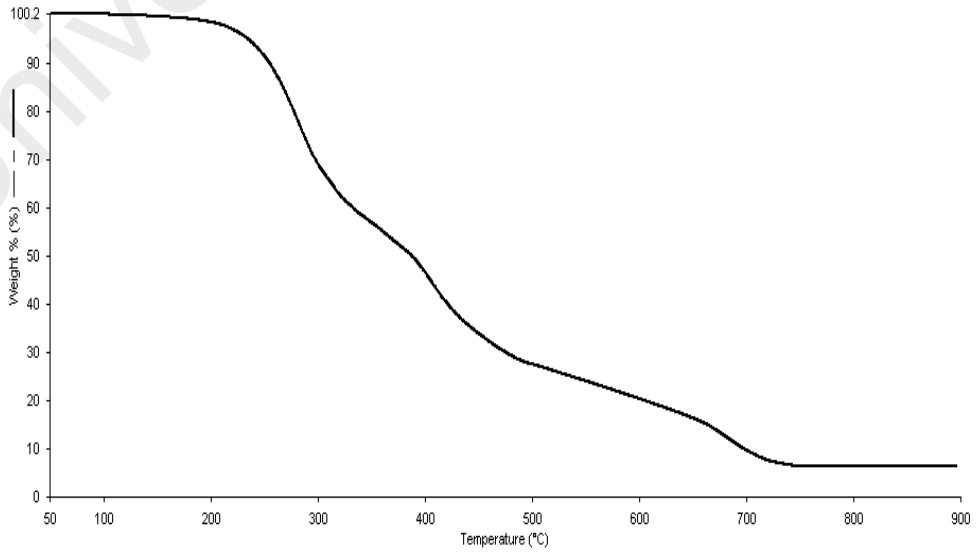

Figure 4.75 TGA trace of $[Fe(CH_3(CH_2)_{14}COO)_2(HL3)]$

4.4.3 Summary

H_2L3 reacted with $[M(CH_3(CH_2)_{14}COO)_2]$ to form a dinuclear Cu(II) complex, $[Cu_2(CH_3(CH_2)_{14}COO)(L3)(HL_3)]$, and mononuclear Ni(III), Co(II) and Fe(III) complexes (general formula $[M(R)_2(L3)]$. These complexes were paramagnetic, with thermal decomposition temperatures in the range of 142 °C to 209 °C. However, these complexes did not have liquid crystal properties.

References

[1] Ti, T.J., *Synthesis and Characterization of Zn(II), Cu(II), Ni(II) and Co(II) Complexes as Molecular Spintronic Materials*, M.Sc thesis, 2011, Univeristy of Malaya: Malaysia.

[2] Abe, Y., Nakabayashi, Kyoko., Matsukawa, Nahoko., Takashima, Hiroshi., Iida, Masayasu., Tanase, Tomoaki., Sugibayashi, Makiko., Mukai, Hidetomo., and Ohta, Kazuchika.,*Inorg. Chim. Act*, 2006. **359**(12): p. 3934-3946.

[3] Reglinski, J., S. Morris, and D.E. Stevenson, *Polyhedron*, 2002. **21**(21): p. 2175-2182.

[4] Nathan, L.C., Koehne, Jessica E., Gilmore, Joshua M., Hannibal, Kelly A., Dewhirst, William E., and Mai, Tuyetha D., *Polyhedron*, 2003. **22**(6): p. 887-894.

[5] Tai, X., Yin, Xianhong., Chen, Qiang., and Tan, Minyu.,*Molecules*, 2003. **8**(5): p. 439-443.

[6] Nakamoto, K., *Infrared and Raman spectra of inorganic and coordination compounds*. 1978: Wiley Online Library.

[7] Nishat, N., Rahisuddin., Haq, MM., and Kumar, Vikrant.,*J. Coord. Chem*., 2006. **59**(15): p. 1729-1738.

[8] Gaye, M., Sarr, Oumar., Sall, Abdou Salam., Diouf, Ousmane., and Hadabere, Seydou., *Bull. Chem. Soc. of Ethiopia*, 1997. **11**(2): p. 111-120.

[9] Aazam, E.S., A.F. El Husseiny, and H.M. Al-Amri, *Arab. J. Chem.*, 2012. **5**(1): p. 45-53.

[10] Salib, K.A., Saleh, Akila A., El-Wafa, Samy Abu., and El-Shafiy, Hoda FO., *J. Coord. Chem*, 2003. **56**(4): p. 283-298.

[11] Siqueira, A.B., Ionashiro, Elias Y., Carvalho, Cláudio T de., Bannach, Gilbert., Rodrigues, Emanuel C., and Ionashiro, Massao.,*Química Nova*, 2007. **30**(2): p. 318-322.

[12] Kurahashi, T. and H. Fujii, *U.,Inorg. Chem.*, 2013. **52**(7): p. 3908-3919.

[13] Chen, C.-J., Wang, I-Wen., Sheu, Hwo-Shuenn., Lee, Gene-Hsiang., and Lai, Chung K., *Tetrahedron*, 2011. **67**(42): p. 8120-8130.

[14] Deacon, G. and R. Phillips, *Coord. Chem. Rev*., 1980. **33**(3): p. 227-250.

[15] Shakirova, O.G., Lavrenova, L. G., Naumov, D. Yu., Daletsky, V. A., and Sheludyakova, L. A.., *Polyhedron*, 2012. **31**(1): p. 64-68.

[16] Kahn, O., *Molecular magnetism*. Vol. 60. 1993: VCH New York.

[17] Tomczyk, D., Nowak, L., Bukowski, W., Bester, K., Urbaniak, P., Andrijewski, G., and Olejniczak, B., *Electrochimica Acta*, 2014. 121: p. 64-77.

[18] Vafazadeh, R. and M. Kashfi, *Bull. Kor. Chem. Soc*., 2007. **28**(7): p. 1227.

[19] Raman, N., S. Ravichandran, and C. Thangaraja, *J. Chem. Sci.*, 2004. **116**(4): p. 215-219.

[20] Anacona, J. and J. Santaella, *Spectrochimica Acta Part A: Molecular and Biomolecular Spectroscopy*, 2013. **115**: p. 800-804.

[21] Niu, M.-J., Sun, Da-Wei., Li, Huan-Huan., Cao, Zhi-Qiang., Wang, Su-Na., and Dou, Jian-Min., *J. Coord. Chem*, 2013. **67**(1): p. 81-95

[22] Wilson, D., B. Djukic, and M.T. Lemaire,.*Trans. Met. Chem*, 2014. **39**(1): p. 17-24.

[23] Nawar, N. and N.M. Hosny, *Trans. Met. Chem.*, 2000. **25**(1): p. 1-8.

[24] Mulyana, Y., Alley, Kerwyn G., Davies, Kristian M., Abrahams, Brendan F., Moubaraki, Boujemaa., Murray, Keith S., and Boskovic, Colette.,*Dalton Transactions*, 2014. **43**(6): p. 2499-2511.

[25] Ray, A., Sadhukhan, Dipali., Rosair, Georgina M., Gómez-García, Carlos J., and Mitra, Samiran., *Polyhedron*, 2009. **28**(16): p. 3542-3550.

[26] Mukherjee, P., Drew, Michael, GB., Tangoulis, Vassilis., Estrader, Marta., Diaz, Carmen., and Ghosh, Ashutosh., *Polyhedron*, 2009. **28**(14): p. 2989-2996.

[27] Nagajothi, A., Kiruthika, A, Chitra, S, and Parameswari, K.,*Research Journal of Chemical Science*, 2013. **3**(2): p. 35-43.

[28] Turkyilmaz, M., M. Kacan, and Y. Baran, *Inorg. Chim. Act*, 2013. **395**(0): p. 255-259.

CHAPTER 5 CONCLUSIONS AND SUGGESTIONS FOR FUTURE WORKS

5.1 Conclusions

Three Schiff bases, H_2L1, H_2L2 and H_2L3 were successfully prepared from the reactions between 2-hydroxybenzaldehyde and 1,8-diaminooctane, 1,10-diaminodecane and 1,3-diaminopentane, respectively. These Schiff bases reacted with $[M(CH_3(CH_2)_{14}COO)_2]$ (M = Cu, Ni, Co, Fe; R = to form 16 complexes showing differences in structures and properties (magnetic, thermal, and mesomorphic).

H_2L1formed mononuclear square planar or distorted square complexes with Cu(II), Ni(II) and Co(II) (general formula, [M(L1)]), and formed dinuclear octahedral complex with Fe(II), $[Fe_2(CH_3(CH_2)_{14}COO)_2(L1)(H_2O)_4].2.5H_2O$. All complexes, except Ni(II), were paramagnetic. Their decomposition temperatures ranged from 198°C to 313°C. However, these complexes did not exhibit liquid crystal properties.

H_2L2 formed mononuclear Cu(II) complexes (general formula [M(L2)] by both one-pot and step-wise methods. The complexes were square planar, magnetic and thermally stable. For Ni(II), the step-wise method formed a mononuclear complex, $[Ni(L2)].CH_3CH_2OH$, while the one-pot method formed a dinuclear Ni(II) complex, $[Ni_2(L2)(HL2)_2].H_2O$. Both complexeswere square planar (hence diamagnetic). The mononuclear complex has a higher thermal stability than the dinuclear complex.For Co(II), the step-wise method formed a dinuclear Co(II) complex, $[Co_2(L2)(HL2)_2(EtOH)_4]$, while one-pot method formed a mononuclear Co(III) complex, [Co(L2)(HL2)]. The geometry of Co(II) and Co(III) was octahedral. The thermal stability of both complexes were almost similar (T_{dec} = 205^{o}C). The dinuclear complex was paramagnetic while the mononuclear complex was diamagnetic.For Fe(II), both methods formed dinuclear mixed-valence complexes in good yields. The difference in the two complexes was the presence of coordinated and non-coordinated solvent. The magnetic susceptibility and thermal stability for the complex formed from

the one-pot method were slightly higher than from the step-wise method. All of these complexes did not exhibit liquid crystal properties

H_2L3 formeda dinuclearCu(II) complex, $[Cu_2(CH_3(CH_2)_{14}COO)(L3)(HL_3)]$, and mononuclear complexes with Ni(III), Co(II) and Fe(III) complexes. These complexes were paramagnetic, with thermal decomposition temperatures in the range of 142 °C to 209 °C. However, these complexes also did not have liquid crystal properties.

5.2 Suggestions for Future Works

All hexadecanoato-Schiff base complexes were not mesomorphic. However, they may be made to be mesogenicby reacting them with neutral N-donor amide ligands, such as shown in **Figure 5.1.**

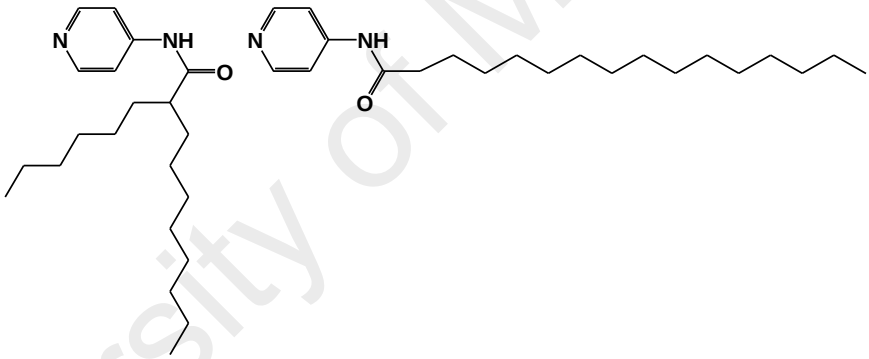

Figure 5.1 Structural formulae of neutral N-donor ligands

The thermal SCO behavior of cobalt(II) and iron(II) complexes should be further probed using SQUID magnetometer on both heating and cooling cycles. It would also be interesting to know the thermoelectric behavior of Co(III) and mixed-valence Fe complexes by measuring their electronic conductivities at different temperatures.Lastly, the potential uses of these complexes, especially Co(II), Fe(II), as catalysts and dye-sensitised cell materials, should be explored.